NORSAR

NORSAR Scientific Report No. 1-2005

Semiannual Technical Summary

1 July - 31 December 2004

Frode Ringdal (ed.)

Kjeller, January 2005

SECURITY CLASSIFICATION OF THIS PAGE

REPORT DOCUMENTATION PAGE

Form Approved
OMB No. 0704-0188

1a. REPORT SECURITY CLASSIFICATION Unclassified	1b. RESTRICTIVE MARKINGS Not applicable
2a. SECURITY CLASSIFICATION AUTHORITY Not Applicable	3. DISTRIBUTION/AVAILABILITY OF REPORT Approved for public release; distribution unlimited
2b. DECLASSIFICATION/DOWNGRADING SCHEDULE	
4. PERFORMING ORGANIZATION REPORT NUMBER(S) Scientific Rep. 1-2005	5. MONITORING ORGANIZATION REPORT NUMBER(S) Scientific Rep. 1-2005
6a. NAME OF PERFORMING ORGANIZATION NORSAR 6b. OFFICE SYMBOL (*If applicable*)	7a. NAME OF MONITORING ORGANIZATION HQ/AFTAC/TTS
6c. ADDRESS (*City, State, and ZIP Code*) Post Box 53 NO-2027 Kjeller, Norway	7b. ADDRESS (*City, State, and ZIP Code*) Patrick AFB, FL 32925-6001
8a. NAME OF FUNDING/SPONSORING ORGANIZATION Army Space and Missile Defense Command/ 8b. OFFICE SYMBOL (*If applicable*) ASMDC	9. PROCUREMENT INSTRUMENT IDENTIFICATION NUMBER Contract No. F08650-01-C-0055
8c. ADDRESS (*City, State, and ZIP Code*) 1515 Wilson Blvd., Suite 720 Arlington, VA 22209	10. SOURCE OF FUNDING NUMBERS PROGRAM ELEMENT NO. R&D; PROJECT NO. NORSAR Phase 3; TASK NO. SOW Task 5.0; WORK UNIT ACCESSION NO. Sequence No. 004A2
11. TITLE (*Include Security Classification*) Semiannual Technical Summary, 1 July - 31 December 2004 (Unclassified)	
12. PERSONAL AUTHOR(S)	
13a. TYPE OF REPORT Scientific Summary 13b. TIME COVERED FROM 1 Jul 04 TO 31 Dec 04 14. DATE OF REPORT (*Year, Month, Day*) 2005 January 15. PAGE COUNT 93	
16. SUPPLEMENTARY NOTATION	

17. COSATI CODES			18. SUBJECT TERMS (*Continue on reverse if necessary and identify by block number*)
FIELD	GROUP	SUB-GROUP	
8	11		NORSAR, Norwegian Seismic Array

19. ABSTRACT (*Continue on reverse if necessary and identify by block number*)

This report describes the research activities carried out at NORSAR under Contract No. F08650-01-C-0055 for the period 1 July - 31 December 2004. In addition, it provides summary information on operation and maintenance (O&M) activities at the Norwegian National Data Center (NDC) during the same period. Research activities described in this report, as well as transmission of selected data to the United States NDC, are funded by the United States Government. The O&M activities, including operation of transmission links within Norway and to Vienna, Austria, are being funded jointly by the CTBTO/PTS and the Norwegian Government, with the understanding that the funding of O&M activities for primary IMS will gradually be transferred to the CTBTO/PTS. The O&M statistics presented in this report are included for the purpose of completeness, and in order to maintain consistency with earlier reporting practice.

(cont.)

20. DISTRIBUTION/AVAILABILITY OF ABSTRACT ☐ UNCLASSIFIED/UNLIMITED ☐ SAME AS RPT. ☐ DTIC USERS	21. ABSTRACT SECURITY CLASSIFICATION
22a. NAME OF RESPONSIBLE INDIVIDUAL TSgt Mark C. Gerick	22b. TELEPHONE (*Include Area Code*) (321) 494-3582 22c. OFFICE SYMBOL AFTAC/TTD

DD Form 1473, JUN 86 *Previous editions are obsolete.* SECURITY CLASSIFICATION OF THIS PAGE

This report describes the research activities carried out at NORSAR under Contract No. F08650-01-C-0055 for the period 1 July - 31 December 2004. In addition, it provides summary information on operation and maintenance (O&M) activities at the Norwegian National Data Center (NDC) during the same period. Research activities described in this report, as well as transmission of selected data to the United States NDC, are funded by the United States Government. The O&M activities, including operation of transmission links within Norway and to Vienna, Austria are being funded jointly by the CTBTO/PTS and the Norwegian Government, with the understanding that the funding of O&M activities for primary stations in the International Monitoring System (IMS) will gradually be transferred to the CTBTO/PTS. The O&M statistics presented in this report are included for the purpose of completeness, and in order to maintain consistency with earlier reporting practice.

The NOA Detection Processing system has been operated throughout the period with an uptime of 100%. A total of 2307 seismic events have been reported in the NOA monthly seismic bulletin during the reporting period. On-line detection processing and data recording at the NDC of ARCES and FINES data have been conducted throughout the period. Data from the two small-aperture arrays at sites in Spitsbergen and Apatity, Kola Peninsula, as well as the Hagfors array in Sweden, have also been recorded and processed. Processing statistics for the arrays for the reporting period are given.

A summary of the activities at the Norwegian NDC and relating to field installations during the reporting period is provided in Section 4. Norway is now contributing primary station data from two seismic arrays: NOA (PS27) and ARCES (PS28) one auxiliary seismic array SPITS (AS72) and one auxiliary three-component station (JMIC). These data are being provided to the IDC via the global communications infrastructure (GCI). Continuous data from the three arrays are in addition being transmitted to the US NDC. The performance of the data transmission to the US NDC has been satisfactory during the reporting period.

A summary report on the Spitsbergen array refurbishment is presented in Section 4.4. Installation of the equipment at the array site was completed in September 2004, and the refurbished array is now operational.

Summaries of five scientific and technical contributions are presented in Chapter 6 of this report.

Section 6.1 is entitled “The detection of rockbursts at the Barentsburg coal mine, Spitsbergen, using waveform correlation on SPITS array data”. This contribution is a follow-up to previous studies of rockbursts in this mine, and makes use of the waveform correlation technique described in the previous NORSAR Semiannual Technical Summary. Using waveform correlation on data from the SPITS array, with the signal from the July 26, 2004, rockburst at the Barentsburg coal mine as a template or master waveform, we have identified over 1500 instances between January 1 and August 10, 2004, for which there is evidence for the occurrence of an event located very close to the site of this incident. The distribution in time of detections appears to correspond well with activity at the mine during the period investigated.

Section 6.2 is a study of spectral characteristics of signals and noise at selected primary seismic stations in the International Monitoring System (IMS). Based on the Threshold Monitoring (TM) concept, NORSAR has previously developed a system for continuous assessment of the global event detection capability of the Primary Seismic Network. In order to include new stations in the detectability calculations, the optimum processing parameters for each station have

to be found. The assessment of noise and signal spectra in various distance ranges, including determining the spectral bands with best SNR, forms an important part of the tuning of the threshold monitoring system. In this contribution, such spectra have been studied for a set of 4 arrays and 3 three-component stations recently added to the IMS network. The paper includes a brief discussion of the main spectral features of each station, with comparisons to the low and high Peterson noise models. Not unexpectedly, we find that for most stations, the best SNR is found at relatively low frequencies for teleseismic events, and at higher frequencies for local and regional events. However, the stations generally have some site-specific characteristics that need to be taken into account when tuning the parameters.

Section 6.3 is a study of a recent magnitude 3.5 earthquake in Flisa, southern Norway, which occurred on 7 April 2004. The main motivation for this quite detailed study was the proximity of the earthquake epicenter to the large NAO array as well as the Hagfors array in Sweden. This proximity, along with excellent recordings from several stations in central and northern Europe, enabled us to carry out a detailed analysis of the earthquake, including a precise location, depth estimate and fault plane solution. One foreshock and several aftershocks were observed. After applying the master-event technique, the foreshock and six of the aftershocks could be located relatively to the main event. The fault-plane solution for the main shock was determined in the traditionally way from first onset observations at numerous stations. In addition, some PmP polarities were used to restrict the solution space. The resulting fault-plane solution shows a north-south striking reverse fault plane, which was presumable also the rupture plane of the main shock.

Section 6.4 is a description of data now available in NORSAR's data archives from a temporary deployment during 2002 - 2004 of six seismic stations in northern Norway and Finland. This deployment was carried out under a separate DoE-funded project, in cooperation with Lawrence Livermore National Laboratory (LLNL). Explosions in underground as well as open-pit mines in the Khibiny massif of the Kola Peninsula of northwestern Russia are conducted on a frequent and relatively regular basis. It was decided to supplement the network of permanent stations in northern Fennoscandia and northwest Russia with temporarily deployed stations, in order to record these explosions, as well as other mining explosions and natural events occurring in this general area. Six temporary stations were deployed along two profile lines, extending westwards from the Khibini massif. The rationale for this deployment was to collect data to examine distance as well as azimuthal dependence of seismic discriminants. The southernmost of the two profile lines runs through the permanent seismic array ARCES in northern Norway. During the deployment period of 745 days, a local representative of NORSAR visited the sites nine times to check the station status and to change the RefTek field disks. Dump files of the recorder's hard disks were sent to NORSAR for subsequent data format conversion, quality control, and archiving. The data files are now stored at NORSAR as well as at LLNL.

Section 6.5 is a study of the disastrous Sumatra earthquake of 26 December 2004. This M_W 9.0 event was the largest earthquake ever recorded by NORSAR, and consequently represented a test of the current instrumentation and processing algorithms. NORSAR has established an earthquake alert system, and this system functioned well for the earthquake with reasonably precise location information relayed about 7 and 9 minutes after the first arrivals were recorded in Finland and Norway. The automatic magnitude estimates were considerably lower than later interactive measurements. While this is no surprise, it certainly represents a challenge for

improving on magnitude determination algorithms for large earthquakes. Until January 20, 2005, 736 aftershocks were detected and located on the NOA array, and the automatic locations by and large delineate the main rupture.

AFTAC Project Authorization	:	T/0155/PKO
ARPA Order No.	:	4138 AMD # 53
Program Code No.	:	0F10
Name of Contractor	:	Stiftelsen NORSAR
Effective Date of Contract	:	1 Feb 2001 (T/0155/PKO)
Contract Expiration Date	:	31 December 2005
Project Manager	:	Frode Ringdal +47 63 80 59 00
Title of Work	:	The Norwegian Seismic Array (NORSAR) Phase 3
Amount of Contract	:	$ 3,383,445
Period Covered by Report	:	1 July - 31 December 2004

The research presented in this report was supported by the Army Space and Missile Defense Command and was monitored by AFTAC, Patrick AFB, FL32925, under contract no. F08650-01-C-0055.

The operational activities of the seismic field systems and the Norwegian National Data Center (NDC) are currently jointly funded by the Norwegian Government and the CTBTO/PTS, with the understanding that the funding of IMS-related activities will gradually be transferred to the CTBTO/PTS.

NORSAR Contribution No. 911

Table of Contents

Page

1 Summary

This report describes the research activities carried out at NORSAR under Contract No. F08650-01-C-0055 for the period 1 July - 31 December 2004. In addition, it provides summary information on operation and maintenance (O&M) activities at the Norwegian National Data Center (NDC) during the same period. Research activities described in this report, as well as transmission of selected data to the United States NDC, are funded by the United States Government. The O&M activities, including operation of transmission links within Norway and to Vienna, Austria are being funded jointly by the CTBTO/PTS and the Norwegian Government, with the understanding that the funding of O&M activities for primary stations in the International Monitoring System (IMS) will gradually be transferred to the CTBTO/PTS. The O&M statistics presented in this report are included for the purpose of completeness, and in order to maintain consistency with earlier reporting practice.

The seismic arrays operated by the Norwegian NDC comprise the Norwegian Seismic Array (NOA), the Arctic Regional Seismic Array (ARCES) and the Spitsbergen Regional Array (SPITS). This report presents statistics for these three arrays as well as for additional seismic stations which through cooperative agreements with institutions in the host countries provide continuous data to the NORSAR Data Processing Center (NDPC). These additional stations comprise the Finnish Regional Seismic Array (FINES), the Hagfors array in Sweden (HFS) and the regional seismic array in Apatity, Russia.

The NOA Detection Processing system has been operated throughout the period with an uptime of 100%. A total of 2307 seismic events have been reported in the NOA monthly seismic bulletin during the reporting period. On-line detection processing and data recording at the NDC of ARCES and FINES data have been conducted throughout the period. Data from the two small-aperture arrays at sites in Spitsbergen and Apatity, Kola Peninsula, as well as the Hagfors array in Sweden, have also been recorded and processed. Processing statistics for the arrays for the reporting period are given.

A summary of the activities at the Norwegian NDC and relating to field installations during the reporting period is provided in Section 4. Norway is now contributing primary station data from two seismic arrays: NOA (PS27) and ARCES (PS28) one auxiliary seismic array SPITS (AS72) and one auxiliary three-component station (JMIC). These data are being provided to the IDC via the global communications infrastructure (GCI). Continuous data from the three arrays are in addition being transmitted to the US NDC. The performance of the data transmission to the US NDC has been satisfactory during the reporting period.

So far among the Norwegian stations, the NOA and the ARCES array (PS27 and PS28 respectively) and the radionuclide station at Spitsbergen (RN49) have been certified. Provided that adequate funding continues to be made available (from the PTS and the Norwegian Ministry of Foreign Affairs), we envisage continuing the provision of data from these and other Norwegian IMS-designated stations in accordance with current procedures. The IMS infrasound station at Karasjok (IS37) is expected to be built in 2005 or 2006, provided adequate resources for project planning and execution are made available.

A summary report on the Spitsbergen array refurbishment is presented in Section 4.4. Installation of the equipment at the array site was completed in September 2004, and the refurbished array is now operational.

Summaries of five scientific and technical contributions are presented in Chapter 6 of this report.

Section 6.1 is entitled "The detection of rockbursts at the Barentsburg coal mine, Spitsbergen, using waveform correlation on SPITS array data". This contribution is a follow-up to previous studies of rockbursts in this mine, and makes use of the waveform correlation technique described in the previous NORSAR Semiannual Technical Summary. Using waveform correlation on data from the SPITS array, with the signal from the July 26, 2004, rockburst at the Barentsburg coal mine as a template or master waveform, we have identified over 1500 instances between January 1 and August 10, 2004, for which there is evidence for the occurrence of an event located very close to the site of this incident.

As the objective was to obtain a comprehensive event list, the detection thresholds were purposefully set low. The initial detection list comprised over 7000 candidate events, and many of these were clearly spurious. This made it necessary to devise a system for the automatic screening of false alarms. We developed such a screening procedure, applying f-k analysis to the *individual sensor* correlation traces. This rather unconventional use of f-k analysis turned out to be quite successful. The instances of correlation due to unrelated signals were readily filtered out by applying this type of f-k analysis together with a set of predetermined rules. Many borderline cases with a very low SNR were also removed in this process; these may have corresponded to Barentsburg events but there was insufficient evidence at the SPITS array to support this. This procedure reduced the list of detections from over 7000 to 1578. Of these, a large number correspond to detections made by standard processing at the SPITS array and many others covering a wide range of magnitudes were also registered by two on-site three component instruments close to the Barentsburg mine. The distribution in time of detections appears to correspond well with activity at the mine during the period investigated.

Section 6.2 is a study of spectral characteristics of signals and noise at selected primary seismic stations in the International Monitoring System (IMS). Based on the Threshold Monitoring (TM) concept, NORSAR has previously developed a system for continuous assessment of the global event detection capability of the Primary Seismic Network. In order to include new stations in the detectability calculations, the optimum processing parameters for each station have to be found. The assessment of noise and signal spectra in various distance ranges, including determining the spectral bands with best SNR, forms an important part of the tuning of the threshold monitoring system. In this contribution, such spectra have been studied for a set of 4 arrays and 3 three-component stations recently added to the IMS network:

- AKASG (PS 45) in Ukraine, called the Malin array. This is a 23 element array with an aperture of 15 - 20 km.
- BRTR (PS 43) in Turkey, called the Keskin array. This is a 6 element array with an aperture of about 3 km.
- MKAR (PS 23) in Kazakhstan, called the Makanchi array. This is a 9 element array with an aperture of about 3-4 km.
- SONM (PS 25) in Mongolia, called the Songino array. This is a 10 element array with an aperture of about 4 km.
- KMBO (PS 24) in Kilimambogo, Kenya, which is a three-component station.
- PPT (PS 18) in Pamatai, Tahiti, which is a three-component station.

- THR (PS 21) in Teheran, Iran, which is a three-component station.

The paper includes a brief discussion of the main spectral features of each station, with comparisons to the low and high Peterson noise models. Not unexpectedly, we find that for most stations, the best SNR is found at relatively low frequencies for teleseismic events, and at higher frequencies for local and regional events. However, the stations generally have some site-specific characteristics that need to be taken into account when tuning the parameters.

Section 6.3 is a study of a recent magnitude 3.5 earthquake in Flisa, southern Norway, which occurred on 7 April 2004. The main motivation for this quite detailed study was the proximity of the earthquake epicenter to the large NAO array as well as the Hagfors array in Sweden. This proximity, along with excellent recordings from several stations in central and northern Europe, enabled us to carry out a detailed analysis of the earthquake, including a precise location, depth estimate and fault plane solution.

To calculate a start solution for the hypocenter inversion of the Flisa earthquake, classical location procedures were applied including backazimuth observations, Wadati diagram and an optimized velocity model. The inversions were performed with the HYPOSAT location program, which can use all available data (onset times of first and later onsets, backazimuth and slowness observations, travel time differences between phases, and different types of corrections) to achieve the best least-squares-fit type solution. Investigation of model uncertainties associated with changes made to NORSAR's standard velocity model, revealed that the best fit was achieved when the thickness of the upper crust was increased to 20 km.

One foreshock and several aftershocks were observed. After applying the master-event technique, the foreshock and six of the aftershocks could be located relatively to the main event.

The fault-plane solution for the main shock was determined in the traditionally way from first onset observations at numerous stations. In addition, some PmP polarities were used to restrict the solution space. The resulting fault-plane solution shows a north-south striking reverse fault plane, which was presumable also the rupture plane of the main shock.

Section 6.4 is a description of data now available in NORSAR's data archives from a temporary deployment during 2002 - 2004 of six seismic stations in northern Norway and Finland. This deployment was carried out under a separate DoE-funded project, in cooperation with Lawrence Livermore National Laboratory (LLNL).

Explosions in underground as well as open-pit mines in the Khibiny massif of the Kola Peninsula of northwestern Russia are conducted on a frequent and relatively regular basis. It was decided to supplement the network of permanent stations in northern Fennoscandia and northwest Russia with temporarily deployed stations, in order to record these explosions, as well as other mining explosions and natural events occurring in this general area. Six temporary stations were deployed along two profile lines, extending westwards from the Khibini massif. The rationale for this deployment was to collect data to examine distance as well as azimuthal dependence of seismic discriminants. The southernmost of the two profile lines runs through the permanent seismic array ARCES in northern Norway.

Six RefTek 72A-08 data loggers (Refraction Technology) equipped with three-component GS-13 seismometers (Teledyne Geotech) occupied positions along the two profile lines during the time period from 27 August 2002 to 9 September 2004. Two of the six stations, Ivalo (IVL) and Kaamasmukka (KMM), were located in northern Finland, and the remaining four were deployed in the Finnmark county of northern Norway. These were the sites Neiden (NDN),

Skogfoss (SKF), Skoganvarre (SKV), and Varangerbotn (VGB). During the deployment period of 745 days, a local representative of NORSAR visited the sites nine times to check the station status and to change the RefTek field disks. Dump files of the recorder's hard disks were sent to NORSAR for subsequent data format conversion, quality control, and archiving. The data files are now stored at NORSAR as well as at LLNL.

Section 6.5 is a study of the disastrous Sumatra earthquake of 26 December 2004. This M_W 9.0 event was the largest earthquake ever recorded by NORSAR, and consequently represented a test of the current instrumentation and processing algorithms. NORSAR has established an earthquake alert system, and this system functioned well for the earthquake with reasonably precise location information relayed about 7 and 9 minutes after the first arrivals were recorded in Finland and Norway. The automatic magnitude estimates were considerably lower than later interactive measurements. While this is no surprise, it certainly represents a challenge for improving on magnitude determination algorithms for large earthquakes. Until January 20, 2005, 736 aftershocks were detected and located on the NOA array, and the automatic locations by and large delineate the main rupture.

Following this experience, some challenges for new developments have been identified: a) The processing could be optimized to provide the alert with a delay of some seconds rather than 7 and 9 minutes after data are recorded. Clearly, access to data from local or regional stations would enable even earlier alerts. b) The magnitude estimation (based on P-waves) should be improved for large events. Among the factors to take into account here are both the spectral properties of the signal and the duration of the P-wave train.

Frode Ringdal

2 Operation of International Monitoring System (IMS) Stations in Norway

2.1 PS27 — Primary Seismic Station NOA

The average recording time was 100%, the same as for the previous reporting period.

There were no outages of all subarrays at the same time.

Monthly uptimes for the NORSAR on-line data recording task, taking into account all factors (field installations, transmissions line, data center operation) affecting this task were as follows:

July	:	100%
August	:	100%
September	:	100%
October	:	100%
November	:	100%
December	:	100%

J. Torstveit

NOA Event Detection Operation

In Table 2.1.1 some monthly statistics of the Detection and Event Processor operation are given. The table lists the total number of detections (DPX) triggered by the on-line detector, the total number of detections processed by the automatic event processor (EPX) and the total number of events accepted after analyst review (teleseismic phases, core phases and total).

	Total DPX	Total EPX	Accepted Events		Sum	Daily
			P-phases	Core Phases		
Jul	7,077	801	269	61	330	10.6
Aug	10,130	1,633	252	47	299	9.6
Sep	9,036	756	193	41	234	7.8
Oct	10,020	859	277	51	328	10.6
Nov	11,546	1,072	267	64	331	11.0
Dec	13,994	1,432	743	42	785	25.3
	61,803	6,553	2,001	306	2,307	12.48

Table 2.1.1. *Detection and Event Processor statistics, 1 July - 31 December 2004.*

NOA detections

The number of detections (phases) reported by the NORSAR detector during day 183, 2004, through day 366, 2004, was 61,803, giving an average of 318 detections per processed day (184 days processed).

B. Paulsen

U. Baadshaug

2.2 PS28 — Primary Seismic Station ARCES

The average recording time was 99.65%, as compared to100% for the previous reporting period.

Table 2.2.1 lists the time periods of the outages in the period.

Day	Period
02/08	15.52.20 - 16.04.50
06/08	15.19.50 - 15.29.50
06/08	16.18.50 - 16.29.50
22/10	05.07.00 - 05.13.50
17/12	05.02.50 - 05.08.50

Table 2.2.1. *The main interruptions in recording of ARCES data at NDPC, 1 July - 31 December 2004.*

Monthly uptimes for the ARCES on-line data recording task, taking into account all factors (field installations, transmission lines, data center operation) affecting this task were as follows:

July	:	99.98%
August	:	99.93%
September	:	100%
October	:	99.99%
November	:	100%
December	:	99.99%

J. Torstveit

Event Detection Operation

ARCES detections

The number of detections (phases) reported during day 183, 2004, through day 366, 2004, was 225,733, giving an average of 1227 detections per processed day (184 days processed).

Events automatically located by ARCES

During days 183, 2004, through 366, 2004, 10,017 local and regional events were located by ARCES, based on automatic association of P- and S-type arrivals. This gives an average of 54.4 events per processed day (184 days processed). 56% of these events are within 300 km, and 85% of these events are within 1000 km.

U. Baadshaug

2.3 AS72 — Auxiliary Seismic Station Spitsbergen

The average recording time was 95.46% as compared to 95.76% for the previous reporting period.

Table 2.3.1 lists the time periods of the main downtimes in the reporting period.

Day	Period
04/07	14.42.09 - 15.17.50
14/07	13.25.00 - 13.39.38
16/07	16.19.18 - 16.23.17
21/07	14.06.43 - 14.19.12
10/08	14.44.12 -
12/08	- 23.59.59

Table 2.3.1. *The main interruptions in recording of Spitsbergen data at NDPC, 1 July - 31 December 2004.*

Monthly uptimes for the Spitsbergen on-line data recording task, taking into account all factors (field installations, transmissions line, data center operation) affecting this task were as follows:

July	:	99.82%
August	:	92.30%
September	:	100%
October	:	100%
November	:	100%
December	:	100%

J. Torstveit

Event Detection Operation

Spitsbergen array detections

The number of detections (phases) reported from day 183, 2004, through day 366, 2004, was 366,266, giving an average of 2,012 detections per processed day (182 days processed).

Events automatically located by the Spitsbergen array

During days 183, 2004, through 366, 2004, 29,962 local and regional events were located by the Spitsbergen array, based on automatic association of P- and S-type arrivals. This gives an average of 164.6 events per processed day (182 days processed). 75% of these events are within 300 km, and 89% of these events are within 1000 km.

U. Baadshaug

2.4 AS73 — Auxiliary Seismic Station at Jan Mayen

The IMS auxiliary seismic network includes a three-component station on the Norwegian island of Jan Mayen. The station location given in the protocol to the Comprehensive Nuclear-Test-Ban Treaty is 70.9˚N, 8.7˚W.

The University of Bergen has operated a seismic station at this location since 1970. A so-called Parent Network Station Assessment for AS73 was completed in April 2002. A vault at a new location (71.0^{o}N, 8.5^{o}W) was prepared in early 2003, after its location had been approved by the PrepCom. New equipment was installed in this vault in October 2003, as a cooperative effort bertween NORSAR and the CTBTO/PTS. Continuous data from this station are being transmitted to the NDC at Kjeller via a satellite link installed in April 2000. Data are also made available to the University of Bergen.

J. Fyen

2.5 IS37 — Infrasound Station at Karasjok

The IMS infrasound network will include a station at Karasjok in northern Norway. The coordinates given for this station are 69.5˚N, 25.5˚E. These coordinates coincide with those of the primary seismic station PS28.

A site survey for this station was carried out during June/July 1998 as a cooperative effort between the Provisional Technical Secretariat of the CTBTO and NORSAR. The site survey led to a recommendation on the exact location of the infrasound station. This location needs to be surveyed in detail. The next step will be to approach the local authorities to obtain the permission necessary to establish the station. Station installation is expected to take place in 2005 or 2006, provided that adequate resources for project planning and execution are made available.

S. Mykkeltveit

2.6 RN49 — Radionuclide Station on Spitsbergen

The IMS radionuclide network includes a station on the island of Spitsbergen. This station is also among those IMS radionuclide stations that will have a capability of monitoring for the presence of relevant noble gases upon entry into force of the CTBT.

A site survey for this station was carried out in August of 1999 by NORSAR, in cooperation with the Norwegian Radiation Protection Authority. The site survey report to the PTS contained a recommendation to establish this station at Platåberget, near Longyearbyen. The infrastructure for housing the station equipment was established in early 2001, and a noble gas detection system, based on the Swedish “SAUNA” design, was installed at this site in May 2001, as part of PrepCom’s noble gas experiment. A particulate station (“ARAME” design) was installed at the same location in September 2001. A certification visit to the station took place in October 2002, and the particulate station was certified on 10 June 2003. The equipment at RN49 is being maintained and operated in accordance with a contract with the CTBTO/PTS.

S. Mykkeltveit

3 Contributing Regional Seismic Arrays

3.1 NORES

NORES has been out of operation since a thunderstorm destroyed the station electronics on 11 June 2002.

J. Torstveit

3.2 Hagfors (IMS Station AS101)

Data from the Hagfors array are made available continuously to NORSAR through a cooperative agreement with Swedish authorities.

The average recording time was 99.71% as compared to 100% for the previous reporting period.

There were no outages in the reporting period.

Monthly uptimes for the Hagfors on-line data recording task, taking into account all factors (field installations, transmissions line, data center operation) affecting this task were as follows:

July	:	99.99%
August	:	99.81%
September	:	98.45%
October	:	99.98%
November	:	99.98%
December	:	100%

J. Torstveit

Hagfors Event Detection Operation

Hagfors array detections

The number of detections (phases) reported from day 183, 2004, through day 366, 2004, was 175,422, giving an average of 953 detections per processed day (184 days processed).

Events automatically located by the Hagfors array

During days 183, 2004, through 366, 2004, 5,082 local and regional events were located by the Hagfors array, based on automatic association of P- and S-type arrivals. This gives an average of 27.6 events per processed day (184 days processed). 65% of these events are within 300 km, and 89% of these events are within 1000 km.

U. Baadshaug

3.3 FINES (IMS station PS17)

Data from the FINES array are made available continuously to NORSAR through a cooperative agreement with Finnish authorities.

The average recording time was 98.97% as as compared to 100% for the previous reporting period.

Monthly uptimes for the FINES on-line data recording task, taking into account all factors (field installations, transmissions line, data center operation) affecting this task were as follows:

July	:	100%
August	:	95.36%
September	:	98.62%
October	:	99.83%
November	:	100%
December	:	100%

J. Torstveit

FINES Event Detection Operation

FINES detections

The number of detections (phases) reported during day 183, 2004, through day 366, 2004, was 49,444, giving an average of 269 detections per processed day (184 days processed).

Events automatically located by FINES

During days 183, 2004, through 366, 2004, 2644 local and regional events were located by FINES, based on automatic association of P- and S-type arrivals. This gives an average of 14.4 events per processed day (184 days processed). 76% of these events are within 300 km, and 86% of these events are within 1000 km.

U. Baadshaug

3.4 Apatity

The average recording time was 90.96% in the reporting period compared to 99.94% during the previous period.

The main outages in the period are given in Table 3.4.1.

Date	Time
16/12 - 17/12	16.20.00 - - 14.30.00

Table 3.4.1. *The main interruptions in recording of Apatity data at NDPC, 1 July - 31 December 2004.*

Monthly uptimes for the Apatity on-line data recording task, taking into account all factors (field installations, transmissions line, data center operation) affecting this task were as follows:

July	:	99.95%
August	:	99.97%
September	:	98.45%
October	:	99.95%
November	:	75.10%
December	:	70.52%

J. Torstveit

Apatity Event Detection Operation

Apatity array detections

The number of detections (phases) reported from day 183, 2004, through day 366, 2004, was 241,476, giving an average of 1446 detections per processed day (167 days processed).

As described in earlier reports, the data from the Apatity array is transferred by one-way (simplex) radio links to Apatity city. The transmission suffers from radio disturbances that occasionally result in a large number of small data gaps and spikes in the data. In order for the communication protocol to correct such errors by requesting retransmission of data, a two-way radio link would be needed (duplex radio). However, it should be noted that noise from cultural activities and from the nearby lakes cause most of the unwanted detections. These unwanted detections are “filtered” in the signal processing, as they give seismic velocities that are outside accepted limits for regional and teleseismic phase velocities.

Events automatically located by the Apatity array

During days 183, 2004, through 366, 2004, 4654 local and regional events were located by the Apatity array, based on automatic association of P- and S-type arrivals. This gives an average

of 27.9 events per processed day (167 days processed). 28% of these events are within 300 km, and 70% of these events are within 1000 km.

U. Baadshaug

3.5 Regional Monitoring System Operation and Analysis

The Regional Monitoring System (RMS) was installed at NORSAR in December 1989 and has been operated at NORSAR from 1 January 1990 for automatic processing of data from ARCES and NORES. A second version of RMS that accepts data from an arbitrary number of arrays and single 3-component stations was installed at NORSAR in October 1991, and regular operation of the system comprising analysis of data from the 4 arrays ARCES, NORES, FINES and GERES started on 15 October 1991. As opposed to the first version of RMS, the one in current operation also has the capability of locating events at teleseismic distances.

Data from the Apatity array was included on 14 December 1992, and from the Spitsbergen array on 12 January 1994. Detections from the Hagfors array were available to the analysts and could be added manually during analysis from 6 December 1994. After 2 February 1995, Hagfors detections were also used in the automatic phase association.

Since 24 April 1999, RMS has processed data from all the seven regional arrays ARCES, NORES, FINES, GERES (until January 2000), Apatity, Spitsbergen, and Hagfors. Starting 19 September 1999, waveforms and detections from the NORSAR array have also been available to the analyst.

Phase and event statistics

Table 3.5.1 gives a summary of phase detections and events declared by RMS. From top to bottom the table gives the total number of detections by the RMS, the number of detections that are associated with events automatically declared by the RMS, the number of detections that are not associated with any events, the number of events automatically declared by the RMS, and finally the total number of events worked on interactively (in accordance with criteria that vary over time; see below) and defined by the analyst.

New criteria for interactive event analysis were introduced from 1 January 1994. Since that date, only regional events in areas of special interest (e.g, Spitsbergen, since it is necessary to acquire new knowledge in this region) or other significant events (e.g, felt earthquakes and large industrial explosions) were thoroughly analyzed. Teleseismic events of special interest are also analyzed.

To further reduce the workload on the analysts and to focus on regional events in preparation for Gamma-data submission during GSETT-3, a new processing scheme was introduced on 2 February 1995. The GBF (Generalized Beamforming) program is used as a pre-processor to RMS, and only phases associated with selected events in northern Europe are considered in the automatic RMS phase association. All detections, however, are still available to the analysts and can be added manually during analysis.

	Jul 04	Aug 04	Sep 04	Oct 04	Nov 04	Dec 04	Total
Phase detections	172,013	148,724	172,319	157,960	182,110	175,767	1,008,894
- Associated phases	7,380	5,814	8,863	6,919	6,557	6,901	42,434
- Unassociated phases	164,633	142,910	163,456	151,041	175,553	168,866	966,459
Events automatically declared by RMS	1,489	1,320	1,965	1,529	1,501	1,793	9,597
No. of events defined by the analyst	108	95	160	106	92	89	650

Table 3.5.1. RMS phase detections and event summary 1 July - 31 December2004.

U. Baadshaug
B. Paulsen

4 NDC and Field Activities

4.1 NDC Activitities

NORSAR functions as the Norwegian National Data Center (NDC) for CTBT verification. Six monitoring stations, comprising altogether 119 field instruments, will be located on Norwegian territory as part of the future IMS as described elsewhere in this report. The four seismic IMS stations are all in operation today, and three of them are currently providing data to the IDC on a regular basis. The radionuclide station at Spitsbergen was certified on 10 June 2003, whereas the infrasound station in northern Norway will need to be established within the next few years. Data recorded by the Norwegian stations is being transmitted in real time to the Norwegian NDC, and provided to the IDC through the Global Communications Infrastructure (GCI). Norway is connected to the GCI with a frame relay link to Vienna.

Operating the Norwegian IMS stations continues to require increased resources and additional personnel both at the NDC and in the field. The PTS has established new and strictly defined procedures as well as increased emphasis on regularity of data recording and timely data transmission to the IDC in Vienna. This has led to increased reporting activities and implementation of new procedures for the NDC operators. The NDC carries out all the technical tasks required in support of Norway's treaty obligations. NORSAR will also carry out assessments of events of special interest, and advise the Norwegian authorities in technical matters relating to treaty compliance.

Verification functions; information received from the IDC

After the CTBT enters into force, the IDC will provide data for a large number of events each day, but will not assess whether any of them are likely to be nuclear explosions. Such assessments will be the task of the States Parties, and it is important to develop the necessary national expertise in the participating countries. An important task for the Norwegian NDC will thus be to make independent assessments of events of particular interest to Norway, and to communicate the results of these analyses to the Norwegian Ministry of Foreign Affairs.

Monitoring the Arctic region

Norway will have monitoring stations of key importance for covering the Arctic, including Novaya Zemlya, and Norwegian experts have a unique competence in assessing events in this region. On several occasions in the past, seismic events near Novaya Zemlya have caused political concern, and NORSAR specialists have contributed to clarifying these issues.

International cooperation

After entry into force of the treaty, a number of countries are expected to establish national expertise to contribute to the treaty verification on a global basis. Norwegian experts have been in contact with experts from several countries with the aim of establishing bilateral or multilateral cooperation in this field. One interesting possibility for the future is to establish NORSAR as a regional center for European cooperation in the CTBT verification activities.

NORSAR event processing

The automatic routine processing of NORSAR events as described in NORSAR Sci. Rep. No. 2-93/94, has been running satisfactorily. The analyst tools for reviewing and updating the solutions have been continually modified to simplify operations and improve results. NORSAR is currently applying teleseismic detection and event processing using the large-aperture NORSAR array as well as regional monitoring using the network of small-aperture arrays in Fennoscandia and adjacent areas.

Communication topology

Norway has implemented an independent subnetwork, which connects the IMS stations AS72, AS73, PS28, and RN49 operated by NORSAR to the GCI at NOR_NDC. A contract has been concluded and VSAT antennas have been installed at each station in the network. Under the same contract, VSAT antennas for 6 of the PS27 subarrays have been installed for intra-array communication. The seventh subarray is connected to the central recording facility via a leased land line. The central recording facility for PS27 is connected directly to the GCI (Basic Topology). All the VSAT communication is functioning satisfactorily.

Jan Fyen

4.2 Status Report: Provision of data from Norwegian seismic IMS stations to the IDC

Introduction

This contribution is a report for the period July - December 2004 on activities associated with provision of data from Norwegian seismic IMS stations to the International Data Centre (IDC) in Vienna. This report represents an update of contributions that can be found in previous editions of NORSAR's Semiannual Technical Summary. It is noted that as of 31 December 2004, two out of the three Norwegian seismic stations providing data to the IDC have been formally certified.

Norwegian IMS stations and communications arrangements

During the reporting interval 1 July - 31 December 2004, Norway has provided data to the IDC from the three seismic stations shown in Fig. 4.2.1. The NORSAR array (PS27, station code NOA) is a 60 km aperture teleseismic array, comprised of 7 subarrays, each containing six vertical short period sensors and a three-component broadband instrument. ARCES is a 25-element regional array with an aperture of 3 km, whereas the Spitsbergen array (station code SPITS) has 9 elements within a 1-km aperture.

The intra-array communication for NOA utilizes a land line for subarray NC6 and VSAT links based on TDMA technology for the other 6 subarrays. The central recording facility for NOA is located at the Norwegian National Data Center (NOR_NDC).

Continuous ARCES data has been transmitted from the ARCES site to NOR_NDC using a 64 kbits/s VSAT satellite link, based on BOD technology.

Continuous SPITS data has been transmitted to NOR_NDC via a VSAT terminal located at Platåberget in Longyearbyen (which is the site of the IMS radionuclide monitoring station RN49 installed during 2001).

Seven-day station buffers have been established at the ARCES and SPITS sites and at all NOA subarray sites, as well as at NOR_NDC for ARCES, SPITS and NOA.

The NOA and ARCES arrays are primary stations in the IMS network, which implies that data from these stations is transmitted continuously to the receiving international data center. Since October 1999, this data has been transmitted (from NOR_NDC) via the Global Communications Infrastructure (GCI) to the IDC in Vienna. The SPITS array is an auxiliary station in the IMS, and the SPITS data have been available to the IDC throughout the reporting period on a request basis via use of the AutoDRM protocol (Kradolfer, 1993; Kradolfer, 1996). In addition, continuous data from all three arrays is transmitted to the US NDC.

Uptimes and data availability

Figs. 4.2.2 and 4.2.3 show the monthly uptimes for the Norwegian IMS primary stations ARCES and NOA, respectively, for the period 1 July - 31 December 2004, given as the hatched (taller) bars in these figures. These barplots reflect the percentage of the waveform data that is available in the NOR_NDC tape archives for these two arrays. The downtimes inferred from these figures thus represent the cumulative effect of field equipment outages, station site to NOR_NDC communication outage, and NOR_NDC data acquisition outages.

Figs. 4.2.2 and 4.2.3 also give the data availability for these two stations as reported by the IDC in the IDC Station Status reports. The main reason for the discrepancies between the NOR_NDC and IDC data availabilities as observed from these figures is the difference in the ways the two data centers report data availability for arrays: Whereas NOR_NDC reports an array station to be up and available if at least one channel produces useful data, the IDC uses weights where the reported availability (capability) is based on the number of actually operating channels.

Use of the AutoDRM protocol

NOR_NDC's AutoDRM has been operational since November 1995 (Mykkeltveit & Baadshaug, 1996). The monthly number of requests by the IDC for SPITS data for the period July - December 2004 is shown in Fig. 4.2.4.

NDC automatic processing and data analysis

These tasks have proceeded in accordance with the descriptions given in Mykkeltveit and Baadshaug (1996). For the period July - December 2004, NOR_NDC derived information on 700 supplementary events in northern Europe and submitted this information to the Finnish NDC as the NOR_NDC contribution to the joint Nordic Supplementary (Gamma) Bulletin, which in turn is forwarded to the IDC. These events are plotted in Fig. 4.2.5.

Data access for the station NIL at Nilore, Pakistan

NOR_NDC continued to provide access to the seismic station NIL at Nilore, Pakistan, through a VSAT satellite link between NOR_NDC and Pakistan's NDC in Nilore.

Current developments and future plans

NOR_NDC is continuing the efforts towards improving and hardening all critical data acquisition and data forwarding hardware and software components, so as to meet the requirements related to operation of IMS stations.

The NOA array was formally certified by the PTS on 28 July 2000, and a contract with the PTS in Vienna currently provides partial funding for operation and maintenance of this station. The ARCES array was formally certified by the PTS on 8 November 2001, and a contract with the PTS is in place which also provides for partial funding of the operation and maintenance of this station. Provided that adequate funding continues to be made available (from the PTS and the Norwegian Ministry of Foreign Affairs), we envisage continuing the provision of data from all Norwegian seismic IMS stations without interruption to the IDC in Vienna.

U. Baadshaug
S. Mykkeltveit
J. Fyen

References

Kradolfer, U. (1993): Automating the exchange of earthquake information. *EOS, Trans., AGU*, 74, 442.

Kradolfer, U. (1996): AutoDRM — The first five years, *Seism. Res. Lett.*, 67, 4, 30-33.

Mykkeltveit, S. & U. Baadshaug (1996): Norway's NDC: Experience from the first eighteen months of the full-scale phase of GSETT-3. *Semiann. Tech. Summ., 1 October 1995 - 31 March 1996*, NORSAR Sci. Rep. No. 2-95/96, Kjeller, Norway.

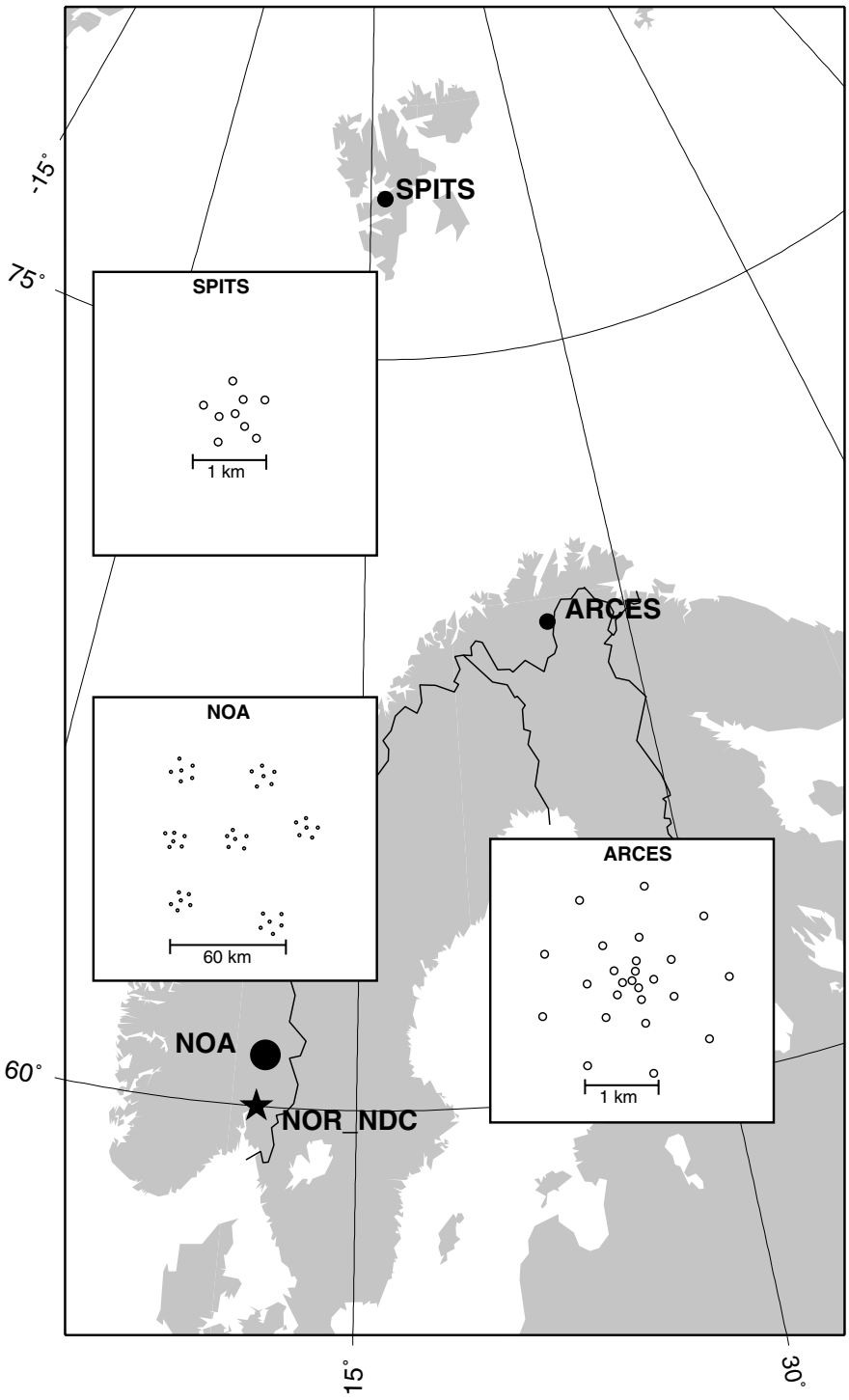

Fig. 4.2.1. The figure shows the locations and configurations of the three Norwegian seismic IMS array stations that provided data to the IDC during the period July - December 2004. The data from these stations are transmitted continuously and in real time to the Norwegian NDC (NOR_NDC). The stations NOA and ARCES are primary IMS stations, whereas SPITS is an auxiliary IMS station.

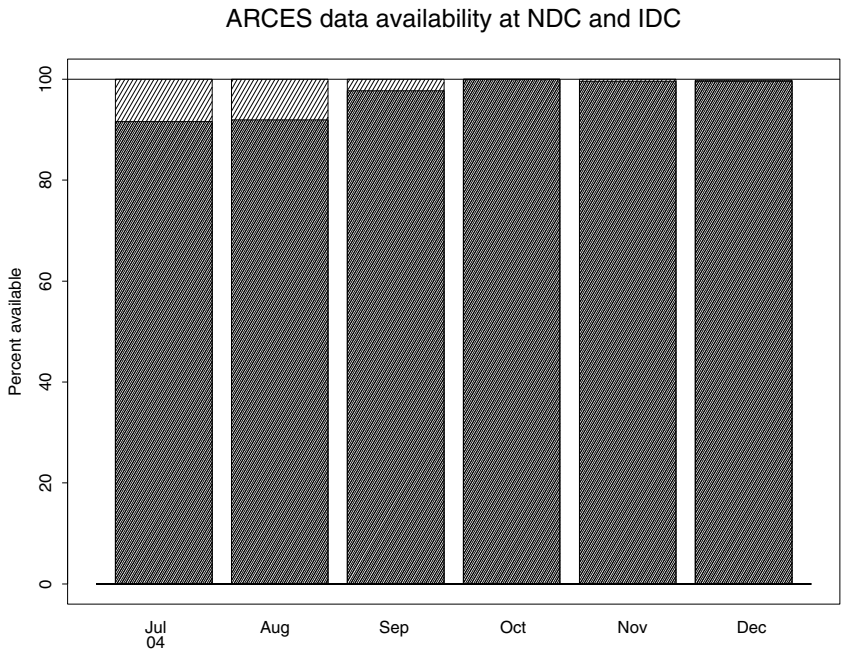

Fig. 4.2.2. The figure shows the monthly availability of ARCES array data for the period July - December 2004 at NOR_NDC and the IDC. See the text for explanation of differences in definition of the term "data availability" between the two centers. The higher values (hatched bars) represent the NOR_NDC data availability.

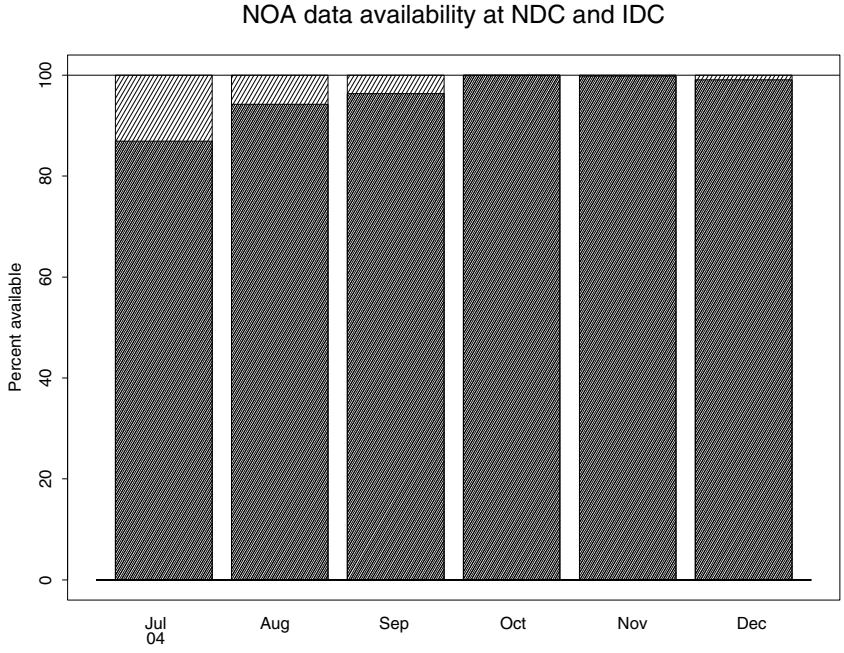

Fig. 4.2.3. The figure shows the monthly availability of NORSAR array data for the period July - December 2004 at NOR_NDC and the IDC. See the text for explanation of differences in definition of the term "data availability" between the two centers. The higher values (hatched bars) represent the NOR_NDC data availability.

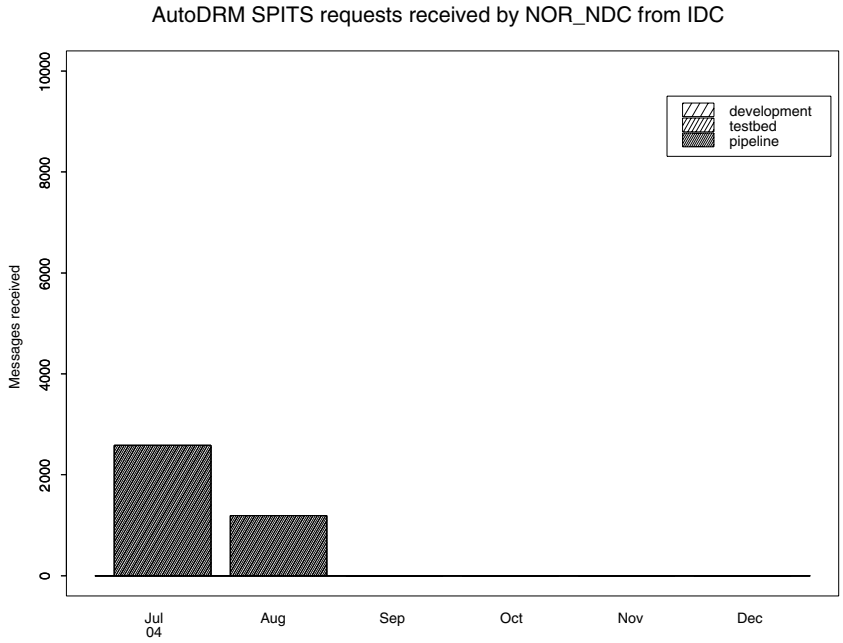

Fig. 4.2.4. The figure shows the monthly number of requests received by NOR_NDC from the IDC for SPITS waveform segments during July - December 2004. SPITS was refurbished in August 2004. No requests for data from the upgraded array have been received from the IDC.

Reviewed Supplementary events

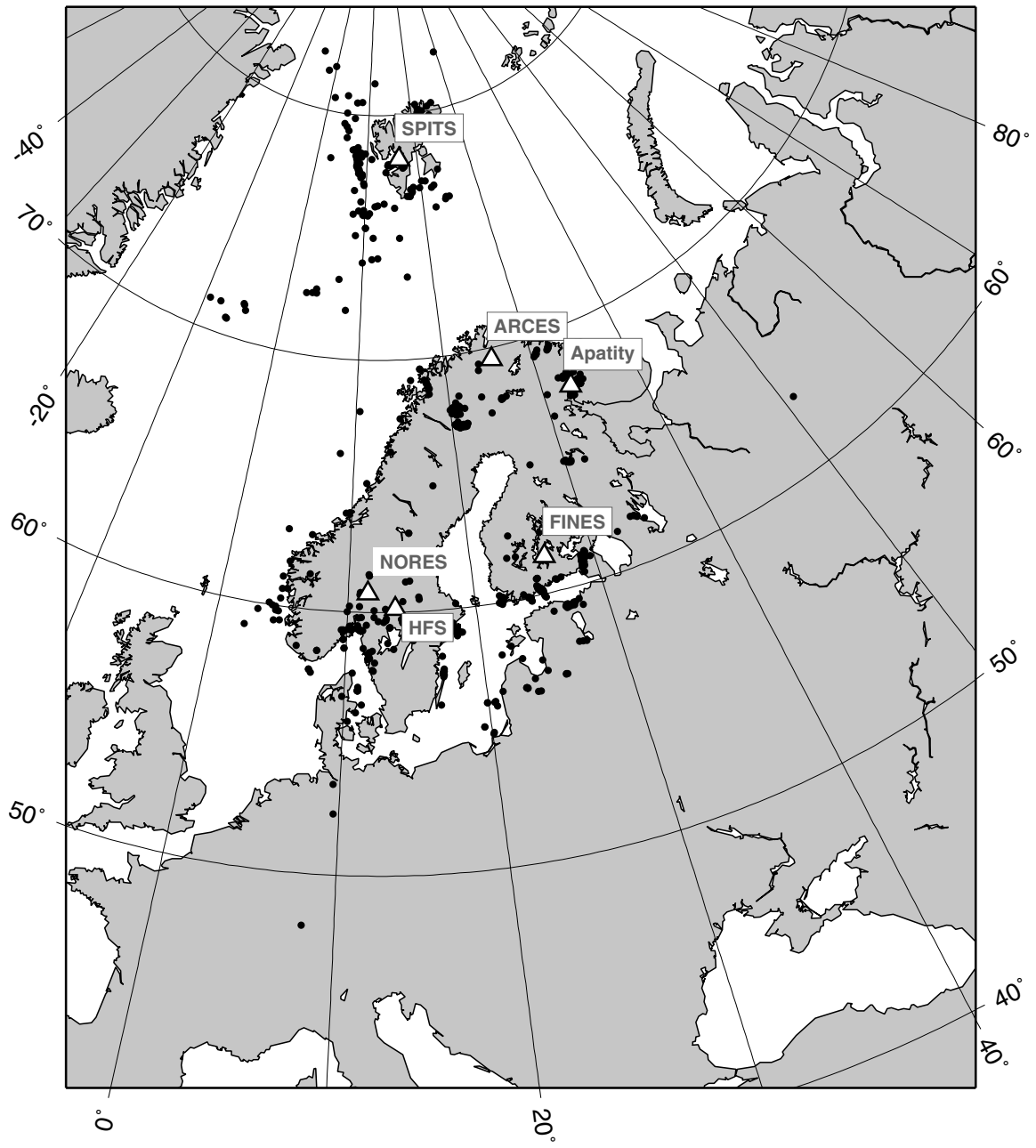

Fig. 4.2.5. The map shows the 700 events in and around Norway contributed by NOR_NDC during July - December 2004 as supplementary (Gamma) events to the IDC, as part of the Nordic supplementary data compiled by the Finnish NDC. The map also shows the seismic stations used in the data analysis to define these events.

4.3 Field Activities

The activities at the NORSAR Maintenance Center (NMC) at Hamar currently include work related to operation and maintenance of the following IMS seismic stations: the NOA teleseismic array (PS27), the ARCES array (PS28) and the Spitsbergen array (AS72). Some work has also been carried out in connection with the seismic station on Jan Mayen (AS73), the infrasound station at Karasjok (IS37) and the radionuclide station at Spitsbergen (RN49). NORSAR also acts as a consultant for the operation and maintenance of the Hagfors array in Sweden (AS101).

NORSAR carries out the field activities relating to IMS stations in a manner generally consistent with the requirements specified in the appropriate IMS Operational Manuals, which are currently being developed by Working Group B of the Preparatory Commission. For seismic stations these specifications are contained in the Operational Manual for Seismological Monitoring and the International Exchange of Seismological Data (CTBT/WGB/TL-11/2), currently available in a draft version.

All regular maintenance on the NORSAR field systems is conducted on a one-shift-per-day, five-day-per-week basis. The maintenance tasks include:

- Operating and maintaining the seismic sensors and the associated digitizers, authentication devices and other electronics components.
- Maintaining the power supply to the field sites as well as backup power supplies.
- Operating and maintaining the VSATs, the data acquisition systems and the intra-array data transmission systems.
- Assisting the NDC in evaluating the data quality and making the necessary changes in gain settings, frequency response and other operating characteristics as required.
- Carrying out preventive, routine and emergency maintenance to ensure that all field systems operate properly.
- Maintaining a computerized record of the utilization, status, and maintenance history of all site equipment.
- Providing appropriate security measures to protect against incidents such as intrusion, theft and vandalism at the field installations.

Details of the daily maintenance activities are kept locally. As part of its contract with CTBTO/PTS NORSAR submits, when applicable, problem reports, outage notification reports and equipment status reports. The contents of these reports and the circumstances under which they will be submitted are specified in the draft Operational Manual.

P.W. Larsen
K.A. Løken

4.4 Spitsbergen array refurbishment

As part of this contract, NORSAR is refurbishing the Spitsbergen array to satisfy the IMS technical specifications. The refurbishment includes upgrading 5 of the array sites to comprise three-component seismometers instead of the original vertical sensors. Both before and after this refurbishment, the Spitsbergen array configuration conforms to the minimum IMS requirement for a new seismic array, having 9 short-period vertical seismometers and one three-component broadband sensor.

As reported in NORSAR Sci. Rep. No. 1 and 2-2004, Guralp Systems was selected as the main vendor for the seismometers, digitizers and data acquisition system.

All equipment was tested at the factory before shipment to the NORSAR Maintenance Center in July 2004, where part of the data acqusition system was tested, in order to prepare for the operation of the software and to be ready for data forwarding after installation on Spitsbergen. Subsequently, the equipment was shipped to the array site on Spitsbergen on August 4, 2004.

NORSAR field personnel arrived at the array site on Spitsbergen in the afternoon, Monday August 9 to complete the installation.

Before this expedition, the power system including batteries and Sterling generators had been installed. Cables from the 9 array sites had been transferred to the new central hut (see Figure 4.4.1), and terminated in a junction box where the old digitizers were reconnected. A new Wilan 2.4 Ghz radio system was also installed with communication to the Longyearbyen settlement, 20 km away. This radio system, together with a 64 Kbps satellite link, provides a full TCP/IP connection between the NDC at Kjeller and the central hut. Figure 4.4.2 shows a schematic view of the components installed.

During August 9, the new array concentrator rack was installed and connected to the new power system, (see Figure 4.4.5). On August 10, at 1400 GMT, the old system was disconnected. During the next two days, at each of the 9 sites, the old CMG-ESP sensor was removed from the borehole, a new CMG-3TB sensor and a new CMG-AM digitizer package were installed in the borehole, a new GPS antenna was installed, a new pitbox including tamper switch was installed and cables were connected.

On August 13, at 0000 GMT, we started to record data from all the 9 newly installed sites.

After the installation, it was found that the borehole became too tightly packed with load bearing cable, cable management unit, strain relief mechanism, sensor and CMG-AM modules (see Figure 4.4.3). A tool that was designed to physically orient the sensors towards north became too big to attach to the sensor and to safely disconnect from the sensor without moving the sensor. Orientation towards north therefore failed.

For several days after installing the broadband seismometers together with all the cabling in an environment of minus 6 degrees Celsius, we experienced mysterious signals, i.e. small ‘events’, oberved at individual sites. Such events are interpreted as instruments ‘pings’, i.e. sudden release of strain in the materials.

We also experienced that some instruments generated a ‘ringing’ for certain local and regional signals.

A new tool was constructed, and during another expedition in September 2004, the instruments were again removed and re-installed for proper orientation.

As of September 8, 2004, all the horizontal components of the 6 three-component sensors were correctly oriented towards north and towards east. See Figure 4.4.4 for a description of the installation process.

Three of the seismometers (SPB3, SPB4 and SPB5) are installed in boreholes backfilled with sand. Initial studies do not give a clear indication that this has been advantageous for lowering the overall noise level. The effect of this will be evaluated further, and if the outcome is positive, we plan to backfill sand in the remaining boreholes this summer/autumn.

SPB4 is very close to the windmill, and due to high sensitivity, flat acceleration response and high sample rate, this site looks very noisy.

The 'pings' have almost completly disappeared after the second installation. For the second installation, the cable support was re-arranged, so as to avoid as much as possible noise between the cables and the sensor.

Another problem discovered after the second installation was that all north-south components had wrong polarity. This turned out to be a production error where two wires were crossed. This was fixed by commanding the digitizer firmware to change polarity of this component. This was done using remote login to the CMG-AM. As of 29 November 2004, all components were correctly oriented both physically and with respect to polarity.

The old installation on Spitsbergen had 9 "short" period sensors (CMG-ESP, flat velocity response in the band 10 seconds to 50Hz) and one broadband sensor (CMG-3T, flat velocity 100 seconds to 50 Hz). The broadband sensor was installed in the same borehole as one of the short period sensors. The installation of two sensors in one borehole was problematic, and we never obtained good broadband recordings. With sensitvity 2*5000 V/m/s for ESP and 0.6 microvolt per count for the digitizer we obtained poor resolution for local high frequency events. Dr. Cansun Guralp suggested that the use of a broadband sensor in all of the boreholes would imply a much simpler and safe installation, and as reported in NORSAR Sci. Rep. No. 1 2004, we tested whether the CMG-3T broadband sensor would be equally good for high frequencies as the CMG-ESP. The conclusion was clearly that the broadband sensor performed as well as the CMG-ESP for high frequencies. We also determined that using a sensor with flat acceleration response would serve our purpose best, as this would enhance the higher frequencies by a factor $2\pi f$ compared to velocity response. In conclusion we chose a response which is flat to aceeleration in the band 100 seconds to 50 Hz for the new broadband sensors (Figure 4.4.6).

On 26 December 2004, we recorded the largest earthquake ever during the 35 years of NORSAR operation. This catastrophic earthquake (near the island of Sumatra) was measured on seismometer SPA0\BHZ to have an M_S magnitude of 9.0. The P signal is long lasting and emergent. If m_b is measured within 5 seconds after the P onset, then m_b is 6.5. However, if the measurement window is expanded to 2 minutes, we obtain m_b=7.8. Figure 4.4.7 shows selected broadband recordings from stations operated by NORSAR. On this figure, we see from top to bottom recordings from:

PS28 - ARCES- ARA0\sz with sensor GS-13, flat velocity 2000 V/m/s, Nanometrics HRD24 digitizer, 0.158 microvolt/count. Largest amplitude 177,634 counts.

PS28 - ARCES- ARE0\bz with sensor CMG-3TB, flat velocity 2*2500 V/m/s, Nanometrics HRD24 digitizer, 0.158 microvolt/count. Largest amplitude 8,387,948 counts, clipped and distorted.

PS27 - NOA - NC405\bz with sensor KS54000, flat acceleration 5000 V/m/s/s, Science Horizons AIM24BB digitizer, 3.8 microvolt/count. Largest amplitude 601,991 counts.

PS27 - NOA - NC602\sz with sensor Teledyne 20171, flat velocity 650 V/m/s plus Brick amplifier 39.8, Science Horizons AIM24-1 digitizer, 0.209 microvolt/count. Largest amplitude 830,907 counts.

PS27 - NOA - NC602\bz with sensor CMG-3TB, flat velocity 2*2500V/m/s , Science Horizons AIM24BB digitizer, 3.8 microvolt/count. Largest amplitude 2,828,908 counts.

AS72 - SPITS - SPA0\BHZ with sensor CMG-3TB, flat acceleration 2*938 V/m/s /s, Guralp DM24 (CMG-AM) digitizer, 1.7 microvolt/count. Largest amplitude 910,299 counts.

AS73 - JMIC - JMIC\BHZ with sensor STS-2, flat velocity 20000 V/m/s /s, Nanometrics Europadigitizer, 2.5 microvolt/count. Largest amplitude 10,804,307, clipped and distorted.

The system response for the new SPITS has not shown any amplitude above 910,000 counts since the installation. We have verified that we can record magnitude 9.0 earthquake without clipping. We have so far not recorded any local or regional signal that come close to the clipping level of the instrumentation. For normal noise conditions, we have seen that we reach system noise for periods longer than 20 seconds. This indicates that the transfer function of the sensor is not optimum for the local noise conditions. It is possible to combine the benefits of velocity sensors for surface waves with acceleration sensors for regional events into one instrument with a “hybrid” response. Such a response could, e.g., be flat to velocity from 1 to 100 seconds and flat to acceleration from 1 Hz to 100 Hz. The manufacturer, Guralp Systems, has indicated that they can change the sensor to a hybrid response in the field.

A hybrid response would seem to be a better choice than the current response. However, we have so far not seen any clipped signals for local or regional events, so a higher sensitivity (e.g by a factor of 5) flat to acceleration over the entire band would also give an improvement for the long period signals. This would be a much simpler alternative to implement. Before making a decision, we need to consider the costs associated with the change, the work effort involved in changing the response in the field (the weather conditions are important in this respect), and we also need to consider carefully the technical risk factors. The system sensitivity will be studied further to gain more experience before any change of response will be decided.

J. Fyen

Fig. 4.4.1. The picture shows the new Spitsbergen array central hut located close to site SPB4, and was taken during installation of a new power support system in April 2004. The annex contains one tank holding 1000 liters of kerosene and one tank holding 1000 liters of water (with anti-freeze solution). The kerosene is used in the Sterling engines to heat the nitrogen gas, and the water is used to cool the gas. The heat transferred to the coolant is used for heating the hut.

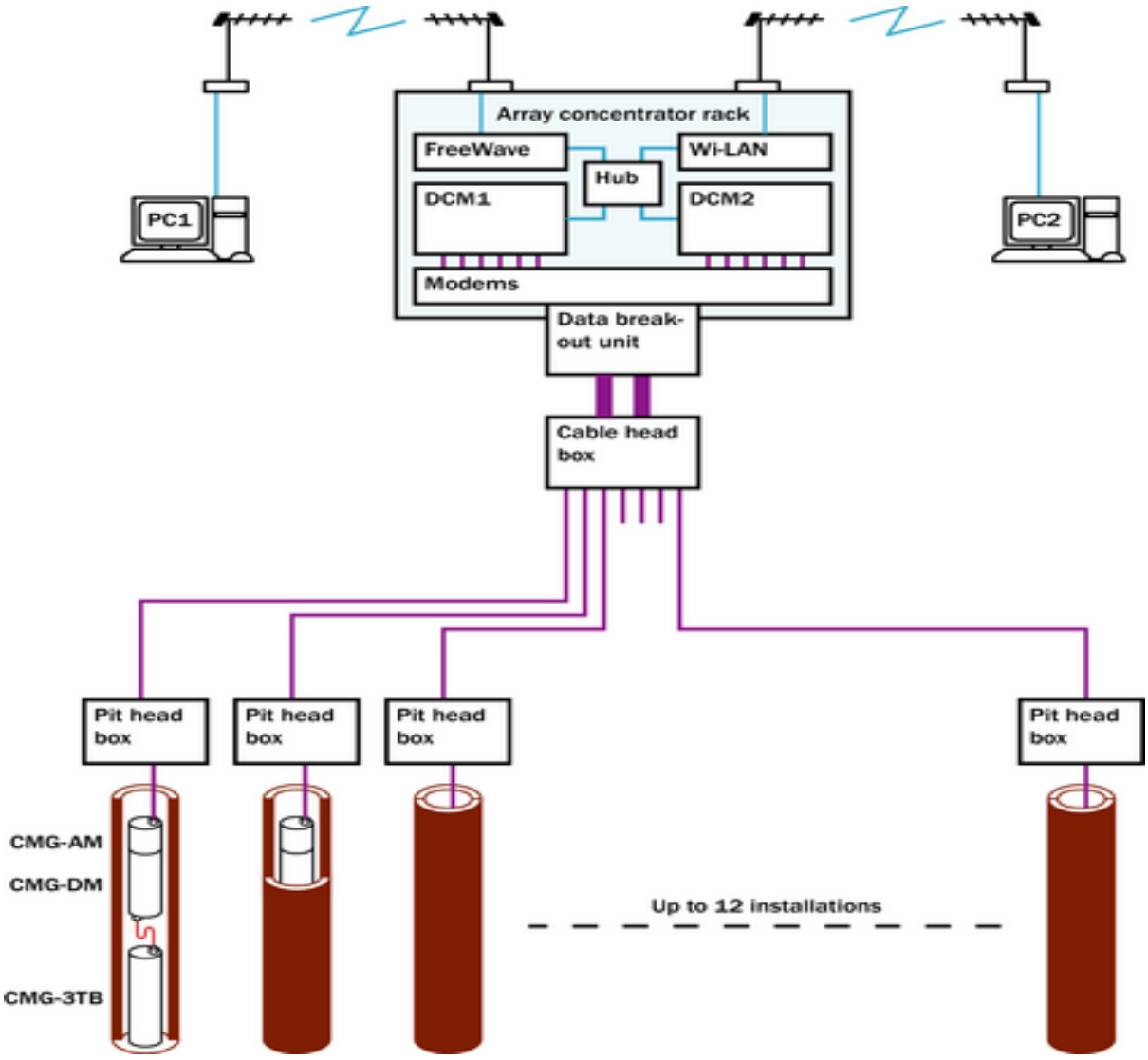

Fig. 4.4.2. Schematic view of the new Spitsbergen installation. All borehole sensors were removed, and new CMG-3TB three-component sensors were installed in the 6 sites A0, B1-B5. New, equivalent, vertical only sensors, CMG-3TV, were installed in the 3 sites A1-A3. In all of the 9 boreholes, new digitizer and authenticator devices were installed. The digitizer, CMG-DM24, and the authenticator, CMG-AM (an ARM processor with Linux and Spyrus PCMCIA digital signature card), and modem, are packaged into one device named CMG-AM. Power and communication to each pit are through the old buried cables. In the central hut, the array concentrator rack distributes power to all the 9 pits, houses the modems for 57600 bps ppp communication with the CMG-AM, and houses 4 CMG-DCM (also Linux ARM processors) that function as routers for the data streams between the boreholes and the central data acquisition system. Two of the CMG-DCM are spare. The CMG-DCM communicates with the central data acquisition system (in Longyearbyen, 20 km away) over a Wi-Lan 2.4 Ghz radio link using TCP/IP. The central hut has a local Ethernet network for the CMG-DCMs, the radio(s) and other devices (e.g. to connect to field engineer laptop). The freewave backup radio is not installed due to regulations in the 900 Mhz band. In Longyearbyen, at the facilities used for station RN49, we have 2 PCs with Linux operating systems that are used as central data acquisition systems.

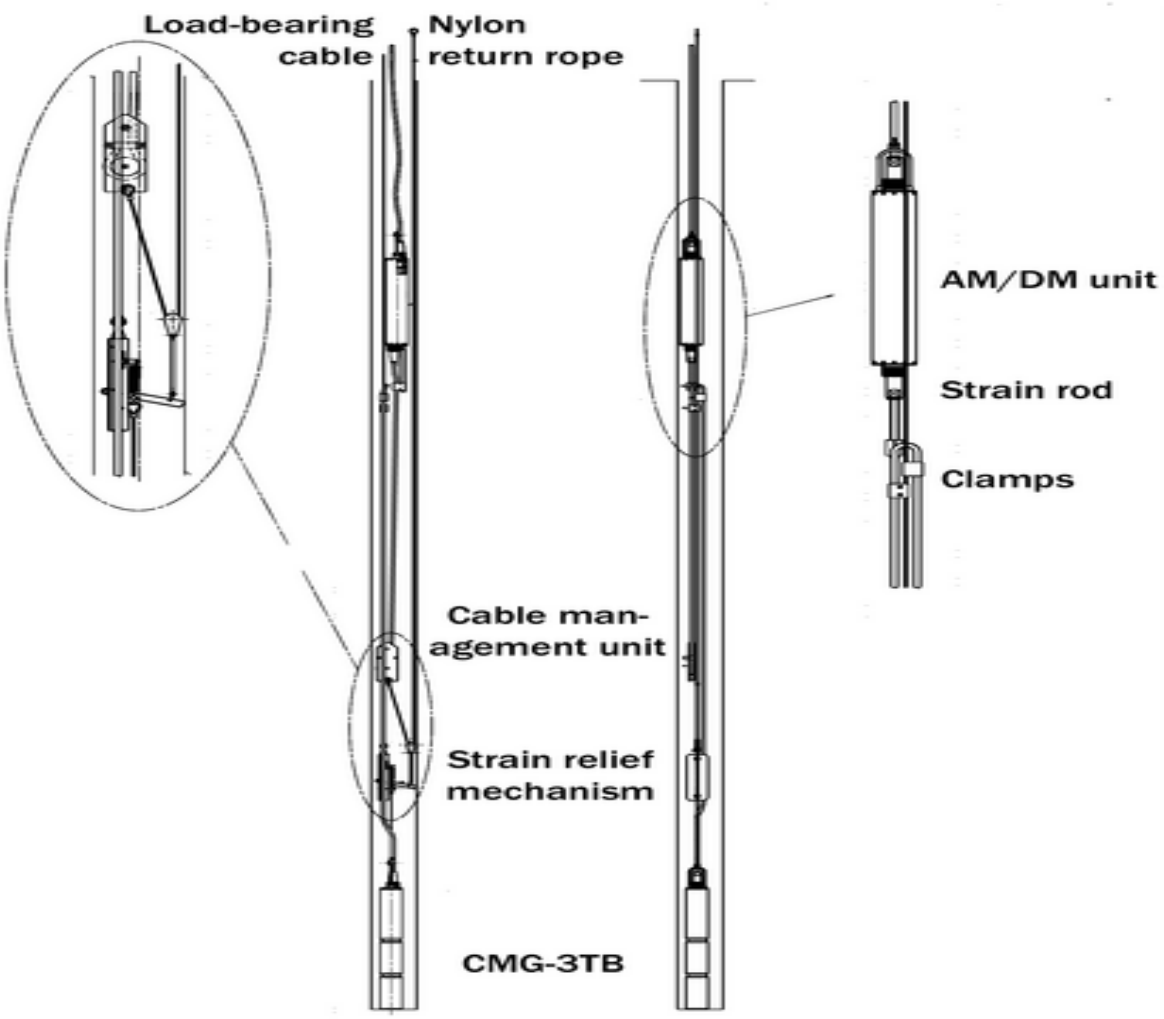

Fig. 4.4.3. Schematic view of borehole components.

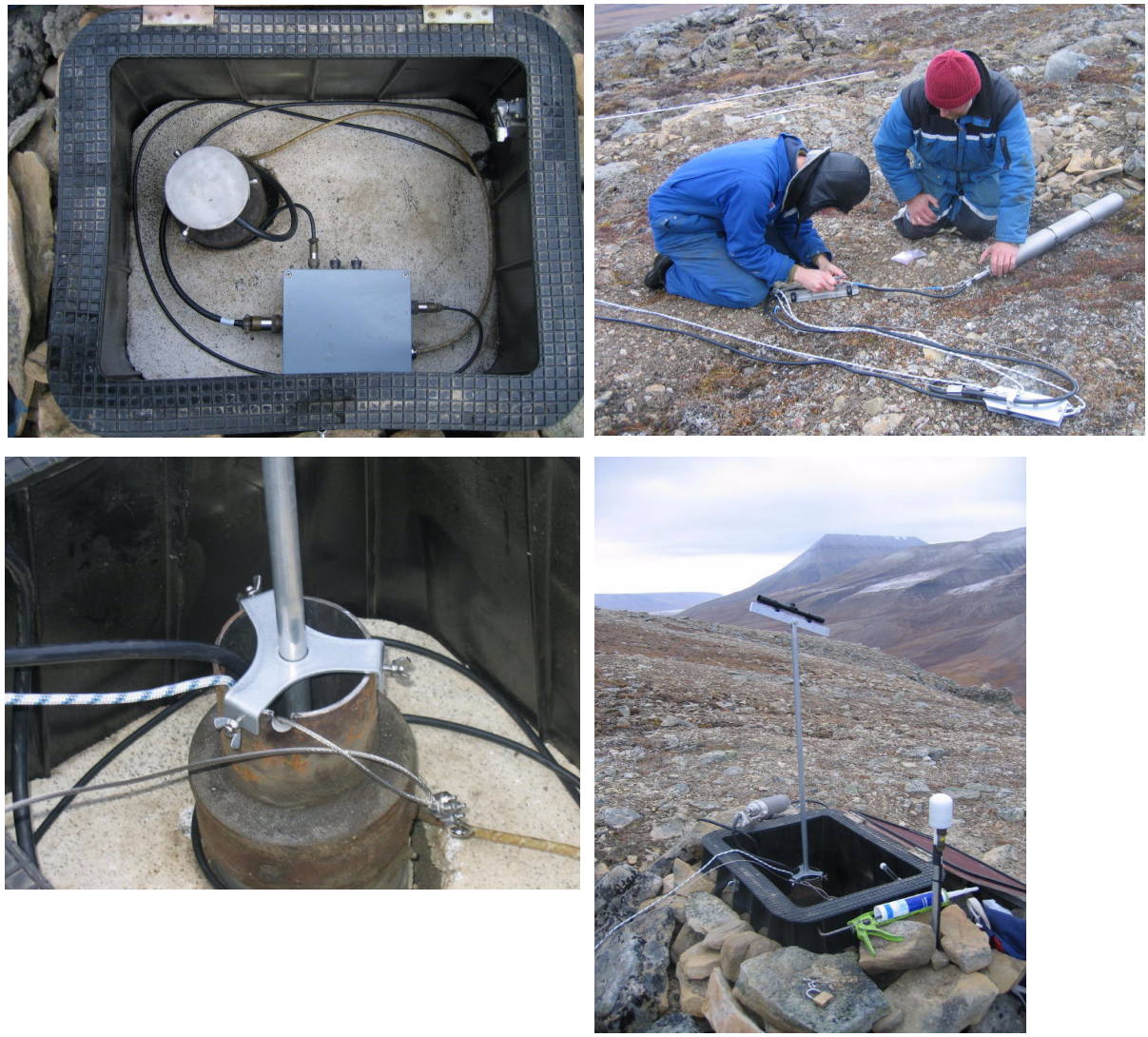

Fig. 4.4.4. The figure illustrates the re-installation of the CMG-3T sensor and CMG-AM in the borehole in order to physically rotate horizontal component NS towards North. The upper left part shows the vault head casing with pitbox and borehole lid. The upper right part shows adjustment of the cable management unit. The lower left and lower right figures show top part of a steel rod that connects into a hollow trapes on the top of the sensor. The trapes ensures that the steel rod can only connect to the sensor in one orientation. Testing at Hamar showed that the steel bar key could be removed without altering the sensor position. The sensor is about 5 meters down. A precise GPS measurement was made to find a point about 20 meters from the borehole and exactly in direction to the North. By aiming with a binocular and twisting the sensor with a steel bar we then oriented the sensor towards North with a precision of better than 2 degrees. This procedure had been tested several times at Hamar with a setup where the sensor was installed in a 6 meter borehole casing above ground, and with an inspection hole to confirm direction.

Fig. 4.4.5. The figure shows, in the upper left part, the battery bank and the unit for controlling battery charging and control of the Stirling generators. In the lower left part, the array concentrator rack is displayed. The upper and lower right hand parts show the two Stirling generators. The windmill is the primary source for charging the batteries. The control unit measures battery charge, room temperature and the temperature of the 1000 liters water tank. A programmable algorithm in the control unit will start and stop the generators as needed. The generators can also be controlled by the use of a GSM phone. Remote access through the network to the control unit will be installed later.

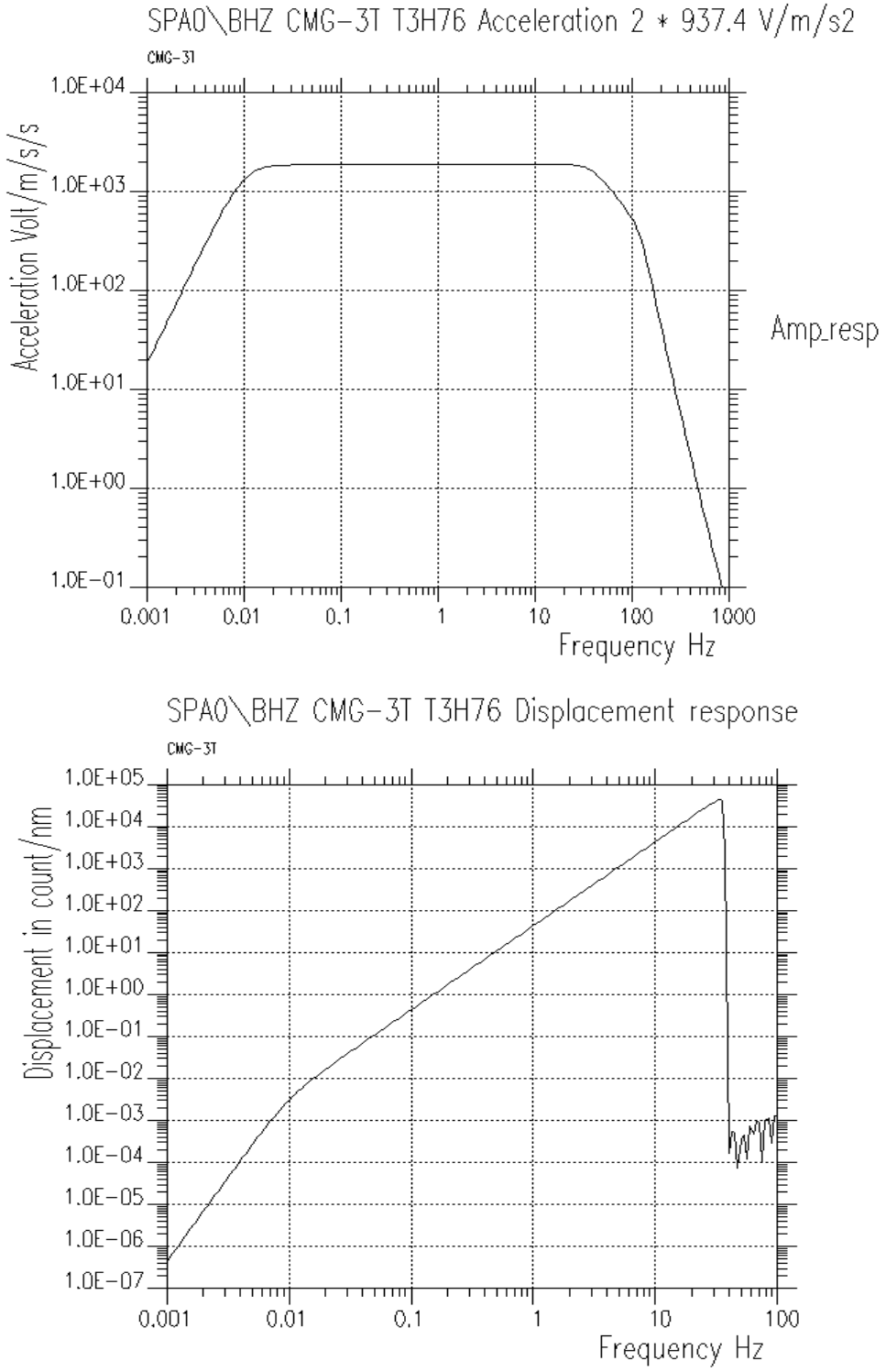

*Fig. 4.4.6. System response of SPA0\BHZ. Upper figure shows the response of sensor only. The sensor is flat to acceleration with 2*937.4 V/m/s/s from 100 seconds to 50 Hz. The lower figure shows the complete system response for SPA0\BHZ with counts/nanometer. All sensor components have the same nominal system response. Displacement response at 1 Hz is 0.023 nm/count.*

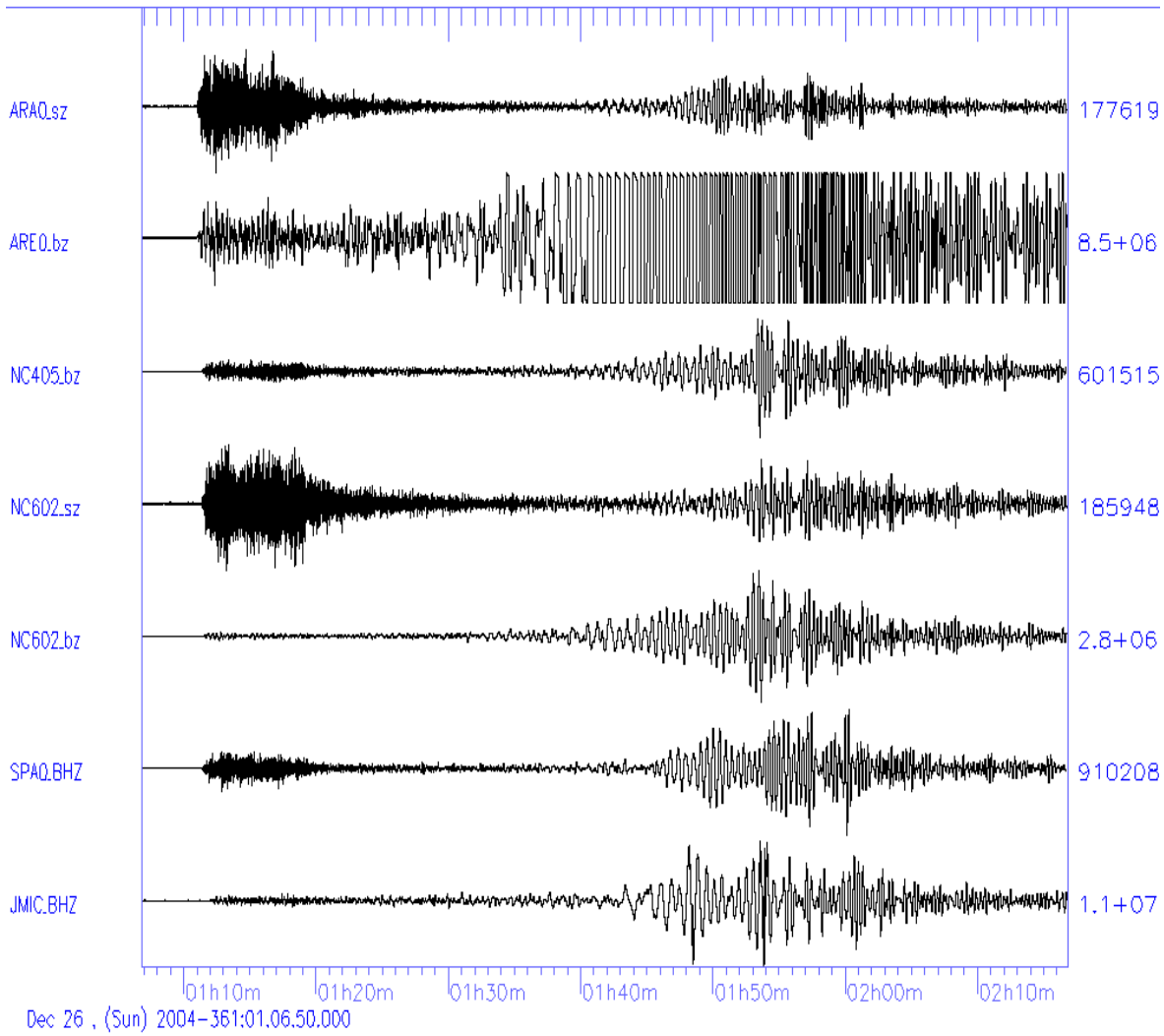

Fig. 4.4.7. Recording of the Sumatra earthquake on 26 December 2004. From top to bottom, we see recording from ARA0\sz, ARE0\bz, NC405\bz, NC602\sz, NC602\bz, SPA0\BHZ and JMIC\BHZ. See the text for a description of the different systems.

5 Documentation Developed

Bungum, H., O. Ritzmann, J.I. Faleide, N. Maercklin, J. Schweitzer, W.D. Mooney, S.T. Detweiler and W. S. Leith (2004): Development of a three-dimensional velocity model for crust and upper mantle of the Barents Sea, Novaya Zemlya, Kara Sea and Kola-Karelia Regions. Proceedings, 26th Seismic Research Review, Orlando, Florida, Sept. 21-23, 2004.

Bungum, H., T. Kvaerna,S. Mykkeltveit, M. Roth, V. Oye, K. Astebol, D.B. Harris and S. Larsen (2004): Energy partitioning for seismic events in Fenniscandia and NW Russia. Proceedings, 26th Seismic Research Review, Orlando, Florida, Sept. 21-23, 2004.

Engdahl, E.R., & J. Schweitzer (2004): Observed and predicted travel times of Pn and P phases recorded at NORSAR from regional events. Eos Trans. AGU, **85 (47)**, Fall Meeting Supplement, Abstract S13B-1050

Gibbons, S. J. & F. Ringdal (2005): . The detection of rockbursts at the Barentsburg coal mine, Spitsbergen, using waveform correlation on SPITS array data. **In**: NORSAR Sci. Rep. 1-2005, 1 July - 31 December 2004, Kjeller, Norway.

Harris, D.B., F. Ringdal, E. Kremenetskaya, S. Mykkeltveit, D. Rock, J. Schweitzer, T. Hauk & J. Lewis (2004): Ground-truth collection for mining explosions in Northern Fennoscandia and Russia. 26th Seismic Research Review – Trends in Nuclear Explosion Monitoring. Orlando, Florida, September 21 – 23, 2004, LA-UR-04-5801, Proceedings, CD Version file 02 – 06; Volume 1, 73–82.

Hicks, E.C, T. Kværna, S. Mykkeltveit, J. Schweitzer and F. Ringdal (2004): Travel-times and attenuation relations for regional phases in the Barents Sea regio*n. Pure appl. geophys.* 161, 1-19, 2004

Kværna, T. & U. Baadshaug (2005): Spectral characteristics of signals and noise at selected IMS stations. **In**: NORSAR Sci. Rep. 1-2005, 1 July - 31 December 2004, Kjeller, Norway.

Kvaerna, T., S. Gibbons, F. Ringdal and D. Harris (2004): Integrated Seismic Event Detection and Location by Advanced Array Processing. 26th Seismic Research Review – Trends in Nuclear Explosion Monitoring. Orlando, Florida, September 21 – 23, 2004, LA-UR-04-5801, Proceedings, CD Version file 8-07; Volume II, 297–306, 2004

Lindholm, C., F. Ringdal & J. Fyen (2005): The Sumatra M=9.0 earthquake as a high-end test of NORSAR's processing capability. **In**: NORSAR Sci. Rep. 1-2005, 1 July - 31 December 2004, Kjeller, Norway.

Maercklin, N., S. Mykkeltveit, J. Schweitzer, D. Rock & D.B. Harris (2005): Data from deployment of temporary seismic stations in northern Norway and Finland. **In**: NORSAR Sci. Rep. 1-2005, 1 July - 31 December 2004, Kjeller, Norway.

Ringdal, F. , T. Kværna, E. Kremenetskaya, V. Asming, S. Kozyrev, S. Mykkeltveit, S. Gibbons and J. Schweitzer (2004): Research in Regional Seismic Monitoring. 26th Seismic Research Review – Trends in Nuclear Explosion Monitoring. Orlando, Florida, September 21 – 23, 2004, LA-UR-04-5801, Proceedings, CD Version file 3–10; Volume I, 297–306, 2004

Ritzmann, O., J.I. Faleide, H. Bungum, N. Maercklin, J. Schweitzer, W. D. Monney, S. T. Detweiler & W. S. Leith (2004): Construction of a 3D seismic velocity model fort he Barents Sea region using sedimnet vs. crystalline crust thickness relationships. Eos Trans. AGU, 85 (47), Fall Meeting Supplement, Abstract S23B-0315.

Schweitzer, J. (2005): The 7 April 2004 Flisa, Southern Norway earthquake sequence — eight hypocenter determinations and one focal mechanism. **In**: NORSAR Sci. Rep. 1-2005, 1 July - 31 December 2004, Kjeller, Norway.

Stevens, J, N. Rimer, H. Xu, J. Murphy, B. Barker, S. Gibbons, C. Lindholm, F. Ringdal, T. Kvaerna and I Kitov (2004):Analysis and Simulation og Cavity-Decupled Chemical Explosions. 26th Seismic Research Review – Trends in Nuclear Explosion Monitoring. Orlando, Florida, September 21 – 23, 2004, LA-UR-04-5801, Proceedings, CD Version file 4-13 ; Volume I, 495-502, 2004

6 Summary of Technical Reports / Papers Published

6.1 The detection of rockbursts at the Barentsburg coal mine, Spitsbergen, using waveform correlation on SPITS array data

6.1.1 Introduction

In several previous Semiannual Technical Summaries, we have studied the detection and location of rockbursts at the Barentsburg coal mine on Spitsbergen. This work has been done in cooperation with the Kola Regional Seismological Centre (KRSC), which operates two seismic stations in the immediate neighborhood of the mine.

In this paper, we apply a waveform correlation procedure to Spitsbergen array data in order to obtain improved detection of such rockbursts. We use available data from the near-mine stations to verify the results, and we compare the results obtained by correlation processing to those obtained through conventional array processing methods.

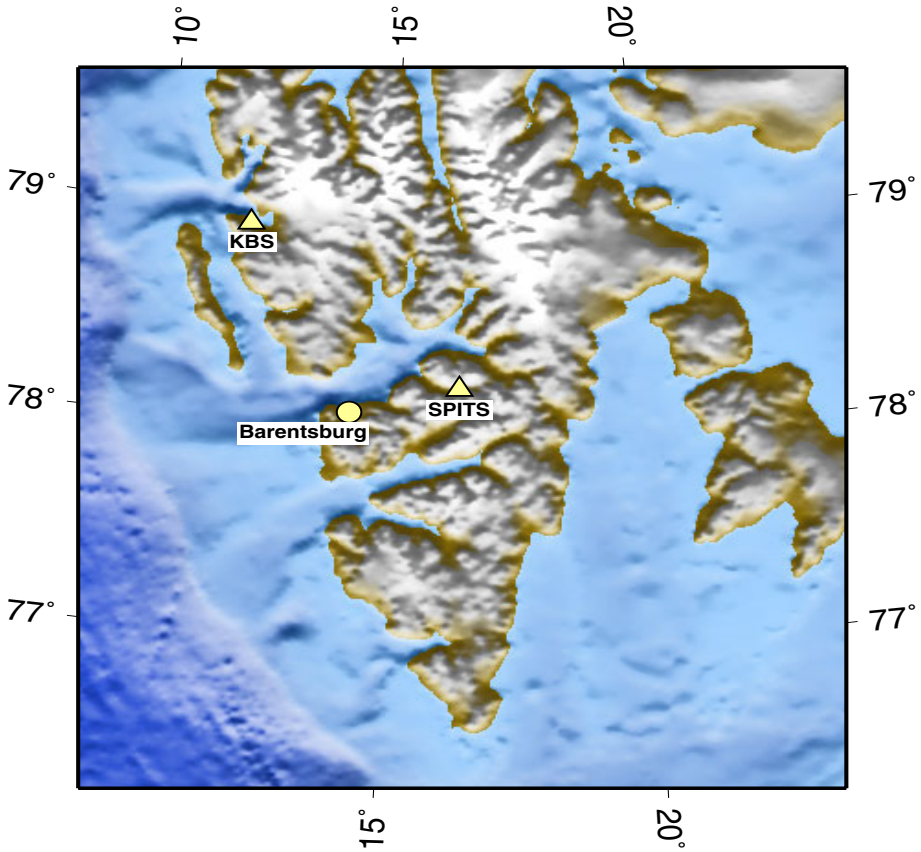

Fig. 6.1.1. Locations of the Barentsburg coal mine, the SPITS seismic array, and the KBS (Kings Bay, Ny Ålesund) 3-component seismic station on the Island of Spitsbergen.

On July 26, 2004, a rockburst at the Barentsburg mine led to the death of a mine worker; this was the third fatal mining accident at this site within four years. The mine is situated approximately 51 km to the west of the Spitsbergen array (see Figure 6.1.1) which recorded the seis-

mic signals from both this event and several previous rockbursts at the mine (see Kværna et al., 2003, Kremenetskaya et al., 2001).

Using data from both SPITS and the KBS 3-component station (at a distance of approximately 120 km), a magnitude estimate of 1.76 was obtained for the event together with origin time 2004-208:06.42.19.44 and coordinates 77.9375°N, 14.0703°E. The SPITS data from this event is displayed in Figure 6.1.2. In Figure 6.1.3, the waveforms from the July 26, 2004, are compared with those from three previous events within the coal mine. The waveforms from the different events display a high degree of semblance in the 1.2 - 2.5 Hz frequency band and far less similarity in the 2.0 - 4.0 Hz band.

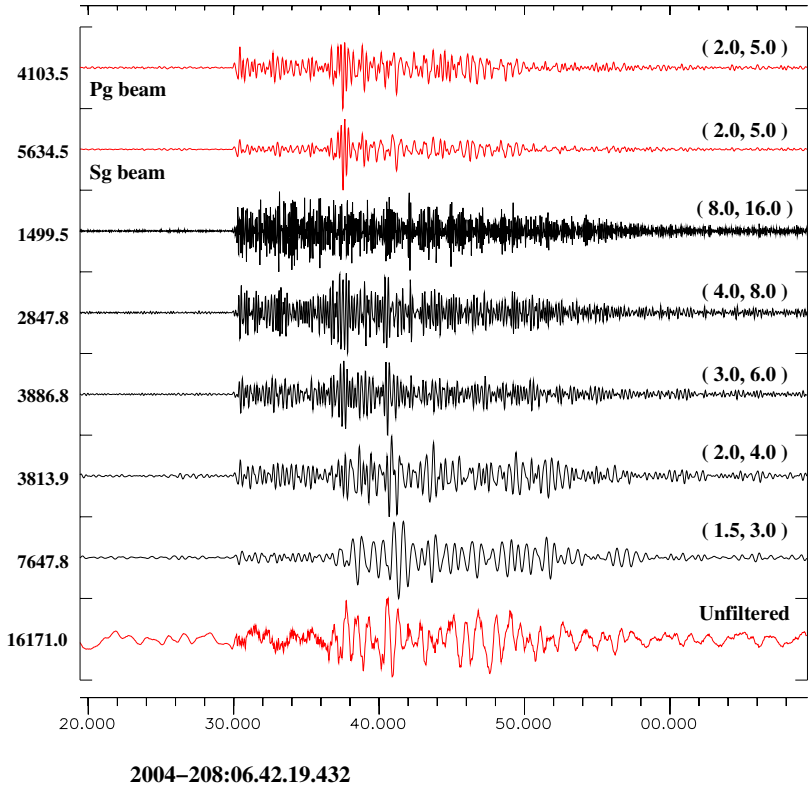

Fig. 6.1.2. Waveforms recorded at the Spitsbergen array resulting from the 26 July 2004 accident at the Barentsburg mine. All traces displayed are the SPA0_sz channel except for the top two traces which are the beams from all sz channels with (vel., azi.) = (5.8, 244) for Pg and (vel., azi.) = (3.4, 244) for Sg. The numbers to the left indicate the maximum amplitude and the frequency band is indicated to the right.

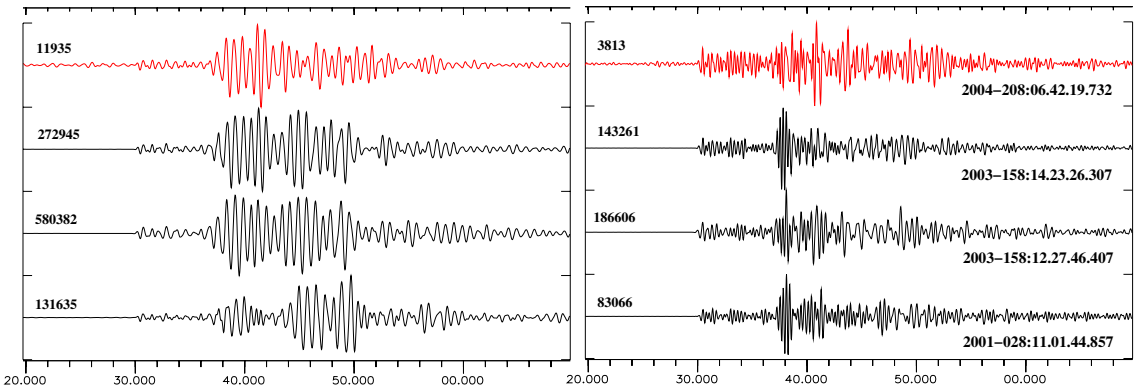

Fig. 6.1.3. SPA0_sz recordings of the July 26, 2004, event (red traces) together with recordings of three previous events in the Barentsburg mine. All traces are aligned according to the best correlation with a 5.0 second long window beginning at a time 2004-208:06.42.30; traces to the left are filtered between 1.2 and 2.5 Hz and traces to the right are filtered between 2.0 and 4.0 Hz.

The goal of the current work is to identify other events which may have occurred within close proximity of the site of the July 26 2004 rockburst and, subsequently, to evaluate the level of seismicity in the region prior to this collapse and examine how this seismicity varied with time. We wish to limit the set of events found to a very small geographical footprint and therefore use an array-based waveform correlation method similar to that described by Gibbons and Ringdal (2004). Whereas location estimates using traditional regional array techniques (see, for example, Ringdal et al. 2003) are likely to be associated with error ellipses of the order of several kilometers (even given the short distance of only 51 km between source and receiver), two events whose waveforms display a sufficiently high correlation are necessarily constrained to have taken place with a region limited by a small multiple of the wavelength at a dominant frequency (Geller and Mueller, 1980). It is also well known that many events too weak to be located adequately by traditional methods can be detected using a matched signal detector.

6.1.2 Event Detection Using Multi-Channel Waveform Cross-Correlation

For the preliminary investigation, a master waveform (a template), filtered between 3.0 and 6.0 Hz, was extracted with a starting time 2004-208:06.42.29.695 and length 20.0 seconds for each channel in the Spitsbergen array. The same time interval was chosen for all of the channels in the array for the sake of simplicity; the aperture of the array is sufficiently small that energy corresponding to a given phase arrives at all sites within less than a second. The fact that a phase arrives later at some stations than others is not an issue; a second event taking place at the same site will result in identically delayed arrivals. It is clear from Figures 6.1.2 and 6.1.3 that a 20.0 second long window includes most of the wavetrain including approximately 14 seconds following the Sg secondary phase arrival. The waveforms were resampled to 40 Hz in order to perform the cross-correlation. The choice of the 3.0 - 6.0 Hz frequency band, under the quarter-wavelength argumentation of Geller and Mueller (1980), constrains the locations of two well-correlated events to be within approximately 150m of each other (based upon a velocity of 3.5 kms^{-1} at a frequency of 6 Hz). However, the “correlation distance” of two different events is likely to vary greatly with local structure and heterogeneity (see, for example, Nakahara 2004); measurements at local distances would be required to verify precise location estimates.

The detection procedure, described by Gibbons and Ringdal (2004), is illustrated in Figure 6.1.4. A continuous, fully-normalised, correlation coefficient is calculated between the data following a given time point and the extracted template waveform for each channel in the array. A zero time-delay beam is then formed from all the correlation traces. A detection is made when the scaled correlation trace (the top channel in Figure 6.1.4) exceeds a preset value, analogous to an SNR threshold in a conventional STA/LTA detection. Specifying a threshold on the scaled trace was found by experience to be considerably easier than specifying an absolute value of the correlation coefficient as a threshold. Correlation coefficients vary greatly depending upon the nature of the signal, in particular the time-bandwidth product of the template waveform, and also on the number of channels used in the array or network. To be able to specify a detection threshold for such a trace requires considerable calibration for each calculation attempted. The scaled correlation beams were examined for a wide range of scenarios and were found to vary typically between -3.5 and +3.5 in the absence of any obvious detections and to very rarely exceed 4.5 unless accompanied by an abnormally high correlation coefficient. A value of 6.0 was found to be quite a robust detection threshold for the majority of scenarios without systematic calibration.

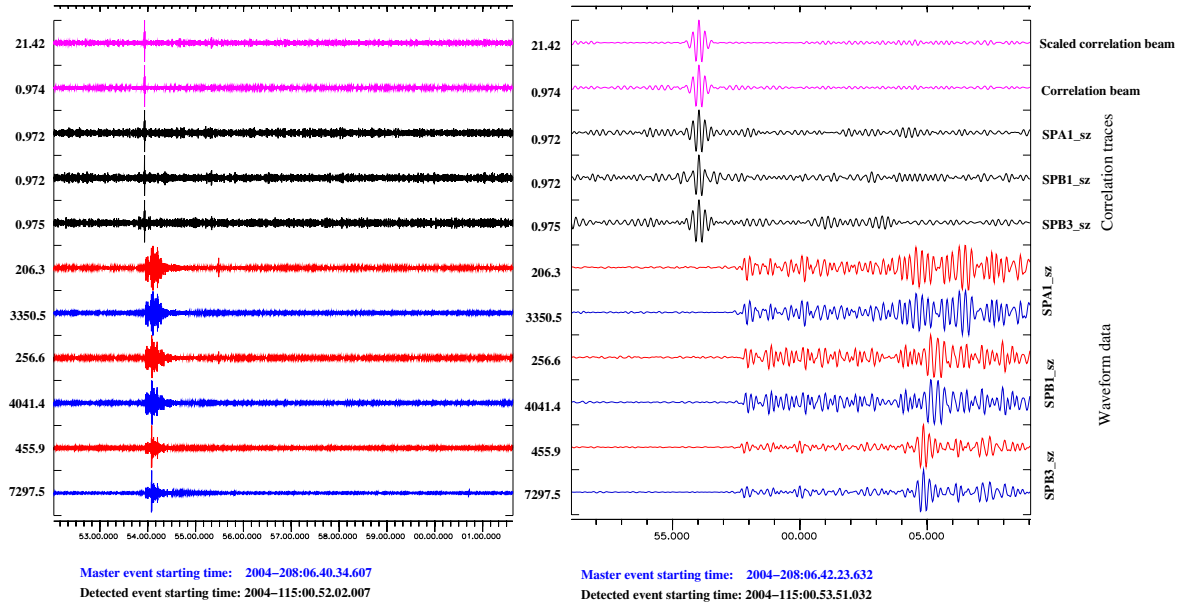

Fig. 6.1.4. The detection by waveform correlation over the Spitsbergen array of an event assumed to originate from the Barentsburg mine. Each of the red traces shows incoming waveform data in a window surrounding the cross-correlation peak and the blue traces indicate data from the master event, aligned according to the maximum correlation coefficient. The black traces indicate the correlation coefficient channels for the indicated traces between the subsequent 20 seconds of the incoming data and the extracted segment from the master event. The lowermost magenta trace, the correlation beam, C(t), is the average of all 9 single channel correlation traces over the SPITS array. For each time-point, t, we define a region of time, I_t, which is the union of two time windows: one prior to and one following t. This typically covers a few seconds of data but avoiding the immediate vicinity of time t. We calculate a scaling factor, R(t), which is the RMS value of C(t') for all t' in I_t. The scaled correlation beam, C'(t), is given by C'(t) = C(t)/R(t), and is displayed in the top trace. The right hand panel is simply a zoomed-in version of the left hand panel. All waveforms are bandpass filtered between 3.0 and 6.0 Hz. Note the alignment of the peaks of the single-channel cross-correlation traces.

In the example displayed in Figure 6.1.4, the cross-correlation coefficient exceeds 0.97 for all channels of the SPITS array; this indicates a remarkable likeness over the full length of the wavetrain, despite the fact that the amplitude of the master event is over an order of magnitude larger than that of the detected event. Note that the likeness between the different events on each channel is far greater than the likeness between the signals from each event on different channels. This indicates at the very least that the source locations of the two events are likely to be separated by a far shorter distance than the interstation distance on the Spitsbergen array.

Figure 6.1.5 illustrates another correlation detection. In this case, no signal is visible in the incoming data and any signal present clearly lies well below the noise level. However, the evidence for the presence of a signal is quite compelling; the value of the correlation beam significantly exceeds the standard deviation of the surrounding values and a close inspection of the waveforms indicate many features in common with the template waveform. Fortunately, this circumstantial evidence is compounded in this case by a clear signal recorded at the BRBB 3-component seismic station (operated by the Kola Regional Seismological Center) in close proximity of the mine.

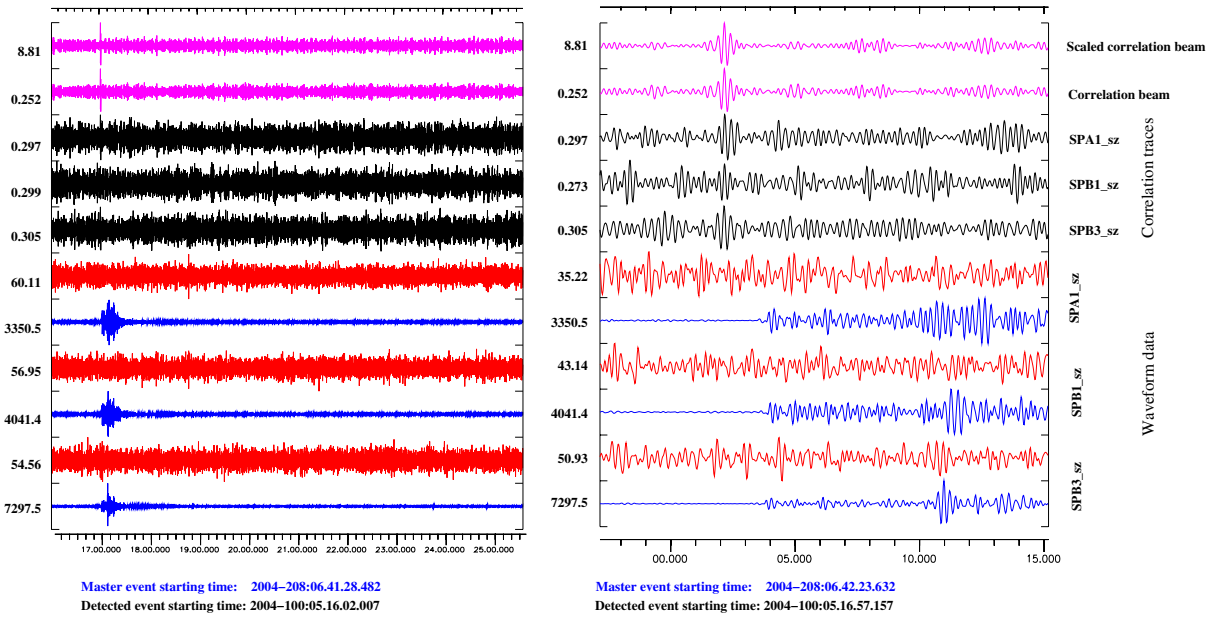

Fig. 6.1.5. A correlation detection presumed to correspond to a weak event at the Barentsburg mine. All traces are analogous to those described in Figure 6.1.5. The signal was not detectable at the SPITS array by a power detector in any frequency band. With the traces aligned according to the correlation coefficient, it is possible to observe a certain correspondence between the extreme values of the data and template waveforms on each of the channels shown. Independent evidence of the presence of an event at the mine was provided by a signal recorded by the BRBB 3-component station located close to the mine. Note that the detection is only possible by considering the full-array correlation beam; the single-channel cross-correlation traces do not even necessarily reach a global maximum at the time indicated by the correlation beam. Note also that the single-channel correlation traces are aligned in the immediate vicinity of the beam maximum.

6.1.3 The automatic screening of false alarms

The correlation detector based upon this template waveform was run on all Spitsbergen data from January 1st, 2004, until August 10th, 2004, the day on which SPITS was temporarily taken out of service for the installation of new instrumentation. A total of 7292 detections as displayed in Figures 6.1.4 and 6.1.5 were made during this period. These included the detections of many events with almost identical waveforms to those from the master event; for 4 of the detections, the array correlation coefficient exceeded 0.99, for 70 detections, the coefficient exceeded 0.90, and, for 158 detections, the coefficient exceeded 0.75. For matches with such a high degree of semblance, it is almost certain that the detection does indeed correspond to an event from the Barentsburg coal mine. However, to only accept detections in which the array correlation coefficient exceeds 0.75 would lead to the exclusion of many events such as that displayed in Figure 6.1.5, whereby the correlation coefficient is only approximately 0.25 due to the exceptionally low signal to noise ratio.

How low can we set our acceptance threshold such that we only include events which are extremely likely to come from the Barentsburg mine? The lower the permitted cross-correlation coefficient is, the more likely it is that our detection pool will include false alarms, which is to say correlation detections which result from sources unrelated to the Barentsburg mine.

An example of such a detection is displayed in Figure 6.1.6; a short high-amplitude Rg phase from an entirely different direction correlates with a short section of the master event coda sufficiently well that a detectable maximum is obtained on the array correlation beam. Not only does the detection exceed our pre-specified threshold, but the correlation coefficient is actually higher than that observed for the detection in Figure 6.1.5, which is assumed to be an event of interest. Given that, from eight months of data, we have obtained over 7000 correlation detections covering the full spectrum from “almost perfect correlation” to “marginal”, we need some form of automatic process to separate such spurious detections from those which are likely to be from the site of interest. An inspection of Figure 6.1.6 suggests a number of possible approaches. One possibility is to calculate correlation coefficients over short sections of the relevant waveforms and to compare with the full waveform correlation coefficient; this method would probably identify the example in Figure 6.1.6 as a spurious detection given that the relatively high correlation coefficient is the result of waveform semblance over a relatively short time window.

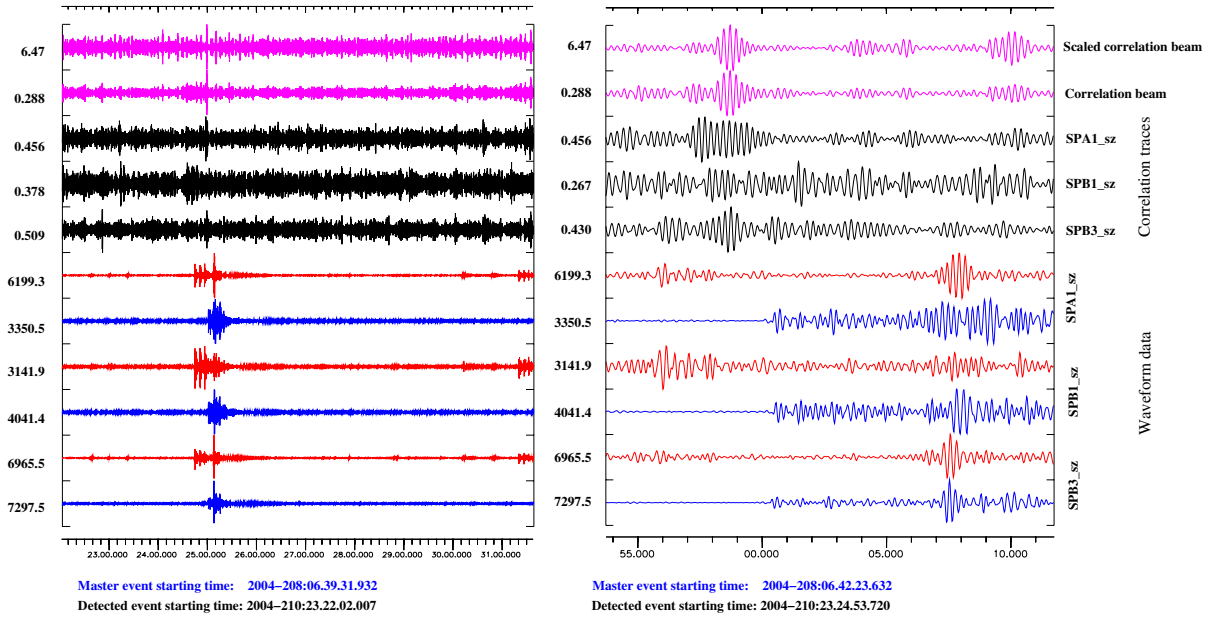

Fig. 6.1.6. A correlation detection which clearly does not correspond to an event from Barentsburg. A signal with a short time-bandwidth product correlates to such an extent with the Sg arrival of the Barentsburg template waveform that the array correlation beam results in a local maximum which triggers a detection. From plots such as these it is quite readily observed that the waveform responsible for this detection is not from our chosen site of interest. Such instances should ideally be screened out automatically. Note the poor alignment of the single channel cross-correlation traces and the fact that the value on the correlation beam is significantly less than the local maxima. on the single channel traces.

However, the most striking difference between the spurious detection in Figure 6.1.6 and the detections in Figures 6.1.4 and 6.1.5 is the alignment of the single-channel correlation coefficient traces. In the first two examples, the maximum of the correlation beam corresponds almost perfectly to local maxima of the single-channel correlation traces whereas, for the example in Figure 6.1.6, there is demonstrable destructive interference of the single-channel traces. Given that each of the single-channel correlation coefficient traces is a time series associated with a geographical site, broadband f-k analysis can be used to indicate any systematic shift in these traces in a very short time-window surrounding the time of maximum correlation on the array beam. If f-k analysis indicates that a maximum on the beam is obtained by a non-zero delay beamforming of the single traces, then it is almost guaranteed that the phase arrivals responsible for the high correlation do not come from the same direction and that, therefore, the correlation detection is spurious. Figure 6.1.7 demonstrates the results from f-k analysis from each of the examples shown in Figures 6.1.4 through to 6.1.6. The spurious detection is associated with a clearly non-zero slowness value.

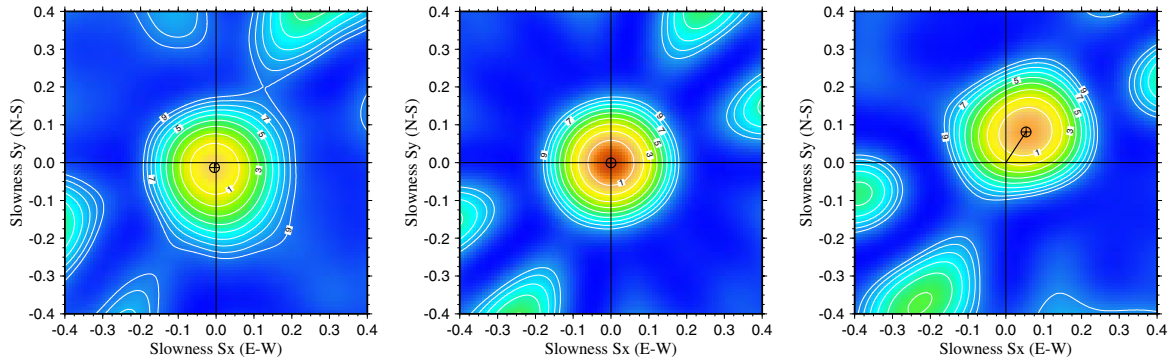

Fig. 6.1.7. Results from broadband f-k analysis on the single-channel waveform correlation traces for times 2004-100:05.17.03.210 (left: see Figure 6.1.5), 2004-157:00.53.57.089 (centre: see Figure 6.1.4), and 2004-210:23.24.59.769 (right: see Figure 6.1.6). In each case, the f-k analysis is performed in a time-window of length 1.5 seconds, centered on the given time. The relative power values obtained from the f-k calculations were 0.68 (left), 0.96 (centre), and 0.82 (right).

Whilst a clear non-zero slowness estimate from the correlation trace f-k analysis (as is shown in the right hand panel of Figure 6.1.7) essentially guarantees a false alarm, a near-zero slowness does not necessarily guarantee a true event. If the f-k power is high (as is shown in the centre panel of Figure 6.1.7), then this is a good indication that a zero time-delay stacking of the single channel correlation coefficient traces results in a beam with little energy loss and that each channel attains a maximum correlation at essentially the same time. If the f-k power is low, it may be that the best we can say is that there is insufficient evidence for a "plane wave" type optimum delay.

From our list of over 7000 correlation detections, we want to be left with only detections which are extremely likely to correspond to events from the Barentsburg mine; this means that we want to eliminate both clear false alarms and detections for which the evidence for a true correlation is not sufficiently compelling. We have already defined $C(t)$ as the correlation beam over the array; we denote the time at which $C(t)$ attains a maximum value by t_M. $C(t_M)$ is the mean value of all the single channel correlation coefficient traces obtained at a time t_M. For the correlation coefficient trace for channel i, we define the closest local maximum to time t_M as $C_i(t_M)$ (which will in general be obtained at a time t' in the immediate vicinity of t_M). If we then define $C_L(t_M)$ as the mean value of all the local maxima, $C_i(t_M)$, then the ratio $C(t_M):C_L(t_M)$ measures the amplitude of the zero-delay correlation beam relative to the amplitudes of the single-channel correlation coefficient traces. This quantity is very similar to the f-k power but is not constrained to the set of time delays permitted by plane wavefront models; a low value of $C(t_M):C_L(t_M)$ indicates that there is considerable "energy loss" in forming the beam.

For each correlation detection, we perform f-k analysis on the correlation coefficient traces and calculate the slowness and f-k power. Calculating, in addition, the quantity $C(t_M):C_L(t_M)$ we consider the detection further only if all of the following three conditions are met:

- Slowness < 0.04 s/km.
- f-k power > 0.39
- $C(t_M):C_L(t_M) > 0.58$.

These rules were arrived at simply from the manual observation of several hundred examples and examining how these quantities varied when we had a clear false alarm or a very likely Barentsburg detection. A total of 1578 detections passed the resulting test. A laborious examination of all aspects of these detections (waveforms, correlation traces, f-k analysis) indicated that there were grounds to suppose that all of these were likely to have occurred in the vicinity of the July 26th 2004 rockburst. There is an inevitable trade-off between the detection threshold imposed and the probability of obtaining false alarms. Were we to insist that the correlation coefficient, $C(t_M)$, were to exceed 0.6 for an event to be considered then we would almost certainly not have a single false alarm within our population. By lowering the detection threshold, we increase the risk of false alarms and must take appropriate steps to identify them.

6.1.4 Magnitude estimation

Once we have identified a segment of data, $v(t)$, which gives a maximum correlation with the template waveform, $v(t_0)$, we can solve for a scalar multiplier, α,which minimises the residual $|v(t) - \alpha v(t_0)|$ in the least squares sense. The validity of such an estimate will clearly diminish if the correlation coefficient is low, with a tendency for a magnitude estimate which is too low. Two temporary 3-component stations, BRBA and BRBB, situated close to the mine, provided data for selected time periods between January 1 and August 10, 2004. The best of these stations, BRBB, was operational at the times of 50 of the correlation detections and every one of these detections corresponded to a signal recorded at BRBB. The BRBA station was operational at the times of 168 correlation detections, although only 78 corresponding events were positively identified in the data. It should be noted however that the noise levels at BRBA are significantly worse than those at BRBB.

Figure 6.1.8 shows magnitude estimates for the events indicated by the cross-correlation detections obtained from both the SPITS data and from the BRBA and BRBB stations. The indications are that the magnitude estimates obtained from the cross-correlation procedure are largely consistent with the independent estimates from the on-site instruments. Poor correlation coefficients can result from both a poor signal to noise ratio and waveform dissimilarity due to differences in the source location. It is unfortunate that so much data from the on-site stations is missing.

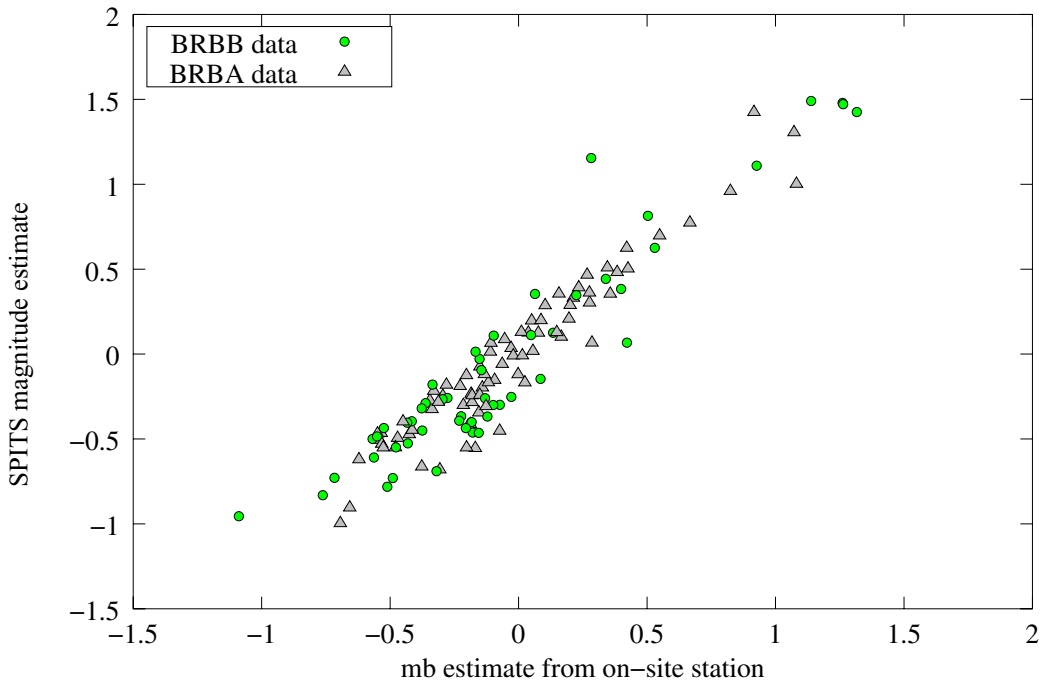

Fig. 6.1.8. Magnitude estimates of events at the Barentsburg mine from the scaling factor obtained from SPITS correlation detections and from STA values obtained from data at the on-site stations BRBA and BRBB. The master event (which was recorded by neither BRBA or BRBB) was fixed to m_b = 2.0 for the purpose of scaling.

6.1.5 A comparison of matched signal detection and detection by conventional array processing

Given a correlation detection for a presumed Barentsburg event, we know exactly when we ought to expect the appropriate P- and S- arrivals at the SPITS array. We can therefore search the detection list for SPITS and examine how many of the correlation detections correspond to events which were detected with appropriate phase propagation parameters. If we obtain a correlation detection at a time t_C, then we search for a Pg detection in the time interval [t_C - 1.2, t_C + 1.2] and an Sg detection in the interval [t_C + 5.0, t_C + 7.2]. A detection is accepted as a Barentsburg Pg phase if the apparent velocity falls within the range [6.0, 8.5] and the azimuth falls in the range [230.0, 260.0]. Similarly, a phase detection is accepted as a Barentsburg Sg if the apparent velocity falls within the range [3.0, 4.6] and the azimuth falls in the range [230.0, 260.0]. These intervals are quite large as we anticipate a certain variation in the arrival time estimates and variable frequency band slowness estimates. A site-specific reprocessing using fixed frequency band f-k analysis and autoregressive onset time estimation would almost certainly allow us to impose greater restrictions on these parameters; however, since our aim is to see how many of these events were detected by the standard processing, such an exercise is not required.

Figure 6.1.9 displays the frequency of correlation detections together with magnitude estimates from the cross-correlation calculations and a colour code to indicate whether or not a signal detection was made using the standard processing at SPITS. Altogether 1578 events were detected by the correlation method, whereas a total of 304 events were detected through con-

ventional array processing (148 with both P and S phases at SPITS, 63 with a P-phase only and 93 with an S-phase only). In the upper plot, a magnitude of -1 was chosen as a cut-off point given that no evidence exists from the on-site stations for events weaker than this. Although it is not yet clear how reliable such simple scaling magnitude estimates are as the SNR decreases, Figure 6.1.9 suggests that the detection threshold for such events has been lowered by between 0.5 and 1.0 magnitude units. An independent confirmation of this can be obtained by simply comparing the number of detections by each method, using a procedure similar to the one described by Ringdal (1974). Let us denote by C and m_c the number of events detected by the correlation procedure and the corresponding 50% detection thresholds, respectively, and let P and m_p denote similar values for conventional array processing. We then find the following approximate relationship:

$$m_p - m_c = -\frac{1}{b}\log\ (\frac{P}{C})$$

where the logarithm is to base 10 and b is the slope of the commonly used magnitude-frequency relationship for earthquakes. Setting b=1.0 and using the values above (P=304, C=1578), we obtain m_p - m_c = 0.7 magnitude units as an approximate estimate of the improvement in detectability.

It is clear that a more reliable estimate of both the absolute and relative detectability levels could be obtained if a sensitive in-mine network were available. A reference set of events detected and confirmed by such a network, as well as corresponding magnitude estimates, could then be used as a basis for a direct estimation of the detection thresholds. Clearly, this in-mine network would need to be more sensitive than the correlation procedure in order to enable such estimation to be made reliably.

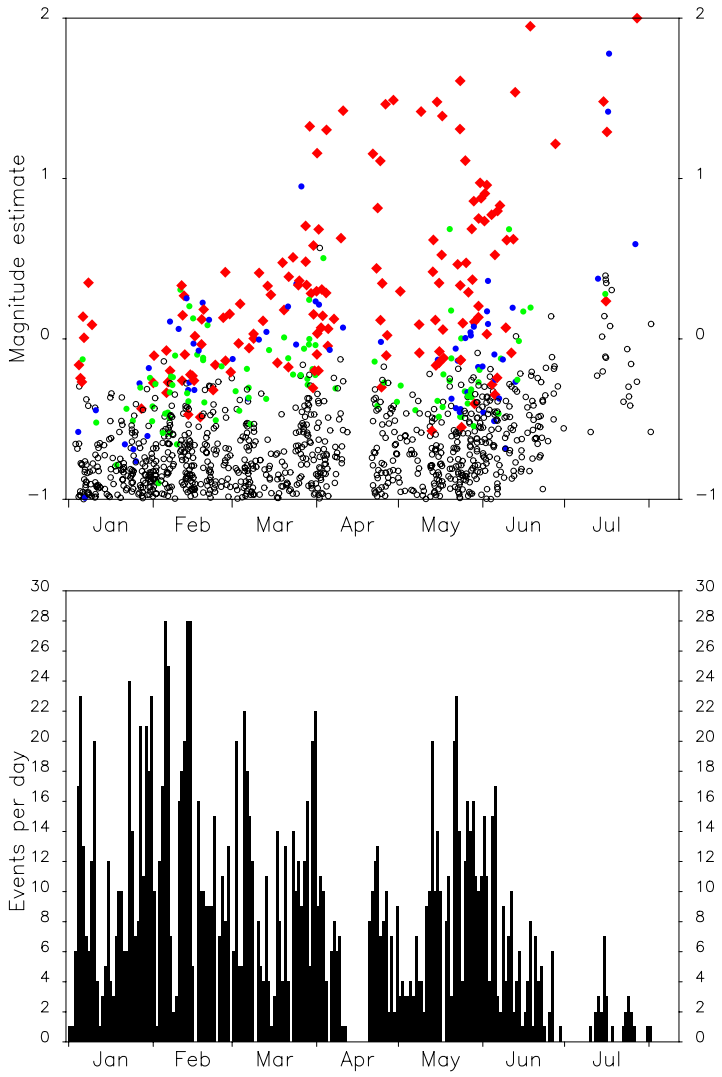

Fig. 6.1.9. The lower panel displays a histogram showing the distribution in time of the 1578 cross-correlation detections which passed the tests described in Section 6.1.3 between January 1 and August 10, 2004. The frequency with which these detections occurred is known to correspond well with industrial activity in the mine. In the upper panel, the magnitude estimate obtained from the cross-correlation calculation is displayed as a function of time. Each point is displayed as a red symbol if both a P and S detection were made at SPITS within the appropriate time windows and with appropriate propagation parameters. If only a P, but no S, phase was detected then the point is displayed as a blue symbol and a green symbol similarly indicates that an appropriate S-phase with no corresponding P-phase was detected. Black symbols indicate that either no detection was made at SPITS in the appropriate time window, or that the slowness estimates which correspond to these detections were not consistent with an event from Barentsburg.

6.1.6 Conclusions

Using waveform correlation on data from the SPITS array, with the signal from the July 26, 2004, rockburst at the Barentsburg coal mine as a template or master waveform, we have identified over 1500 instances between January 1 and August 10, 2004, for which there is evidence for the occurrence of an event located very close to the site of this incident. As the objective was to obtain a comprehensive event list, the detection thresholds were purposefully set low. The initial detection list comprised over 7000 candidate events, and many of these were clearly spurious. This made it necessary to devise a system for the automatic screening of false alarms.

False alarms generally occurred because of coincidental similarity between short sections of the template waveform and arriving phases from other sources. This problem was not encountered by Gibbons and Ringdal (2004) who ran an equivalent detection process for over two years of array data, detecting every known event from the site studied and without obtaining a single detection which did not correspond to a known event. The events sought by Gibbons and Ringdal (2004) were cavity-decoupled chemical explosions which had extremely characteristic high-frequency waveforms. The master signal and incoming data in that study were filtered in the 14 - 18 Hz frequency band as this band gave an optimal SNR. However, at such high frequencies, there is very little coherency between adjacent receivers, even for a regional array such as NORES. This, coupled with the longer length of the master signal, meant that the likelihood of coincidental correlation with unrelated signals was far smaller. The current study used a necessarily shorter time-window of data in a far lower frequency band over which the coherence (over an array with fewer stations) was far greater. Although the use of small aperture arrays is necessary for the detection of low-magnitude events using standard array processing, waveform similarity between stations appears to be a distinct disadvantage when running a matched signal detector; a more robust detector is likely when using a large aperture seismic array or a network, ideally with good azimuth coverage. We plan to carry out a systematic study of the false alarm rate as a function of network (or array) configurations, filter frequency bands and time window lengths selected for the correlation process.

The instances of correlation due to unrelated signals were readily filtered out by applying f-k analysis to the resulting waveform correlation traces and applying a set of predetermined rules. Many borderline cases with a very low SNR were also removed in this process; these may have corresponded to Barentsburg events but there was insufficient evidence at the SPITS array to support this. This procedure reduced the list of detections from over 7000 to 1578. Of these, a large number correspond to detections made by standard processing at the SPITS array and many others covering a wide range of magnitudes were also registered by two on-site three component instruments close to the Barentsburg mine. The distribution in time of detections appears to correspond well with activity at the mine during the period investigated.

References

Geller, R. J. and Mueller, C. S. (1980). Four Similar Earthquakes in Central California. *Geophys. Res. Lett.*, **7**, 821-824.

Gibbons, S. J. and Ringdal, F. (2004). A waveform correlation procedure for detecting decoupled chemical explosions, Semiannual Technical Summary, 1 January - 30 June 2004, NORSAR Sci. Rep. 2-2004, Norway. pp 41-50.

Kremenetskaya, E., Baranov, S., Filatov, Y., Asming, V. E. and Ringdal, F. (2001). Study of seismic activity near the Barentsburg mine (Spitsbergen), Semiannual Technical Summary, 1 October 2000 - 30 June 2001, NORSAR Sci. Rep. 1-2001, Norway. pp 114-121.

Kværna, T., Schweitzer, J., Ringdal, F., Asming, V. and Kremenetskaya, E. (2003): Seismic events associated with the Barentsburg mining accident on 7 June 2003, Semiannual Technical Summary, 1 January - 30 June 2003, NORSAR Sci. Rep. 2-2003, Norway. pp 77-86.

Nakahara, H. (2004). Correlation distance of waveforms for closely located events - I. Implications of the heterogeneous structure around the source region of the 1995 Hyogo-Ken Nanbu, Japan, earthquake (M_W = 6.9), Geophys. J. Int., **157**, 1255-1268.

Ringdal, F., Kværna, T., Kremenetskaya, E. O., Asming, V., Mykkeltveit, S., Gibbons, S. J. and Schweitzer, J. (2003). Research in Regional Seismic Monitoring. Proceedings of the 25th Seismic Research Review - Nuclear Explosion Monitoring: Building the Knowledge Base. September 23-25, 2003, Tucson Arizona. pp 291-300.

Ringdal, F., (1974). Estimation of seismic detection thresholds, Report No. ALEX(01)-TR-74-02, Texas Instruments Inc., Dallas, Texas.

Acknowledgements

We would like to thank Vladimir Asming at the Kola Regional Seismological Center, Apatity, Russia for analysis of 3-component data from the stations close to the Barentsburg mine.

S. J. Gibbons
F. Ringdal

6.2 Spectral characteristics of signals and noise at selected IMS stations

6.2.1 Introduction

The Primary Seismic Network of the International Monitoring System (IMS) has during the last couple of years been extended with new arrays and three-component stations. Based on the Threshold Monitoring (TM) concept, NORSAR has previously developed a system for continuous assessment of the global event detection capability of the Primary Seismic Network (Kværna and Ringdal, 1999; Taylor et al., 1998). In order to include new stations in the detectability calculations, the optimum processing parameters for each station have to be found. This station tuning process generally includes the following steps:

- Selection of recordings of regional and teleseismic events with geographically well-distributed locations
- Assessment of average noise spectra for the purpose of identifying spectral peaks that should be avoided in the continuous processing
- Determination of frequency passbands to be used when filtering the data. These passbands may be different for regional and teleseismic distances
- Determination of the beam deployment and signal loss of the arrays

For a set of 4 arrays and 3 three-component stations recently added to the IMS network, we will in the following present samples of the results from the tuning process, with emphasis on the noise spectra and the frequency ranges providing the best SNR.

6.2.2 Station and event distributions

A map of the arrays and three-component stations that have been tuned is shown in Figure 6.2.1. These are:

- AKASG (PS 45) in Ukraine, called the Malin array. This is a 23 element array with an aperture of 15 - 20 km.
- BRTR (PS 43) in Turkey, called the Keskin array. This is a 6 element array with an aperture of about 3 km.
- MKAR (PS 23) in Kazakhstan, called the Makanchi array. This is a 9 element array with an aperture of about 3-4 km.
- SONM (PS 25) in Mongolia, called the Songino array. This is a 10 element array with an aperture of about 4 km.
- KMBO (PS 24) in Kilimambogo, Kenya, is a three-component station.
- PPT (PS 18) in Pamatai, Tahiti, is a three-component station.
- THR (PS 21) in Teheran, Iran, is a three-component station.

Fig. 6.2.1. Map of 4 arrays (filled red circles) and 3 three-component stations of the IMS Primary Seismic Network that are to be included in the TM-based detectability calculations.

For each of the arrays and three-component stations we have selected data for a set of geographically well-distributed shallow events. The event locations are shown in Figures 6.2.2 and 6.2.3. A basic assumption for the tuning procedure is that the characteristics of these events can be extrapolated down to the event detection threshold of the network, and we therefore have to avoid the largest magnitude events. On the other hand, we also have to require a sufficient signal-to noise ratio (SNR) such that the characteristics of the signals can be reliably estimated. We have therefore targeted the first-arriving P-phases with SNRs between 20 and 80. From searching the IDC Reviewed Event Bulletin for the time period October 2001 - October 2004 we ended up with 120 - 150 events for five of these stations. 89 events were found for station THR, whereas we were only able to find 33 events at station PPT, out of which several were deep events located in subduction zones. The reason for the small event population at PPT is the generally high background noise level and the low seismicity in the Central Pacific.

AKASG (50.70 N, 29.22 E)

BRTR (39.73 N, 33.64 E)

MKAR (46.79 N, 82.29 E)

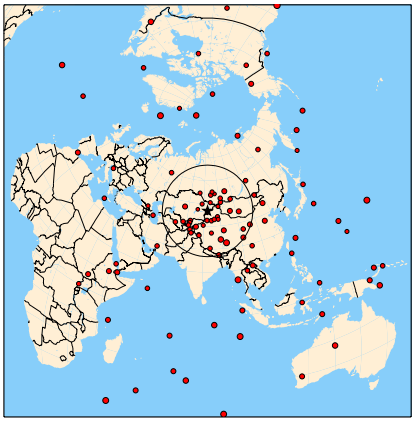

SONM (47.83 N, 106.39 E)

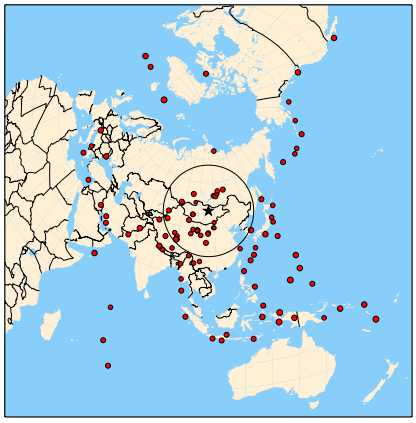

Fig. 6.2.2. Locations of the events used for tuning of the 4 arrays considered in this study. The circles encompassing the arrays represent a distance of 20 degrees.

KMBO (1.13 S, 37.25 E)

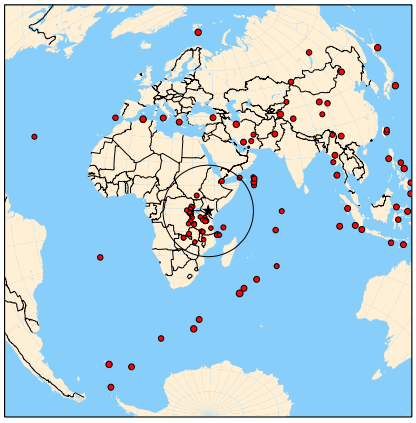

PPT (17.57 S, 149.58 W)

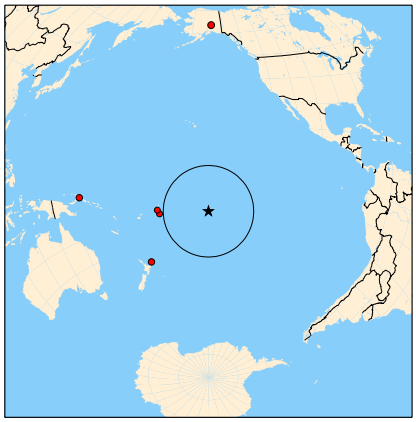

THR (35.91 N, 51.13 E)

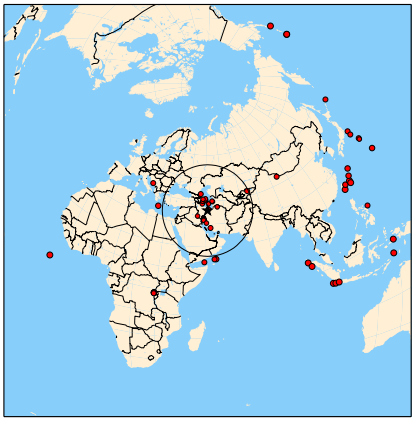

Fig. 6.2.3. Locations of the events used for tuning of the 3 three-component stations considered in this study. The circles encompassing the stations represent a distance of 20 degrees.

6.2.3 Noise and signal spectra

For each event in the database we have calculated the spectra of the noise preceding the P-phase. The noise windows started 50 second before the P onset and had a length of 40 seconds. The multitaper spectral method (Thomson, 1982) was used for estimation. For arrays we calculated the average noise spectra of all vertical-component channels, as well as the noise spec-

trum of the vertical component beam. The beam was steered with the azimuth and slowness of the arriving P-phase.

The motivation for this analysis was to get information about the absolute noise levels at the different stations and to identify frequencies or frequency ranges with particularly high noise levels. Figure 6.2.4 shows the displacement power spectra of the investigated arrays, both the average of the individual vertical component channels and of the beams. Figure 6.2.5 shows the displacement power spectra of the vertical component of the three-component stations. A summary of the spectral levels as compared to the Peterson noise models (Peterson, 1993) for given frequencies is given in Table 6.2.1. The numbers in red color represent values below the Peterson low noise model (PLNM). Such values are found on some of the array beams at selected frequencies.

Table 6.2.1. Displacement power levels at discrete frequencies

Frequency (Hz)												
	0.5	0.8	1.0	2.0	3.0	4.0	5.0	6.0	7.0	8.0	9.0	10.0
Peterson Low Noise Model (Displacement Power, nm^2/Hz)												
	2.36e+01	5.60e-01	3.80e-02	1.49e-03	3.00e-04	2.00e-04	9.94e-05	1.07e-05	8.29e-06	5.86e-06	3.43e-06	1.00e-06
Average Noise Levels (Decibels above Peterson Low Noise Model)												
AKASG	9.81	13.67	18.14	19.89	21.05	25.68	27.43	24.77	24.37	25.40	24.59	26.57
BRTR	8.49	11.03	10.78	13.42	19.40	17.80	16.11	16.73	15.87	16.02	16.33	
MKAR	5.59	10.94	10.92	5.40	5.96	7.78	10.67	8.74	8.82	8.85	9.63	9.49
SONM	4.53	7.66	7.49	10.20	13.97	15.03	16.40	16.19	18.24	19.36	19.76	30.04
KMBO	9.56	11.98	10.55	8.67	11.72	14.36	20.78	28.27	32.50	33.74	30.31	27.41
PPT	34.99	38.85	37.30	39.20	34.11	37.11	37.58	38.20	37.62	42.13	39.29	42.59
THR	3.27	7.51	7.49	8.71	11.39	10.93	12.01	12.01	9.87	10.14	12.01	13.00
Beam Noise Levels (Decibels above Peterson Low Noise Model)												
AKASG	-1.26	1.74	7.58	8.03	9.10	13.29	15.27	12.46	12.79	14.40	13.03	15.33
BRTR	5.33	5.95	3.80	5.02	11.48	10.20	8.64	8.47	7.96	8.49	8.59	
MKAR	3.68	6.57	5.64	-3.39	-3.91	-2.22	1.22	-0.78	-0.25	-0.27	0.45	0.42
SONM	2.52	3.30	0.86	-0.50	3.74	4.87	6.58	6.48	8.29	9.01	10.52	20.02

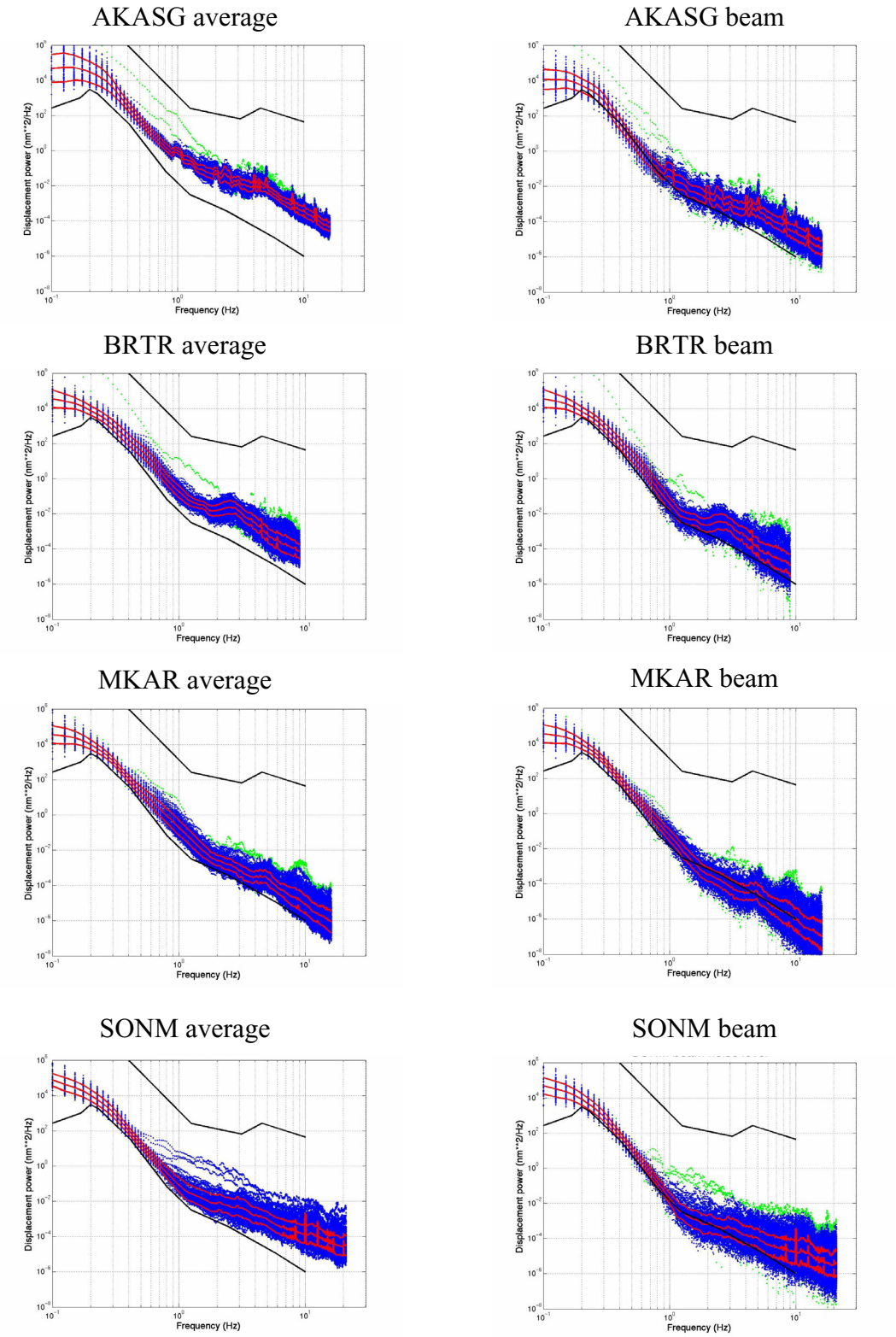

Fig. 6.2.4. Average displacement spectra (left) and beam spectra (right) of noise preceding the P-phases for the four arrays. The average ± one standard deviation of all noise samples are shown red. Green indicate spectral levels exceeding 3 standard deviations. The low and high Peterson noise models are indicated by black solid lines.

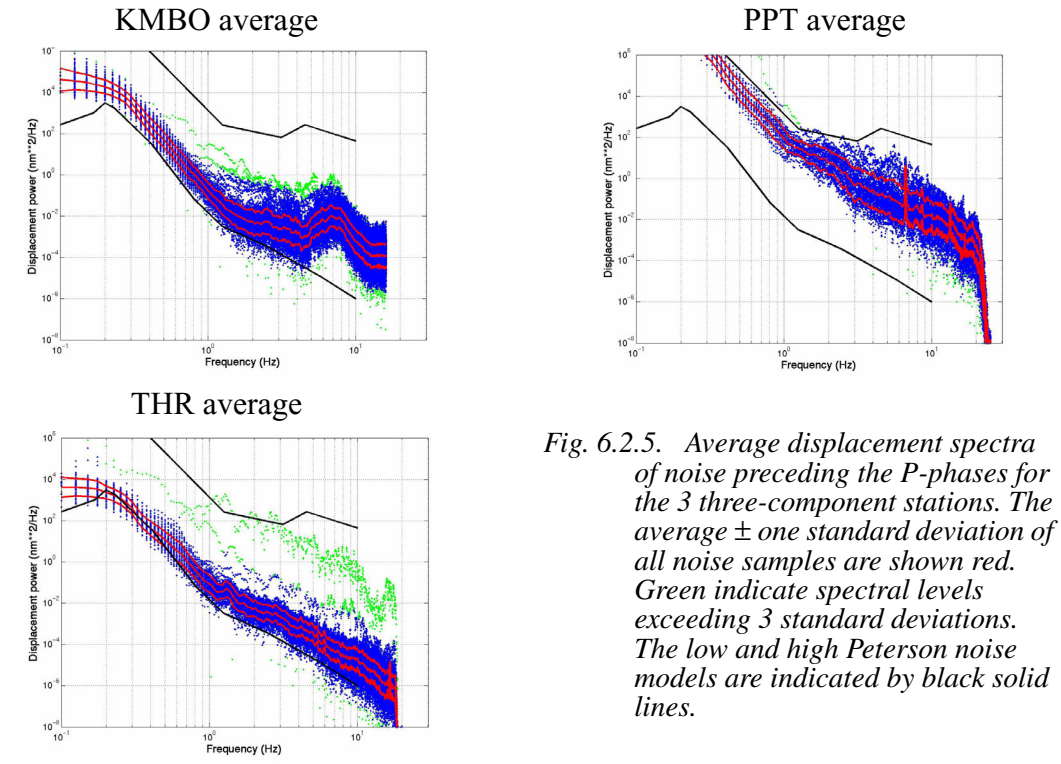

Fig. 6.2.5. Average displacement spectra of noise preceding the P-phases for the 3 three-component stations. The average ± one standard deviation of all noise samples are shown red. Green indicate spectral levels exceeding 3 standard deviations. The low and high Peterson noise models are indicated by black solid lines.

The spectra shown in Figures 6.2.4 and 6.2.5 provide information about the absolute noise levels at the different stations. However, continuous data processing is most of the time applied to uncorrected data, and the shape of the uncorrected noise spectra is not only dependent on the actual noise field, but also on the instrument response of the recording system. For estimation of the network event detection capability we need for each station to know the frequency range for which we usually have the best SNR, preferably combined with a good recovery of the signal amplitudes. Figure 6.2.6 shows the uncorrected array beam spectra together with SNR versus distance for the P-phases for the four arrays. The SNR of the beamformed P-signal was measured via the STA/LTA in narrow frequency bands. The SNR values were then normalized to the maximum, and some averaging was done when grouping the events into distance bins. Figure 6.2.7 shows similar plots for the three-component stations. For most stations we see that the highest SNR is found at generally low frequencies for teleseismic events, whereas for local and regional events the best SNR is generally found at higher frequencies. This is mostly a result of the attenuation of the high frequencies at larger distances, but the receiver site conditions, the local noise field and the instrument response also play a role in determining the frequency range for which we find the highest SNR.

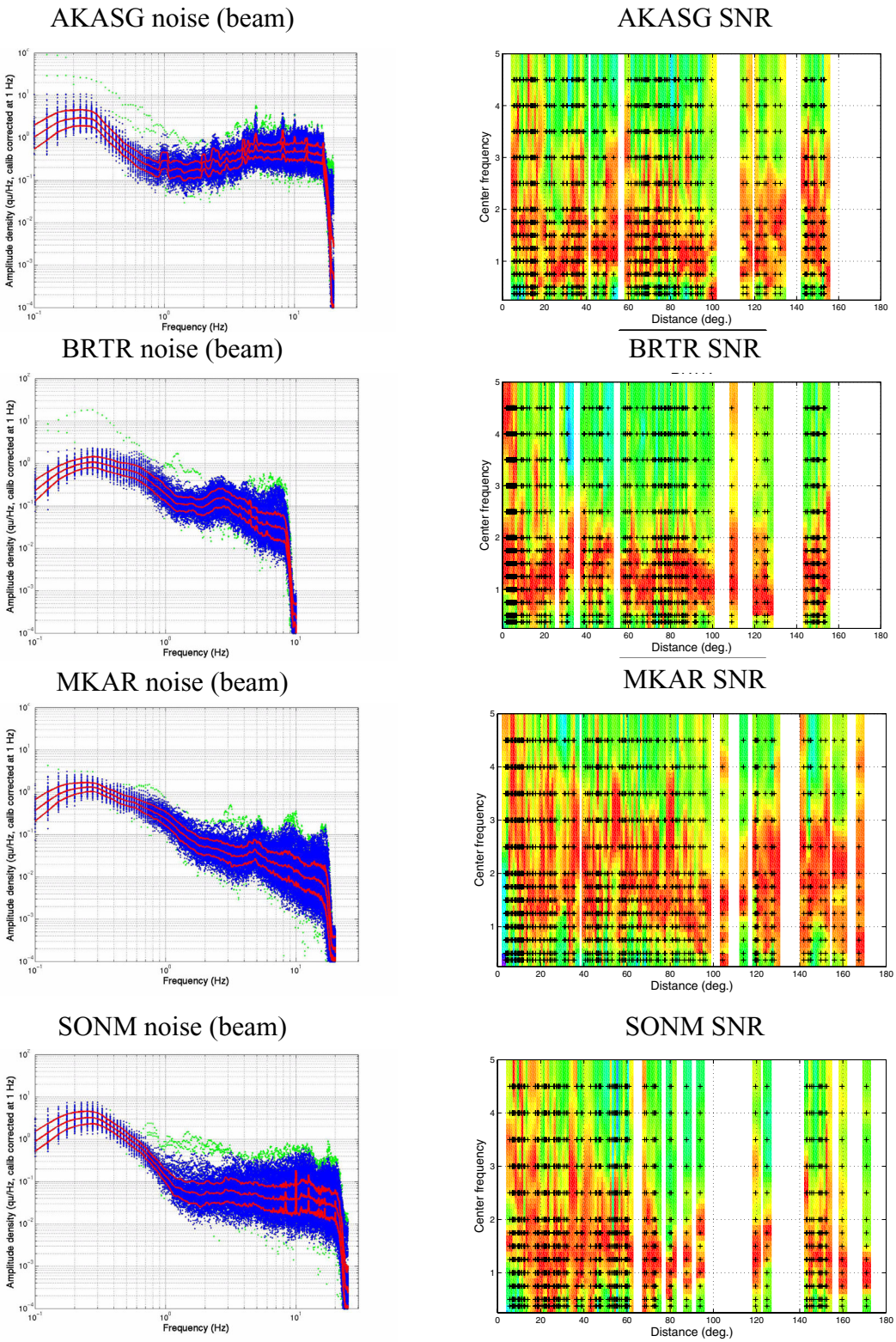

Fig. 6.2.6. Uncorrected beam noise spectra (left) and SNR vs. distance (right) for the P-phases for the four arrays. On the plots to the left, the average ± one standard deviation of all noise samples are shown red, while green indicate spectral levels exceeding 3 standard deviations. The plots to the right show the normalized SNR as a function of distance. The frequencies with the highest SNR are marked red.

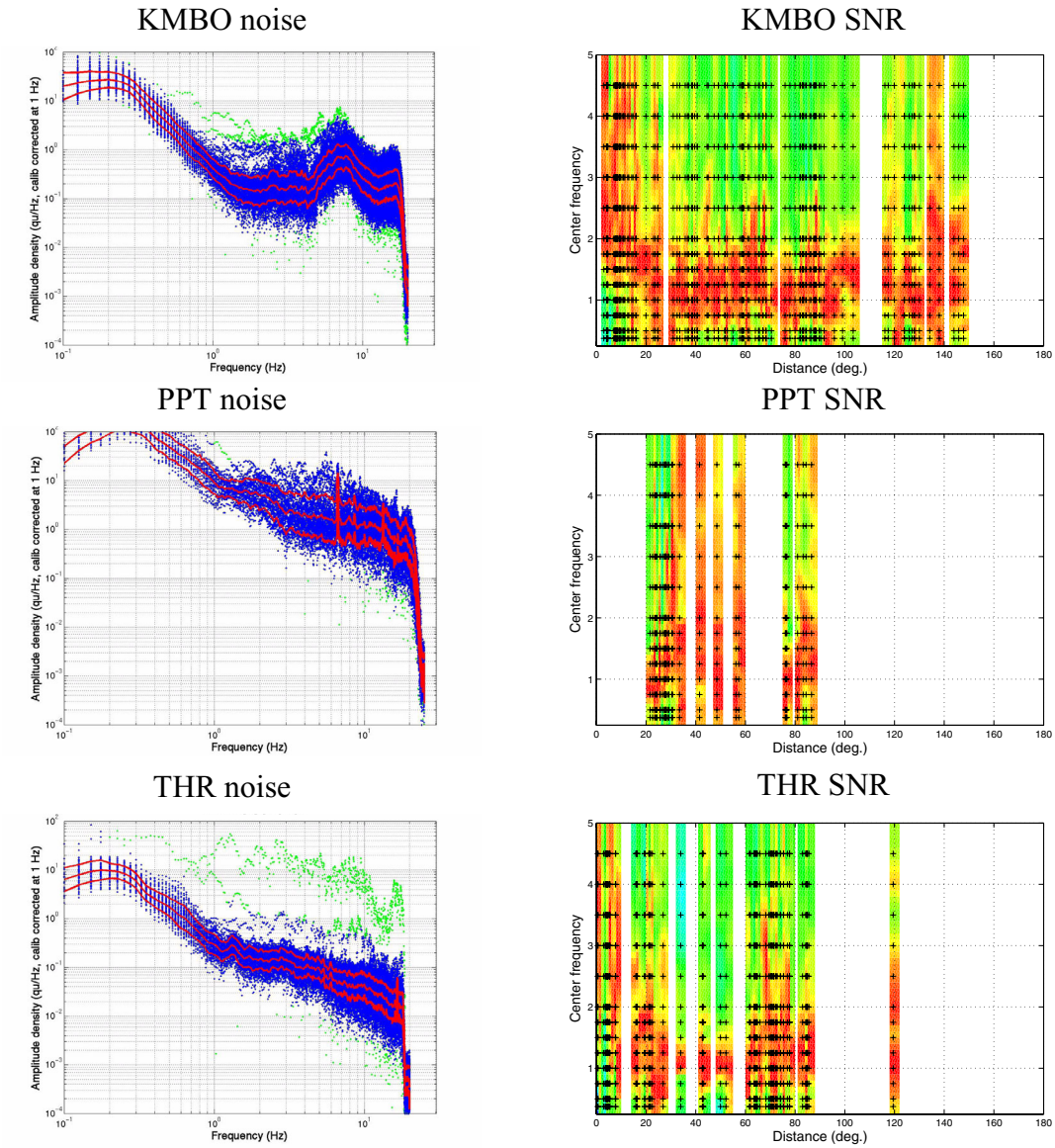

Fig. 6.2.7. Uncorrected noise spectra (left) and SNR vs. distance (right) for the P-phases for the 3 three-component stations. On the plots to the left, the average ± one standard deviation of all noise samples are shown red, while green indicate spectral levels exceeding 3 standard deviations. The plots to the right show the normalized SNR as a function of distance. The frequencies with the highest SNR are marked red.

6.2.4 Discussion

We will in the following discuss the noise and signal characteristics of the investigated arrays and three-component stations.

AKASG

Background Noise Levels:

The background noise levels at Malin, Ukraine (AKASG) ranges from about 10 dB above

the Peterson Low Noise Model (PLNM) at 0.5 Hz increasing to about 25 dB above PLNM at 4 Hz. Above 4 Hz the background noise level stays about 25 dB above PLNM.

Beam Noise Levels:

AKASG is a 23 element array with an aperture of 15 - 20 km. With uncorrelated noise we would expect about 13 dB noise reduction by beamforming. The noise beam spectra of Figure 6.2.4 and the values given in Table 6.2.1 confirm this. As a result we find that the noise level after beamforming is lower than the PLNM below 1 Hz.

Noise Peaks

As seen from Figures 6.2.4 and 6.2.6 there are a number of pronounced peaks in the AKASG noise spectra (1Hz, 2 Hz, 2.5 Hz, 4 Hz, 8 Hz), which we assume are caused by nearby cultural noise sources.

Uncorrected spectra

The AKASG array is equipped with instruments that have a flat acceleration response in the higher frequency range. Consequently the uncorrected noise has relatively high levels above 4 Hz (see Figure 6.2.6). The noise peaks stand out clearly in the uncorrected spectra. Without introducing instrument response corrections, the frequency range between 1 and 2 Hz has the lowest noise levels.

SNR vs. distance

For distances larger than 20 degrees, the highest SNR is usually found between 1 and 2 Hz, but some of the teleseismic events have high SNR up to 3 Hz. For local/regional distances up to 20 degrees high SNR is observed up to 4 Hz.

BRTR

Background Noise Levels:

Between 0.5 and 2 Hz the background noise levels at Keskin, Turkey (BRTR) ranges from 8.5 to 13.5 dB above the Peterson Low Noise Model (PLNM). Between 2 and 3 Hz there is a relative increase in the background noise level from 13.5 to 19.5 dB above PLNM. For frequencies above 5 Hz we find average noise levels about 16 dB above PLNM.

Beam Noise Levels:

BRTR is a 6 element array with an aperture of about 3 km. With uncorrelated noise we would expect 7-8 dB noise reduction by beamforming. The noise beam spectra of Figure 6.2.4 and the values given in Table 6.2.1 confirms this for frequencies above 1Hz. For frequencies below 1 Hz less noise reduction if found through beamforming, indicating that the noise is correlated between the array sensors for such low frequencies.

Noise Peaks

As seen from Figures 6.2.4 and 6.2.6 there is a pronounced noise peak between 2 and 3 Hz, which we assume is caused by nearby cultural noise sources.

Uncorrected spectra

The BRTR array is equipped with instruments that have a flat velocity response above about 1 Hz. Because of the noise peak around 3 Hz, we find that there is a local minimum between 1.2 and 2 Hz in the uncorrected noise spectra.

SNR vs. distance

For distances larger than 15 degrees, we find the highest SNR between 0.8 and 2 Hz. For distances less than 10 degrees we also find high SNR is observed above 3 Hz.

MKAR

Background Noise Levels:

The background noise levels at the Makanchi array in Kazakhstan (MKAR) stays within 11 dB of the PLNM for the frequency range 0.2 - 10 Hz. In particular, the noise levels around 2 and 3 Hz is within 6 dB of the PLNM.

Beam Noise Levels:

MKAR is a 9 element array with an aperture of about 3-4 km. With uncorrelated noise we would expect about 9 dB noise reduction by beamforming. The noise beam spectra of Figure 6.2.4 and the values given in Table 6.2.1 confirms this for frequencies above 2 Hz, such that the beam noise level at MKAR fall below or close to the PNLM for these frequencies. For frequencies below 2 Hz less noise reduction is found through beamforming, indicating that the noise in this frequency range is correlated between the array sensors.

Noise Peaks

As seen from Figures 6.2.4 and 6.2.6 there is a small noise peak around 5 Hz.

Uncorrected spectra

The MKAR array is equipped with instruments that have a flat velocity response above about 1 Hz. The average uncorrected noise spectrum generally decreases from 0.3 to 15 Hz, except for the frequency range 3.5 - 5 Hz which is influenced by the small 5 Hz noise peak.

SNR vs. distance

For distances larger than 15 degrees, we find the highest SNR between 0.8 and 3.5Hz. For distances less than 10 degrees the highest SNR is observed above 2 Hz.

SONM

Background Noise Levels:

The background noise levels at the Songino array in Mongolia (SONM) stays within 8 dB of the PLNM for the frequency range 0.2 - 1 Hz. Between 2 and 9 Hz there is a relative increase in the noise levels from 10 to 20 dB above PLNM.

Beam Noise Levels:

SONM is a 10 element array with an aperture of about 4 km. With uncorrelated noise we would expect about 10 dB noise reduction by beamforming. The noise beam spectra of Figure 6.2.4 and the values given in Table 1 confirms this for frequencies above 1 Hz, such that the beam noise level at SONM is comparable to the PNLM in the 1 to 2 Hz range. For frequencies below 1 Hz less noise reduction is found through beamforming, indicating that the noise in this frequency range is correlated between the array sensors.

Noise Peaks

There are several pronounced noise peaks around 10 Hz.

Uncorrected spectra

The SONM array is equipped with instruments that have a flat velocity response above 1 Hz. The average uncorrected noise spectrum is almost constant in the frequency range 1.5 to 8 Hz.

SNR vs. distance

For distances larger than 80 degrees, we find the highest SNR between 0.8 and 2 Hz. For distances between 20 and 80 degrees the highest SNR is found between 0.8 and 3 Hz. For local and regional distances, the higher frequencies become more important.

KMBO

Background Noise Levels:

The background noise levels at the Kilimambogo station in Kenya (KMBO) stays within 15 dB of the PLNM for the frequency range 0.2 - 4 Hz. Between 4 and 6 Hz there is a large relative increase in the noise levels from 15 to 30 dB above PLNM.

Noise Peaks

There are no narrow noise peaks, but the frequency range from 4.5 to 10 Hz is characterized by high noise levels.

Uncorrected spectra

The KMBO station is equipped with instruments that have a flat velocity response above 1 Hz, and the high noise levels between 4.5 and 10 Hz stand out clearly.

SNR vs. distance

For distances above 20 degrees, we generally find the highest SNR between 0.8 and 2 Hz. For distances less than 20 degrees, generally high SNR is found in the frequency range 1.2 to 4.5 Hz.

PPT

Background Noise Levels:

The Pamatai station on Tahiti (PPT) has high noise levels in the entire investigated frequency band, varying between 35 and 40 dB above PLNM. The high noise levels are most likely caused by the proximity to the Pacific Ocean and man-made activity on the island of Tahiti.

Noise Peaks

There is a pronounced noise peak between 6 and 7 Hz, together with smaller peaks between 8 and 15 Hz.

Uncorrected spectra

Except for the 6-7 Hz range, the uncorrected PPT noise spectra generally decrease with increasing frequencies. The peak between 6 and 7 Hz stands out clearly.

SNR vs. distance

As previously explained we had difficulties finding a sufficiently large number of events at PPT that could be used for tuning purposes. A total of 33 events were found, having epicentral distances from 20 to 90 degrees from the station. In this distance range the best SNR was generally found in the frequency range 0.8 to 3 Hz.

THR

Background Noise Levels:

The Teheran station in Iran (THR) has relatively low noise levels in the entire investigated frequency band. The values vary from 3 dB above PLNM at 0.5 Hz up to 12 dB above the PLNM for frequencies higher than 3 Hz.

Noise Peaks

Station THR has a few smaller noise peaks, for example at 1.5 Hz and about 15 Hz.

Uncorrected spectra

Except for the 1.5 Hz range, the uncorrected THR noise spectra generally decrease with increasing frequencies. The peak at about 15 Hz stands out clearly.

SNR vs. distance

For distances above 20 degrees, we generally find the highest SNR between 0.8 and 2 Hz. For distances less than 20 degrees, generally high SNR is found in the frequency range 1 to 5 Hz.

References

Kværna, T. and F. Ringdal (1999). Seismic threshold monitoring for continuous assessment of global detection capability, *Bull. Seism. Soc. Am.*, 89, 946-959.

Peterson, J. (1993). Observations and modeling of seismic background noise, *U.S. Geol. Surv. Open File Report*, 93-322.

Taylor, L, T. Kværna and F. Ringdal (1998). Threshold Monitoring operations Manual, *NORSAR Contribution No. 639*, NORSAR, Kjeller, Norway

Thomson, D. J. (1982). Spectrum Estimation and Harmonic Analysis. *Proc IEEE*, 70(9), 1055-1096.

Tormod Kværna
Ulf Baadshaug

6.3 The 7 April 2004 Flisa, Southern Norway earthquake sequence - eight hypocenter determinations and one focal mechanism

6.3.1 Introduction

On 7 April 2004, a moderately felt magnitude 3.5 earthquake occurred close to Flisa, a small settlement in eastern Norway. Geologically, the earthquake was located northeast of the Oslo Graben at the border of the Baltic Shield. This event was observed at numerous seismic stations and arrays in central and northern Europe, in particular the four Fennoscandian IMS arrays (ARCES, FINES, Hagfors, and NORSAR) observed clear P and S onsets. However, most important is that the event occurred in the vicinity of the NORSAR array (closest epicentral distance less than 20 km) and that therefore a precise event location can be achieved. Fig. 6.3.1 shows the geology of the region and a blue circle, indicating the source area of the event.

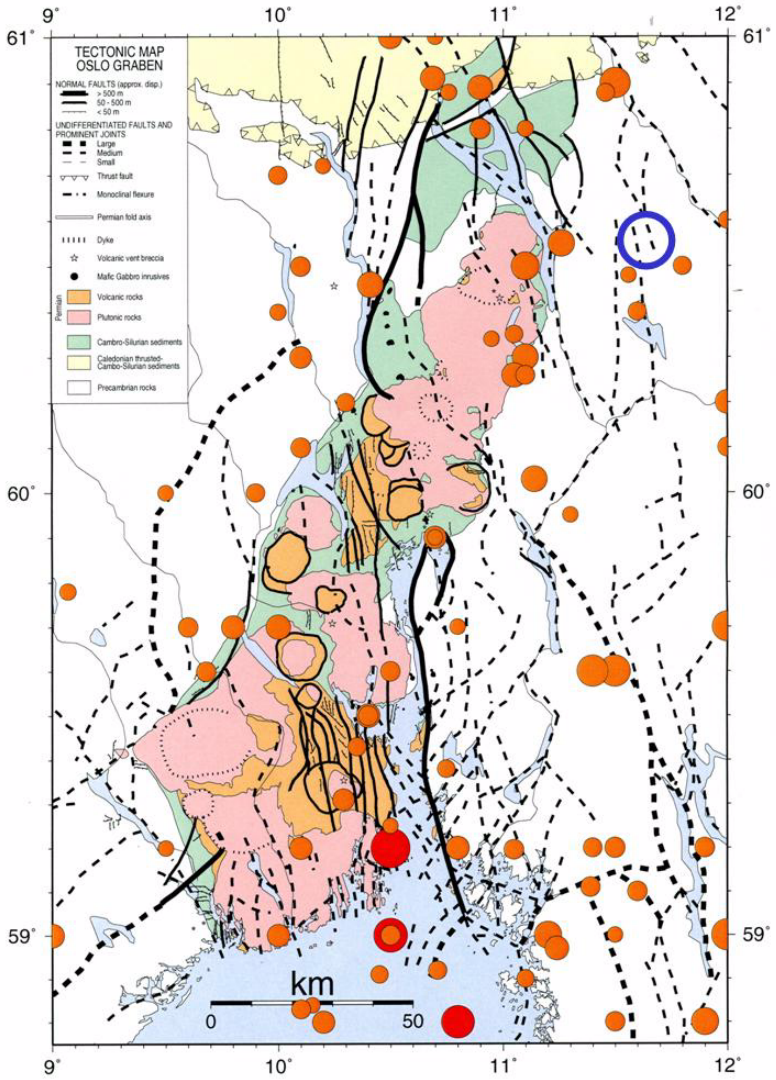

Fig. 6.3.1. Tectonic map of the Oslo Graben area with the source region (blue circle) of the Flisa earthquake sequence (modified from Hicks, 1996). Red symbols show recent seismicity in the region.

Travel-time calibration of the stations of the CTBTO International Monitoring System (IMS) is a major task for CTBT related research at many institutions. For such calibration the availability of recordings from well located seismic events is essential.

A seismic event located so close to an array with 63 single sensors distributed over 42 sites gives a rare opportunity to obtain a very precise location and thereby contribute to the data base of useful ground-truth events. For this event clear P and S onsets were found at all 42 sites of the NORSAR array.

6.3.2 Absolute location of the main shock

Although many observations were available from stations all over Fennoscandia and Central Europe, only the closest stations were used for the event location. The hypocenter determination of the main shock included several steps.

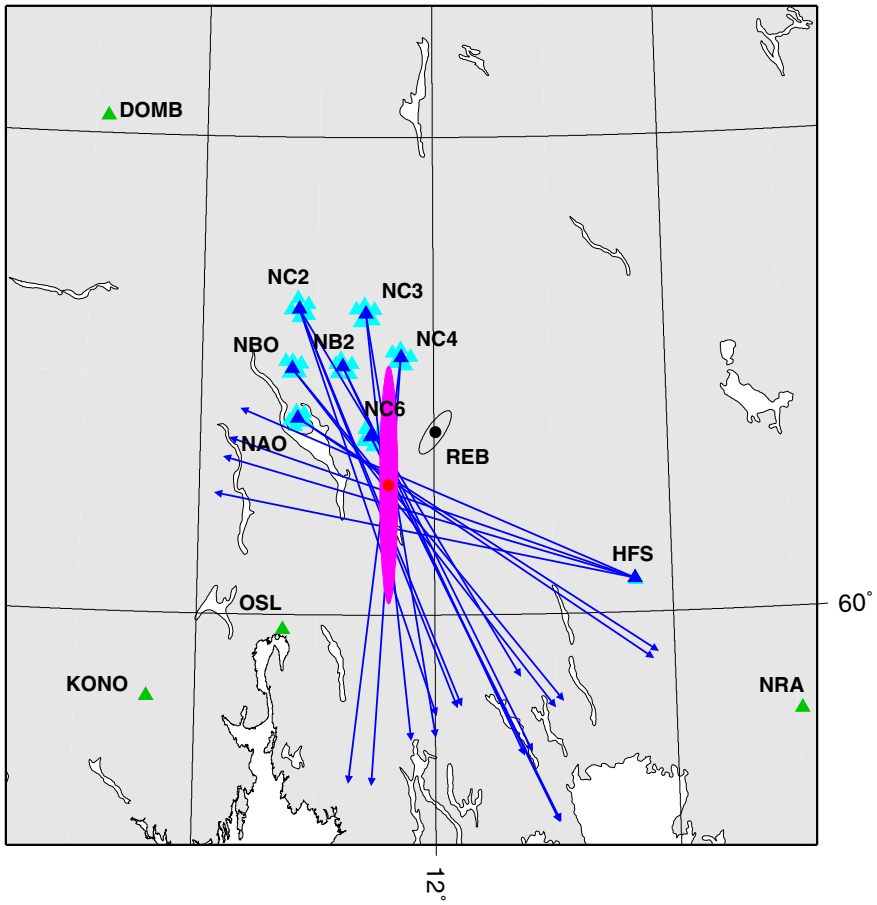

Fig. 6.3.2. The map shows all stations used to locate the main shock. Backazimuth observations at Hagfors and the NORSAR subarrays are shown by blue lines. Also shown are the epicenter (red dot) and the epicentral area (magenta ellipse) as estimated from these observations (99.99% confidence area), and the event location as published in the Reviewed Event Bulletin (REB) of the IDC in Vienna. All single array sites are plotted with blue symbols (the reference sites in dark blue) and all nearby located single sites of the Norwegian and the Swedish national networks are shown in green.

In an initial step, all backazimuth observations of P- and S-type onsets from the NORSAR array and the Hagfors array in Sweden were used to define an initial epicenter. The seven sub-arrays of NORSAR were individually analyzed as small aperture arrays and the backazimuth determined by plane-wave-fit. 158 crossing points could be calculated between the backazimuth observations. Then a common mean crossing point was determined together with its uncertainty. This crossing point defines the starting epicenter for the final inversion. Fig. 6.3.2 shows a map of all backazimuth observations and the calculated epicenter; the uncertainty region is indicated in magenta, which is just the formal error calculated from the single backazimuth uncertainties. This error ellipse does not take in account the actual close geometry between event and observing stations and therefore the error ellipse becomes too elongated in the south-north direction. In addition, the event location as given in the REB by the IDC in Vienna is also shown, which is definitely outside the possible source area already defined by the backazimuth observations.

The second step was the determination of an initial estimate for the final inversion of the hypocenter. Readings at stations with a P and an S onset with the same ray-path geometry, e.g., Pb and Sb or Pn and Sn (assuming a constant v_p/v_s ratio), the v_p/v_s ratio, and the source time are a function of the P-onset time and the travel-time difference between P and S onset (Wadati, 1933). For the Flisa event all observed first P and S onsets at epicentral distances of less than 1° were used for the Wadati-diagram. Fig. 6.3.3 shows the results of this analysis. A mean v_p/v_s ratio of 1.74 was found for all observations and it is easy to see that the source time is determined by the time when the S-P travel-time difference becomes zero. The estimated v_p/v_s ratio is very close to $\sqrt{3}$, which is used in NORSAR's standard velocity model for Fennoscandia (Mykkeltveit & Ringdal, 1981).

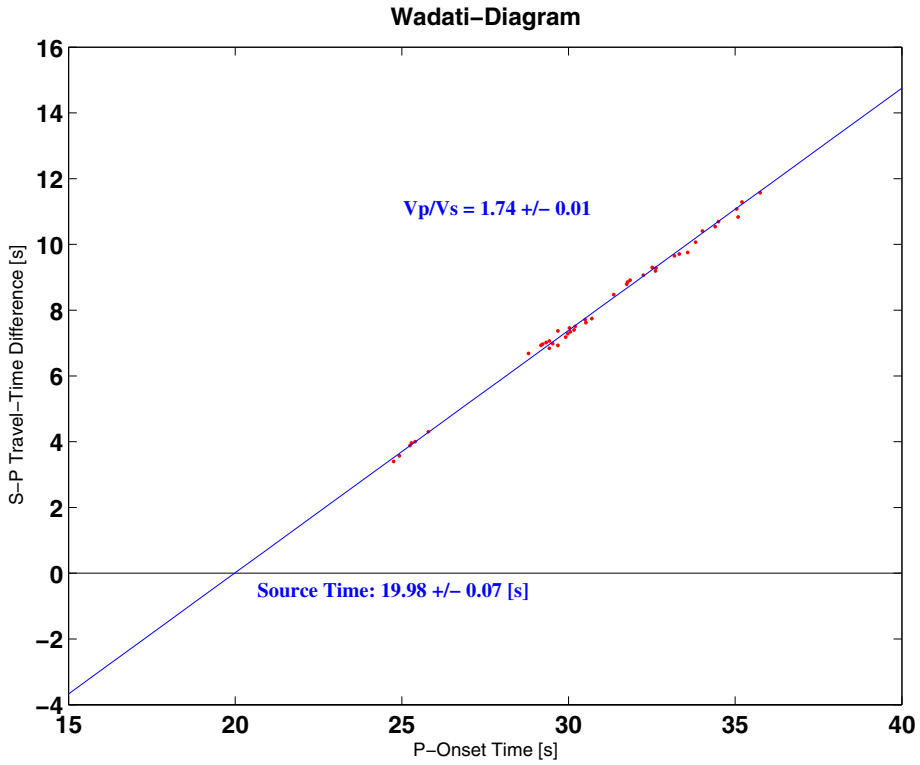

Fig. 6.3.3. The Wadati-diagram for the Flisa main shock defines the mean Vp/Vs ratio and the source time; the given uncertainties correspond to one standard deviation.

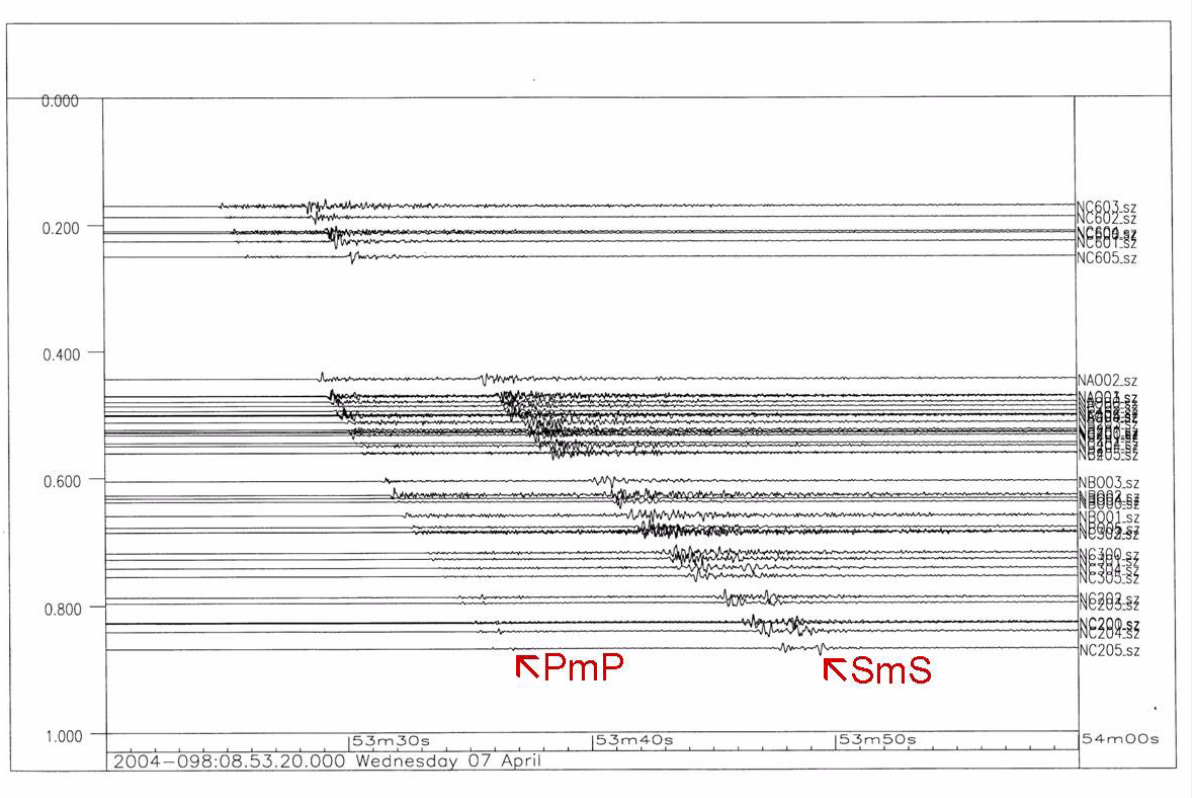

Fig. 6.3.4. Seismogram section of the original vertical traces as recorded at the 42 sites of the NORSAR array. The vertical axes is the distance in degrees from the epicenter. Note the clear PmP and SmS onsets from about 0.8° epicentral distance on. All traces are individually normalized.

As can be seen from Fig. 6.3.4, the Moho-reflections PmP and SmS have clear onsets at all sites of the NORSAR subarray NC2. Such reflections from interfaces below the hypocenter give additional constraints for the event's depth.

In former studies (e.g., Aki et al., 1977; Gundem, 1984; Bischoff et al., 2004) the mean depth to the Moho below the NORSAR array was estimated to be about 35 km. Taking this and the slightly higher v_p/v_s ratio into account, a first, modified velocity model was derived to locate the event (see Table 6.3.1).

Table 6.3.1. The initial velocity model used for locating the Flisa earthquake

Depth (km)	P Velocity (kms^{-1})	S Velocity (kms^{-1})
0.0	6.20	3.569
16.0	6.20	3.569
16.0	6.70	3.857
35.0	6.70	3.857
35.0	8.15	4.705
95.0	8.15	4.705

In the next step, all the initial results were put together and the event was located by applying the location program HYPOSAT (Schweitzer, 2001). For the final inversion not only the array observations but also readings from four nearby seismic stations were used to reduce the azimuthal gap. The results of this inversion are listed as NORSAR_1 in Table 6.3.3.

However, the model uncertainties may still have an effect on the solution. The inversion algorithm used to calculate the hypocenter cannot simultaneously invert for the velocity structure of the region. To find the best model, a systematical trial-and-error process of several steps was performed. During such inversions, the main question is always which possible model types could explain the data equally well and whether the hypocenter determination in such cases will move away to another source area.

The mean P velocities of the model are assumed to be those obtained from former studies (Aki et al., 1977; Mykkeltveit & Ringdal, 1981; Gundem, 1984). The corresponding S velocities are defined by the results of the Wadati-diagram. Therefore, only changes in the mean depth of the Conrad or the Moho discontinuities may influence the locations.

As a first step, the influence of the Moho discontinuity on the location results was tested. Therefore, the hypocenter inversion was repeatedly performed after moving this discontinuity in 1 km steps from 32 to 38 km depth. The result of this test was that the RMS values varied by 20% and the weighted L1 norm of all residuals by 31%. Rejecting all models with more than 10% RMS or weighted L1 norm deviation from the minimum values, the located epicenter varied within +/- 0.14 km of the initial estimate. The effect on the source depth was a bit larger (+/- 0.8 km). The best data fit was achieved with Moho depths at 34 and 35 km.

During the second test the Moho depth was fixed at 35 km and the Conrad discontinuity was varied in 1 km steps between 13 and 26 km depth. Then the RMS values varied by 26.6% and the weighted L1 norm by 25.9%. Rejecting again all results with more than 10% deviation from the smallest RMS or L1 norm value, the source depth varied by +/- 0.4 km and the epicenter by +/- 0.45 km. The smallest RMS and L1 norm values were achieved with depths of the Conrad discontinuity at 20 and 21 km. This is deeper than in the standard Fennoscandia velocity model, which has a border between upper and lower crust at 16 km (Mykkeltveit & Ringdal, 1981; see also Table 6.3.1). However, Bischoff et al. (2004) had already strong indications from their Rayleigh-wave-dispersion curve study for a thicker upper crust below the NORSAR array and they received in their inversion a depth of the Conrad discontinuity at about 20 km. Therefore, in this study the Conrad discontinuity is assumed to be at 20 - 21 km depth.

In the last two steps, the Conrad discontinuity was fixed, once at 20 and once at 21 km, and the Moho depth was again systematically varied between 33 and 37 km. Rejecting all solutions with more than 10% deviation from the smallest RMS or weighted L1 norm values, the final acceptable depth range for the Moho was determined to be 34 - 35 km. For the best solutions the source parameters varied only slightly: the latitude between 60.551˚ and 60.554˚, the longitude between 11.649˚ and 11.653˚, the depth between 22.1 and 23.3 km, and the source time between 08:53:19.834 and 08:53:20.005.

The solution with the absolute smallest RMS was found for a Conrad discontinuity at 21 km depth and a Moho at 35 km depth. The solution with the smallest weighted L1 norm value was found for the combination: Conrad discontinuity at 20 km depth and Moho at 34 km depth. However, since the differences between these solutions are very small and since they all are

inside the 99.99% confidence region, the selection of such details of the final model is not critical. Therefore, the finally chosen model has the Conrad discontinuity at 20 km depth and the Moho discontinuity is located at a depth of 35 km. These two values are also in best agreement with the results of Bischoff et al., 2004 (see Table 6.3.2).

Table 6.3.2. The final mean velocity model used for locating the Flisa earthquake

Depth (km)	P Velocity (kms^{-1})	S Velocity (kms^{-1})
0.0	6.20	3.569
20.0	6.20	3.569
20.0	6.70	3.857
35.0	6.70	3.857
35.0	8.15	4.705
95.0	8.15	4.705

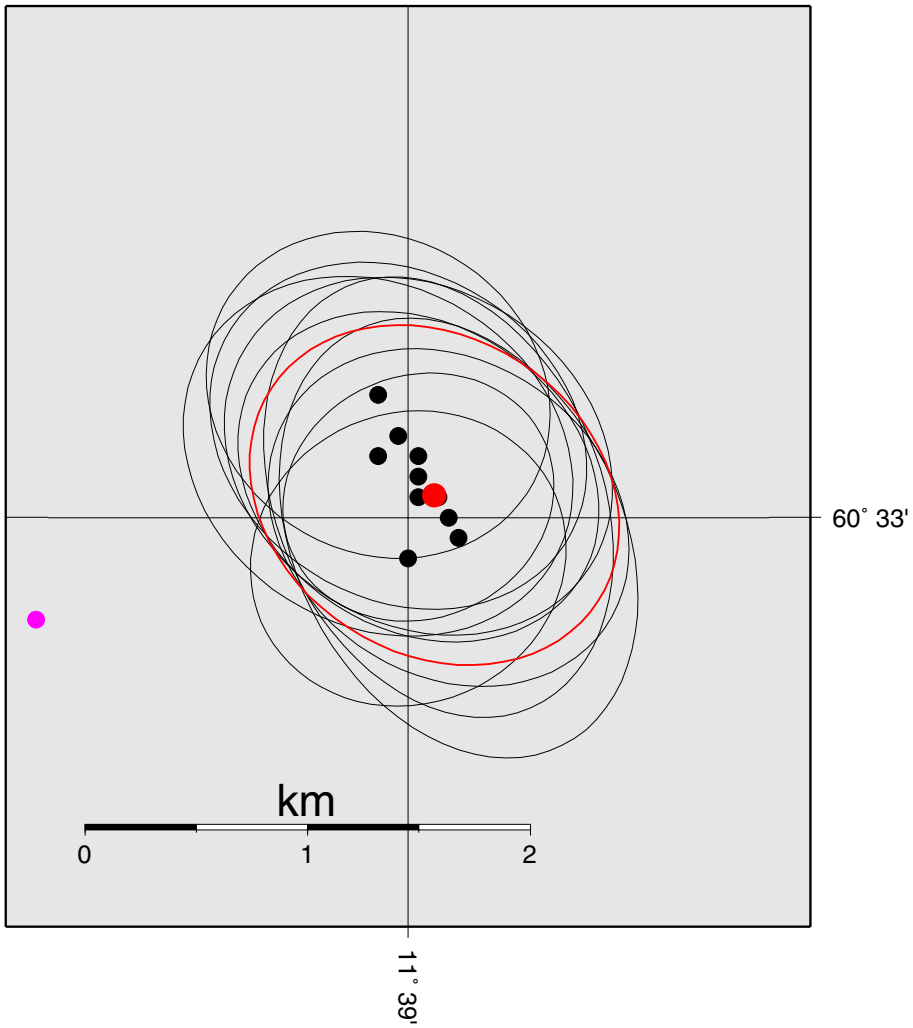

Fig. 6.3.5. Close-up map of locations determined during the model-sensitivity tests. All locations shown in black have RMS and L1 norm values not more than 10% larger than for the final inversion result (red) using the model listed in Table 6.3.2. All error ellipses are for 99.99 confidence level. For comparison the start epicenter from the backazimuth estimates only is also shown (magenta point without error ellipse).

The results of the last inversion are also listed in Table 6.3.3 as solution NORSAR_F. In Fig. 6.3.5 a map with all locations shown including their 99.99% confidence limits (in black), which were found during the model tests and for which the RMS and the weighted L1 norm values are not more than 10% larger than the values for the final inversion. The solution shown in red is the result of the final solution. Note that all solutions calculated for the different models and which have low RMS and weighted L1 norm values lay inside the 99.99 confidence limits of the final solution. The point in magenta shows the epicenter of the start solution, calculated only by the backazimuth observations, and demonstrates the benefits one can achieve from array data.

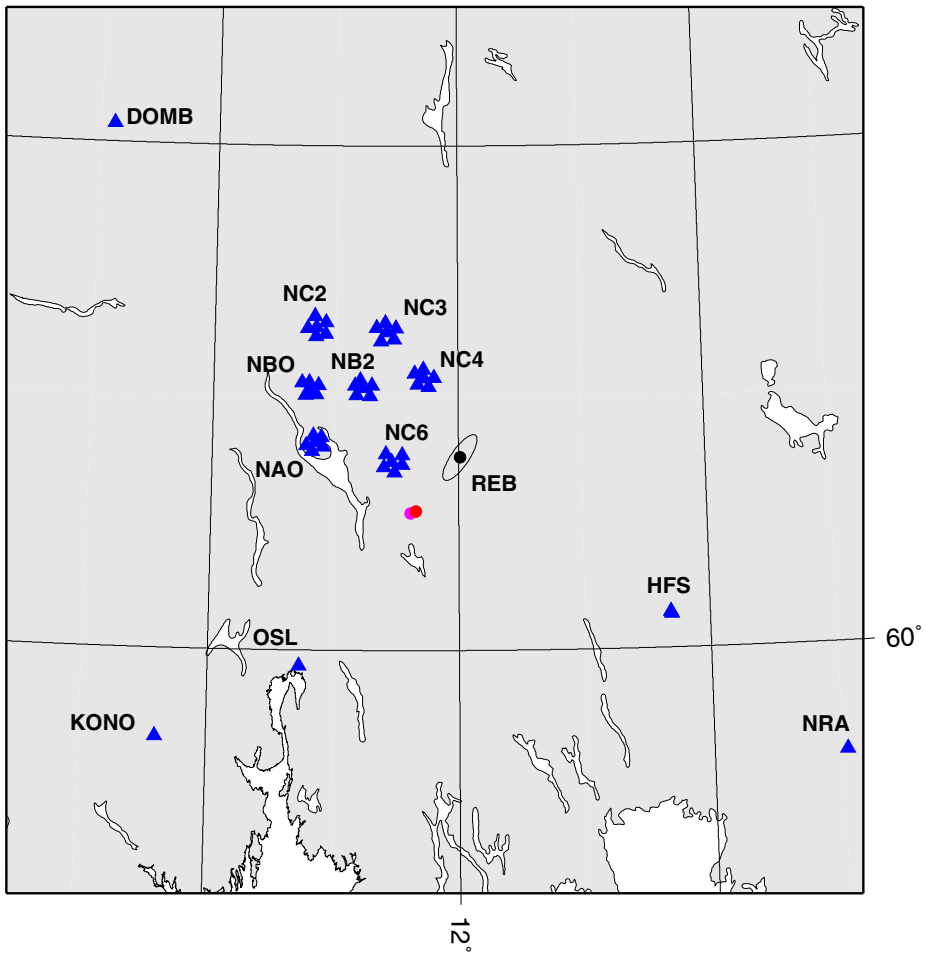

Fig. 6.3.6. The Map shows locations of the Flisa main shock. The red symbol shows the epicenter of the final inversion from this study. The 99.99% confidence ellipse is also plotted but is too small to be seen. In addition we show the epicenter calculated from the backazimuth observations (in magenta), the location results of the IDC, and all stations used in this study to locate the earthquake.

Fig. 6.3.6 shows the results for the final location (NORSAR_F), its 99.99% error ellipse, the stations used, and for comparison the REB location and the epicenter determined only by backazimuth observations (in magenta, now without error ellipse). Note that the error ellipse for the epicenter of the main shock is such small that it is inside of the symbol plotted for the epicenter itself. All numerical values of the location results can be found in Table 6.3.3.

Using the 99.99% (about 3.886 standard deviations in the case of one single parameter) probability limits for the main hypocenter, all the epicenter coordinates are determined within 1 km uncertainty. The model sensitivity tests also showed that the remaining model uncertainties keep the epicenter inside these limits. Therefore, the epicenter of the event can be called a GT-1 event. The uncertainty of the depth determination is slightly larger, in particular due to the influence of the modelling errors. The sensitivity tests showed a bit more than 1 km variation in the depth estimates. Together with the location uncertainty the depth uncertainty is about 2 km. Therefore, this earthquake with a hypocenter in the lower crust can be used to calibrate regional travel-times curves.

Table 6.3.3. Results of the Flisa main shock location. Note that all errors for results of this study are given for 99.99% confidence limits. The IDC uses a 90% confidence limit in its bulletins.

Method	Lat [°]	Lon [°]	Time	Depth [km]	Confidence Limits					Number of Defining Parameters
					Azimuth [°]	Lat / Smaj [km]	Lon/ Smin [km]	Depth [km]	Time [s]	
REB	60.7657	12.0119	08:53:21.18	0.0	35	- 12.0	- 3.9	Fixed	0.73	10
Back-azimuths	60.545	11.613	-	-	-	50.1 -	3.8 -	-	-	158
Wadati	-	-	08:53:19.98	-	-	-	-	-	0.27	43
NORSAR_1	60.5479	11.6501	08:53:20.10	22.7	66.9	0.87/ 0.90	0.84/ 0.87	1.1	0.10	244
NORSAR_F	60.5511	11.6526	08:53:19.96	22.5	123.1	0.74/ 1.06	0.75/ 0.79	0.9	0.09	237

6.3.3 Relative locations for the whole event sequence

In addition to the main shock with its high quality hypocenter determination, one foreshock and seven aftershocks were observed at the NORSAR array and some also at the Hagfors array in Sweden. The foreshock was about 2.5 magnitude units smaller than the main event and was not felt. The aftershocks, which were of even smaller magnitude, were also not felt. Fig. 6.3.7 shows the uncorrected amplitude-power spectra of the main shock, the foreshock and the first aftershock as observed at NC602, one of the seismometer sites closest to the events.

When possible, the onset times of P and S waves were measured by cross-correlation methods. If this was not possible due to a low signal-to-noise (SNR) ratio, the relative onset times were estimated by following common features of the pulse forms from one site to the next. The foreshock and six of the seven known aftershocks could be located relatively to the main shock by applying a master-event algorithm (Schweitzer, 2002). For the foreshock and the first after-

shock recordings from the Hagfors array could also be used. For these two events, a better control of the relative location can be assumed, since the defining data are not exclusively from one direction. Table 6.3.4 gives all details of the estimated relative locations and Fig. 6.3.8 shows a map of all located events. No confidence region is shown for the main shock, since if the main shock is moved all relatively located events will move as a whole group by the same amount. The shown error ellipses for the relatively located events correspond with 99.99% confidence regions.

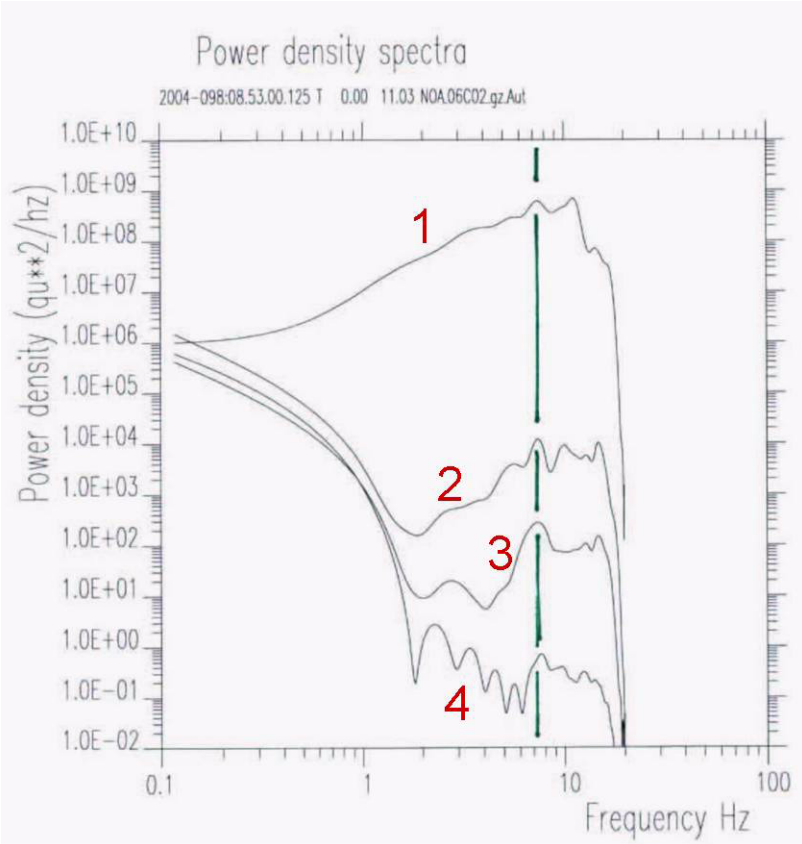

Fig. 6.3.7. Uncorrected power-density spectra of the main shock (1), the foreshock (2), the first aftershock (3), and a noise sample (4) as recorded at the NORSAR array site NC602. The spectral peak for all spectra at about 8 Hz is best explained as a station effect. Note the large range of magnitudes for the different events.

The error ellipse of the foreshock overlaps with the main event, occurring ca. 13 seconds later. This connects these two events closely together to the same rupture plane. Such conclusion cannot be made for the aftershocks, which all occurred in the same source region and depth, but about 1 - 3 km apart from the main shock. For a magnitude 3.5 event the rupture length should not have such an extension. Since all aftershocks are located in the same area, we can either assume that the relative location of these smaller events show some systematic bias or that the first two larger events changed the whole stress field at this place such that the aftershock sequence could occur.

Table 6.3.4. Listing of all relative locations for the whole Flisa earthquake sequence with the main shock as reference event. Given uncertainties for 99.99% confidence limits.

Event	Lat [°]	Lon [°]	N-S [km]	+/- [km]	E-W [km]	+/- [km]	Time [s]	+/- [s]	Depth [km]	+/- [km]
MS	60.5511	11.6526	-	-	-	-	-	-	-	-
FS			-0.214	0.429	-0.099	0.365	-13.43	0.35	-0.001	0.051
AS-1			-1.405	1.784	1.589	1.240	5956.01	1.24	0.353	0.190
AS-2			-1.074	1.853	1.341	0.961	6543.41	1.55	-0.114	0.121
AS-3			-1.945	2.595	1.883	1.171	109659.58	2.14	-0.223	0.190
AS-4			-1.162	0.159	1.407	0.077	112903.46	0.12	-0.038	0.019
AS-5			-1.175	0.618	1.602	0.356	126451.43	0.54	-0.135	0.054
AS-6			-1.536	2.110	1.746	1.188	189400.42	1.79	-0.067	0.194

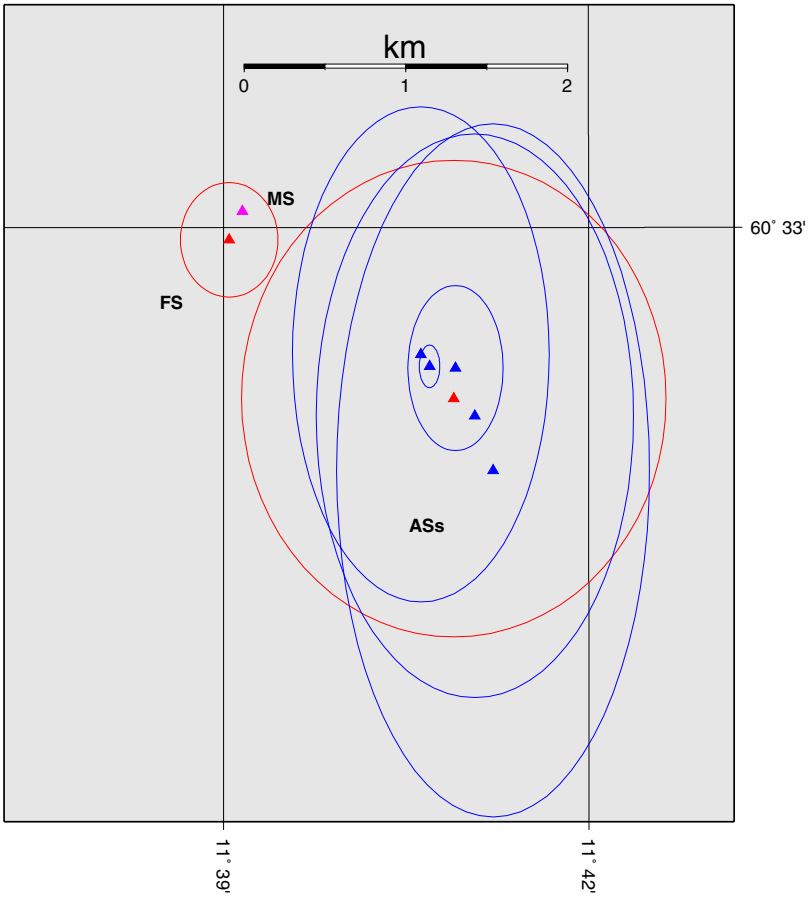

Fig. 6.3.8. A map of all events of the Flisa earthquake sequence as located by a master-event algorithm. The two events shown in red had been relatively located also with Hagfors readings, the magenta triangle show the epicenter of the main shock.

6.3.4 Fault Plane Solution of the Main Shock

As mentioned, the main shock of the Flisa events sequence was observed at almost all stations in Fennoscandia and at many other European stations. Already during the initial analysis of the event it became evident that a polarity change of the first P onsets could be observed for the recordings of the NORSAR array. Fig. 6.3.9 shows first onset recordings from selected NORSAR sites that demonstrate this observation.

After collecting seismograms from all seismic stations up to about 15˚ epicentral distance, a careful analysis of first onset polarities showed that the SNR for all stations from Central Europe was too low for measuring a first onset polarity. However, at almost all stations from Fennoscandia and one in Estonia such a measurement was possible and a classical fault-plane solution could be achieved.

This solution was even better constrained by adding observed polarities from PmP observations at the vertical components of the NORSAR subarray NC2. Fig. 6.3.10 shows a map with the fault-plane solution and the stations from which polarity data were used to derive this solution.

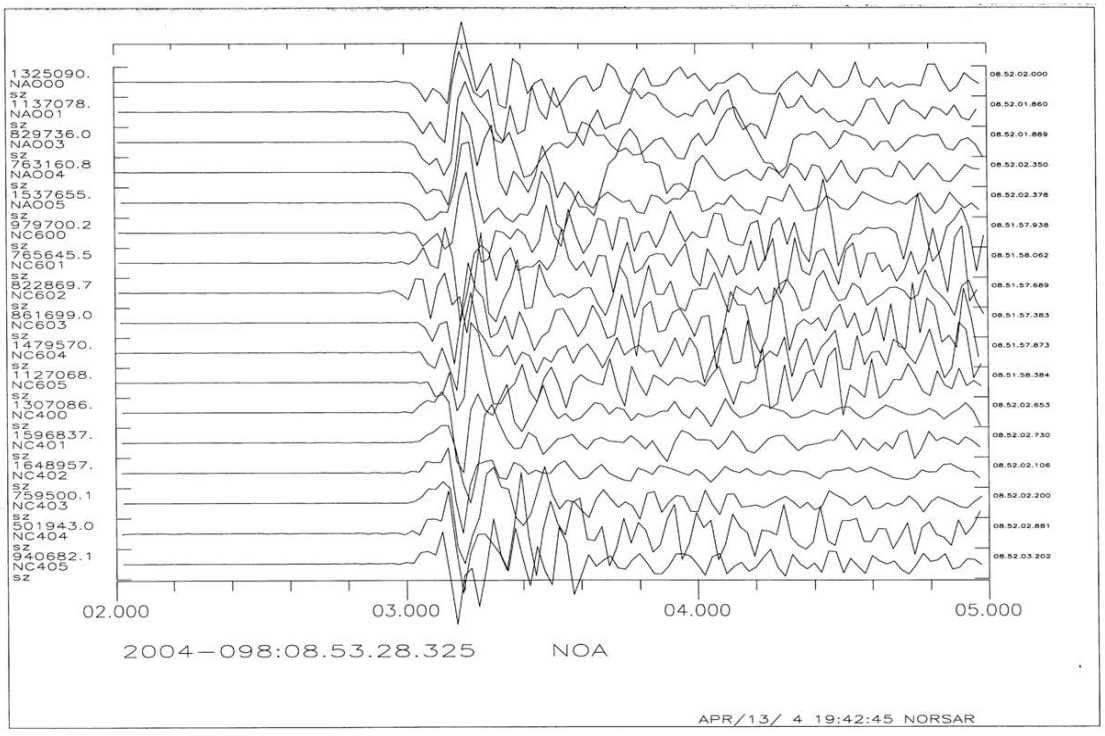

Fig. 6.3.9. P onsets of the Flisa main shock as observed at the NORSAR subarrays NA0, NC4, and NC6. All data are unprocessed but aligned along the first onsets. Note the polarity change from top to bottom.

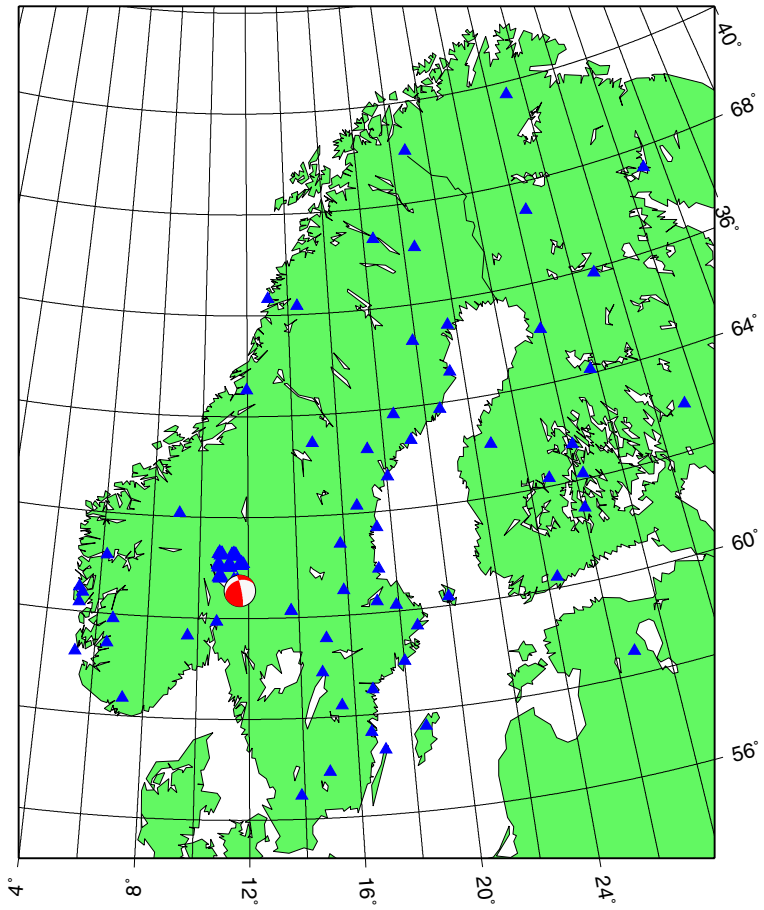

Fig. 6.3.10. The map shows all stations used for determination of the fault plane solution of the Flisa main shock.

The FOCMEC inversion routine (Snoke, 2003) was applied to calculate all possible fault planes, which are in agreement with the observed polarities. The assumption for this type of inversion is that a single double couple can describe the source mechanism. Fig. 6.3.11 shows all observed polarities and the results from FOCMEC. The triangles represent negative and the circles positive first onset polarities.

As fault plane the very steep, north-south striking plane can be assumed since the second plane is horizontally oriented and such a horizontal movement in the lower crust is difficult to achieve. Many earthquakes in and around the Oslo Graben area show similar north-south striking fault planes but a large variability in the orientation of auxiliary plane; almost every type of source mechanism can be observed: normal faulting, strike-slip movements, and reverse faulting (see e.g., Hicks et al., 2000; Lindholm et al., 2000). Although the tectonic features in the lower crust must not the same as at the surface, the geological observations at the surface further support this interpretation as the many mapped faults show a north-south striking direction (see Fig. 6.3.1).

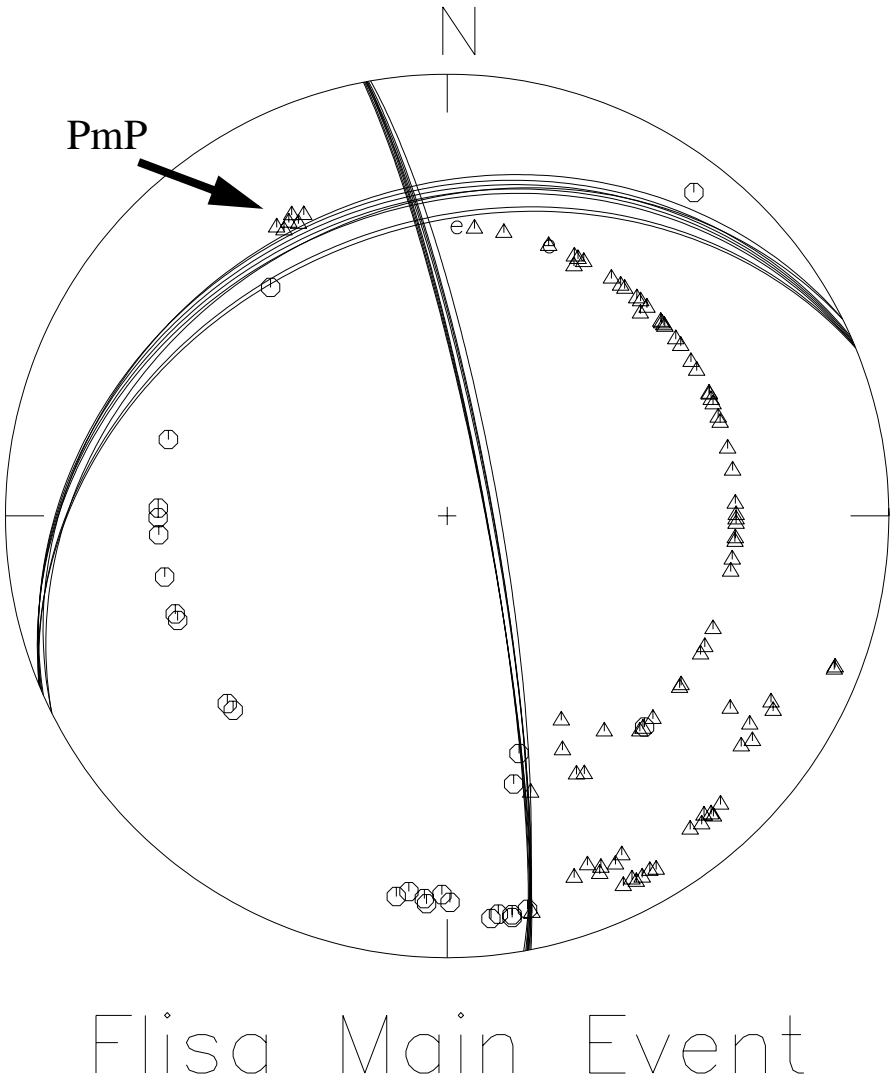

Fig. 6.3.11. Fault-plane solution for the Flisa main shock as derived from first onset polarities. The plot shows all polarities projected on the lower hemisphere. Triangles are negative and circles are positive first onsets. All possible solutions found by FOCMEC (Snoke, 2003) are plotted. The most presumable rupture plane is one of the steep north-south striking fault-planes. Note, the negative polarities of PmP observed at the sites of the NORSAR subarray NC2, which restrict the number of possible solutions.

6.3.5 Conclusions

To calculate a start solution for the hypocenter inversion of the 7 April 2004 Flisa main event, classical location procedures were applied including backazimuth observations, Wadati diagram and an optimized velocity model.

The inversions were performed with the HYPOSAT location program, which can use all available data (onset times of first and later onsets, backazimuth and slowness observations, travel time differences between phases, and different types of corrections) to achieve the best least-squares-fit type solution.

Investigation of model uncertainties associated with changes made to NORSAR's standard velocity model, revealed that the best fit was achieved when the thickness of the upper crust was increased to 20 km. This is also in agreement with recent results of a surface wave study (Bischoff et al., 2004).

Our best location estimate of the Flisa main event is:

Lat:	60.5511˚
Lon:	11.6526˚
Depth:	22.5 km
T0:	08:53:20.0

One foreshock and several aftershocks were observed. After applying the master-event technique, the foreshock and six of the aftershocks could be located relatively to the main event.

The fault-plane solution for the main shock was determined in the traditionally way from first onset observations at numerous stations. In addition, some PmP polarities were used to restrict the solution space. The resulting fault-plane solution shows a north-south striking reverse fault plane, which was presumable also the rupture plane of the main shock.

Acknowledgements

For this study we received data from the University of Bergen for the Norwegian network, from the University in Uppsala for the Swedish network, from the University of Helsinki for the Finnish network, and from ORFEUS the data for all stations contributing to the Virtual European Broadband Seismograph Network (VEBSN). The precise event location and in particular the well defined fault-plane solution would not have been possible without such data exchange, which is gratefully acknowledged.

Johannes Schweitzer

References

Aki, K., A. Christofferson & E. Husebye, E.S. (1977). Determination of the three-dimensional seismic structure of the lithosphere. *J. Geophys. Res.*, **82**, 277-296.

Bischoff, M., J. Schweitzer & T. Meier (2004). Comparison of the Love-Rayleigh discrepancy in central Europe (GRSN) and southern Scandinavia (NORSAR). *NORSAR Sci. Rep.,* **2-2004**, 70-78.

Gundem, M.B. (1984). *2-D seismic synthesis of the Oslo graben*. Cand. Scient. Thesis, University of Oslo, Norway, 164 pp.

Hicks, E. C. (1996). *Crustal stresses in Norway and surrounding areas as derived from earthquake focal mechanism solutions and in-situ stress measurements.* Cand. Scient. Thesis, University of Oslo, Norway, 164 pp.

Hicks, E.C., H. Bungum & C.D. Lindholm (2000). Stress inversion of earthquake focal mechanism solutions form onshore and offshore Norway. *Norsk Geologisk Tidsskrift,* **80**,235-250.

Lindholm, C.D., H. Bungum, E. Hicks & M. Villagran (2000). Crustal stress and tectonics in Norwegian regions determined from earthquake focal mechanisms. In: Nottvedt et al. (eds). Dynamics of the Norwegian Margin. Geological Society London, 167, 429-439.

Mykkeltveit, S., & Ringdal, F. (1981). Phase identification and event location at regional distance using small aperture array data. In: Husebye, E.S. & Mykkeltveit, S. (eds). *Identification of seismic sources – earthquake or underground explosions*, D. Reidel, 467-481.

Schweitzer, J. (2001). HYPOSAT – an enhanced routine to locate seismic events. *Pure appl. geophys.,* **158**, 277-289.

Schweitzer, J.(2002). Some results derived from the seismic signals of the accident of the Russian submarine Kursk. *NORSAR Sci. Rep.*, **1-2002**, 115-121.

Snoke, J. A. (2003). FOCMEC: FOcal MEChanism determinations. In: Lee, W. H. K., H. Kanamori, P. C. Jennings & C. Kisslinger (eds). *International Handbook of Earthquake and Engineering Seismology.* Academic Press, San Diego, Chapter 85.12.

Wadati, K. (1933). On the travel time of earthquake waves. Part. II. Geophys. Mag. (Tokyo) **7**, 101-111.

6.4 Data from deployment of temporary seismic stations in northern Norway and Finland

Sponsored by National Nuclear Security Administration
Contract Nos. DE-FC52-01SF22420 (NORSAR) and W-7405-Eng-48 (LLNL)

6.4.1 Introduction

This short contribution is a description of data now available in NORSAR's data archives from a temporary deployment during 2002 - 2004 of six seismic stations in northern Norway and Finland.

Explosions in underground as well as open-pit mines in the Khibiny massif of the Kola Peninsula of northwestern Russia are conducted on a frequent and relatively regular basis. It was decided to supplement the network of permanent stations in northern Fennoscandia and northwest Russia with temporarily deployed stations, in order to record these explosions, as well as other mining explosions and natural events occuring in this general area. As shown in Fig. 6.4.1, the six temporary stations were deployed along two profile lines, extending westwards from the Khibini massif. The rationale for this deployment was to collect data to examine distance as well as azimuthal dependance of seismic discriminants. As can be seen from Fig. 6.4.1 the southernmost of the two profile lines runs through the permanent seismic array ARCES in northern Norway.

6.4.2 Station equipment and locations

Six RefTek 72A-08 data loggers (Refraction Technology) equipped with three-component GS-13 seismometers (Teledyne Geotech) occupied positions along two profile lines during the time period from 27 August 2002 to 9 September 2004. Table 6.4.1 lists station names and coordinates. Two of the six stations, Ivalo (IVL) and Kaamasmukka (KMM), were located in northern Finland, and the remaining four were deployed in the Finnmark county of northern Norway. These were the sites Neiden (NDN), Skogfoss (SKF), Skoganvarre (SKV), and Varangerbotn (VGB). Fig. 6.4.2 shows a picture for the installation at VBG. During the deployment period of 745 days, a local representative of NORSAR visited the sites nine times to check the station status and to change the RefTek field disks. These were sometimes labeled with the alternative station codes GMM, SFS, and VRB instead of KMM, SKF, and VGB, respectively.

The seismometer coordinates at the stations NDN and VGB were determined directly with a GPS receiver, whereas the seismometer positions at the other stations were estimated from the corresponding data logger location using azimuth and distance to the seismometer. Each data logger location was taken as the median value of all (of the order of thousands) automatic GPS positionings done by the recorder during time corrections (see also the following section). Typically, the individual coordinates measured deviated less than about 20 m from the respective median value. Elevations for the stations in Norway were also verified with topographic maps in the scale 1:50000.

The natural frequency of the GS-13 seismometers is adjustable from 0.75 Hz to 1.1 Hz and was set to 1 Hz here. For calibration purposes, Table 6.4.2 lists the coil generator constant of each sensor at each site, and Table 6.4.3 includes the calculated calibration constants (in nm/count)

at 10 Hz. The vertical component is denoted as Z, and the horizontal components point to north (N) and east (E), respectively.

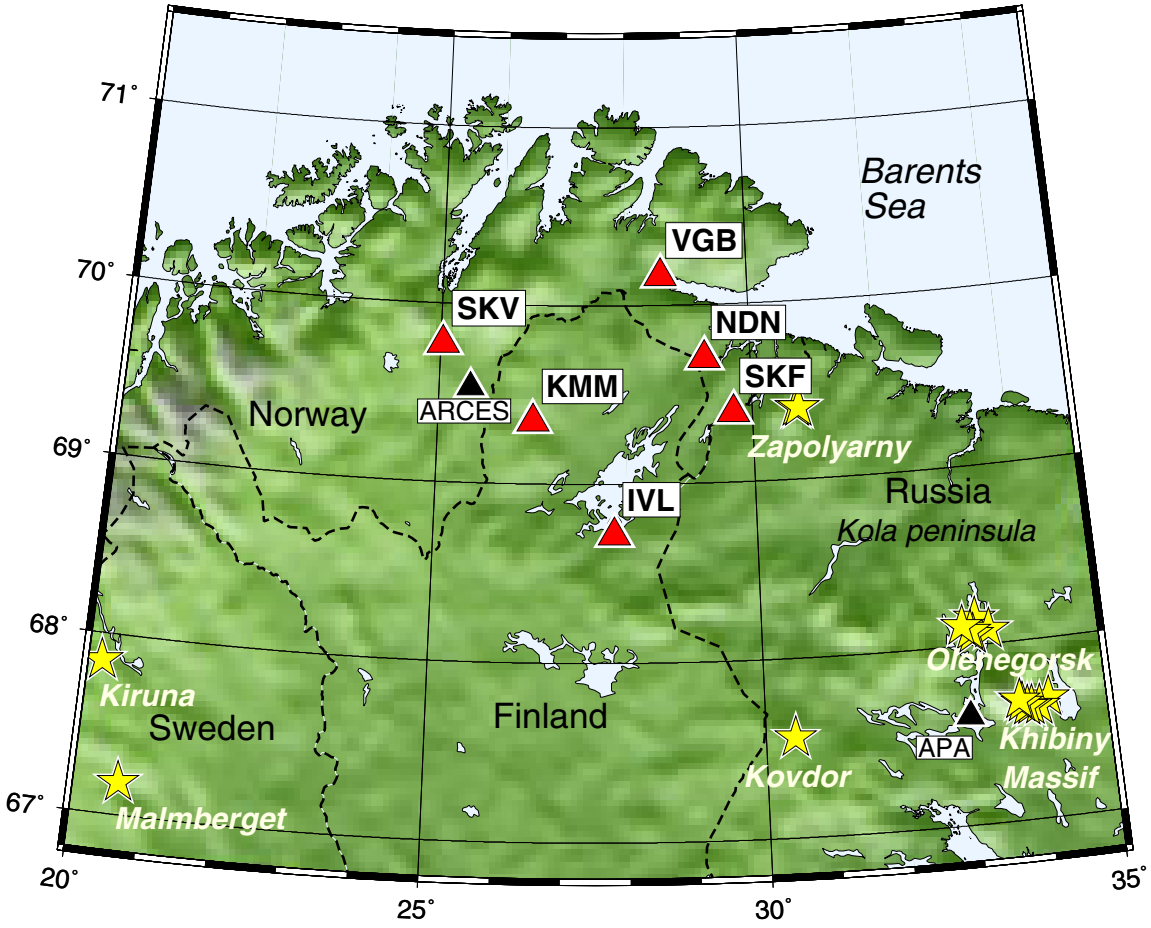

Fig. 6.4.1. Map of six temporary seismic stations (red triangles) in northern Norway and Finland, permanent seismic arrays (black triangles), and mining areas (yellow stars).

Table 6.4.1. Station names and locations

Location	Station	Recorder No.	Lat. N	Lon. E	Elev. [m]
Ivalo	IVL	689	68.71513	27.80159	120
Kaamasmukka	KMM	853	69.34849	26.51432	220
Neiden	NDN	856	69.69850	29.26333	90
Skogfoss	SKF	686	69.39041	29.70506	60
Skoganvarre	SKV	852	69.77436	25.04407	220
Varangerbotn	VGB	855	70.16445	28.57550	6

Fig. 6.4.2. This picture shows the seismometers at station Varangerbotn (VGB), before they were covered by soil, moss, and heather.

Table 6.4.2. Instrumentation (GS-13 sensors)

Station	Rec. No	Rec. Chan.	Comp.	Sensor S/N	Main coil generator constant [Vs/m]
IVL	689	4	Z	115	2130.4
		5	N	292	2366.0
		6	E	294	2344.0
KMM	853	4	Z	133	2311.4
		5	N	128	2305.6
		6	E	283	2304.0
NDN	856	4	Z	114	2118.9
		5	N	111	2130.0
		6	E	113	2133.0
SKF	686	4	Z	112	2159.8
		5	N	285	2369.0
		6	E	288	2344.0
SKV	852	4	Z	286	2343.0
		5	N	296	2335.0
		6	E	297	2353.0
VGB	855	4	Z	265	2337.0
		5	N	273	2339.0
		6	E	284	2323.0

6.4.3 Data recording

The RefTek data loggers recorded digital data continously with a sampling rate of 100 Hz and with a dynamic range of 24 bits. In a testing phase during the first deployment days, the recorder's preamplifier gain was set to 32 at some stations, but was then adjusted to 1 for the remaining period. The adjustment times are given in Table 6.4.3 together with other acquisition parameters.

These digitized data (counts) were written in a native, compressed format (*RefTek C0*) to a hard disk attached to each data logger. The record length was 360054 samples, i.e. about 1 hour. The internal clock of each data logger was also adjusted nominally every hour using the time signal of the GPS satellites. All times are given in GMT.

Dump files of the recorder's hard disks were sent to NORSAR for subsequent data format conversion, quality control, and archiving. In a first step, the compressed data of all three components (channels) were expanded into a modified version of SEG-Y traces that can handle the long record length and keeps data logger specific information such as trace scaling. The recorder log files were also retrieved then. The logs include status information of the instruments, as well as time adjustments applied and its geographic location. In a second step, the SEG-Y traces were converted into the CSS3.0 format as one single file for each record (360054 samples) and the three components of each station. This format conversion was done mainly with the PASSCAL software package, and only the station name assignment utilized NORSAR's in-house EP program. These CSS data (more than 200 GB) are delivered to Lawrence Livermore National Laboratory (LLNL), USA, to be included in their archive system. At NORSAR the final archive format is slightly different. Here, the data from all available stations were merged into single CSS3.0 files of exactly 1 hour length (360000 samples) and starting always at full hours. Additionally, calibration information was added (see also Table 6.4.3). This final format conversion step was also done with EP.

As shown in Fig. 6.4.3, data recording for the various stations ranged between about 38% and 89% of the entire deployment period. Table 6.4.4 and Fig. 6.4.4 provide an overview of the days for which data are available. The stations with the longest uptime are IVL followed by VGB. Small data gaps at all stations are usually related to recorder maintanance (change of disk) or possible hard disk errors, i.e. bad blocks resulting in data decompression failure. The large gaps are caused by full disks, when a station could not be accessed in time for various reasons, or by failures of station power supply or recorder hardware. An example of the latter case is station SKF, which stopped operating already in the middle of 2003. Even though the average uptime must be rated as rather low, a high number of mining events were recorded during this two-year period, and this was the main objective of the deployment.

Except for the data gaps the data quality is generally good for seismic monitoring of events related to the mining activity on the Kola peninsula and for the analysis of teleseismic events. However, the initial quality control of the data revealed some scaling problems at the stations SKF and KMM during limited time periods in 2003. These scaling problems appear as anomalously high amplitudes of the recorded data and are most likely related to recorder hardware malfunction. At station SKF, this affected recordings of the vertical (Z) component from 2003-123:18.52.32 (after a data gap) until the station stopped operating at 2003-197:21.08.32. The data of station KMM show anomalously high amplitudes on all components starting at 2003-205:13.36.56 and a more gradual amplitude decrease to the normal noise level at 2003-

224:02.40.57. Besides that, data from the east (E) component of station NDN appear to be unusable for the entire recording period.

6.4.4 Example of data recorded

On 16 November 2002, one underground (total yield 257 tons for one ripple-fired explosion) and one open-pit explosion (total yield 430 tons for four separate ripple-fired explosions) were carried out in one of the mines in the Khibiny massif. The explosions were only 300 m apart, with the underground explosion occurring about 3 minutes before the open-pit explosion. These explosions were described in Ringdal et al. (2004), who noted a remarkable difference between the two sources in terms of spectral content: At lower frequencies, the underground explosion was stronger by a factor of 10 in amplitude, whereas the open-pit explosion was the stronger for high frequencies. Fig. 6.4.5 shows all data available from the temporary stations for these two explosions, for six different filter bands, ranging from 2-4 Hz in the upper left corner to 10-20 Hz in the lower right corner. In addition, data are shown for the central three-component station ARA0 of the ARCES array. The epicentral distances are 260 km for SKF, 279 km for IVL, 401 km for ARCES and 430 km for SKV. The spectral pattern found by Ringdal et al. (2004) for the station IVL is confirmed by all stations. Note that there is an interfering teleseismic signal (from an mb 5.4 event in the Kuriles) at about the time of the P-arrival for the underground explosion, most clearly seen for stations ARA0 and SKV in the lower passbands.

This work was performed, in part, under the auspices of the U.S. Department of Energy by the University of California, Lawrence Livermore National Laboratory under Contract W-7405-Eng-48 (UCRL Number: UCRL-SR-209656).

Reference

Ringdal, F., T. Kværna, E. Kremenetskaya, V. Asming, S. Kozyrev, S. Mykkeltveit, S. J. Gibbons, and J. Schweitzer (2004). Research in regional seismic monitoring. *Semiannual Technical Summary 1 January - 30 June 2004*, NORSAR Sci. Rep. 2-2004, Kjeller, Norway.

Nils Maercklin
Svein Mykkeltveit
Johannes Schweitzer
Don Rock, Lawrence Livermore National Laboratory
David B. Harris, Lawrence Livermore National Laboratory

Table 6.4.3. Data acquisition parameters and calibration constants

Station	Rec. No.	Rec. Chan. & Comp.	Sample rate [Hz]	Pre-amp. gain	Calibration constant at 10 Hz [nm/count]	Start time
IVL	689	4, Z	100	32	0.0004444425	2002-239:15.13.54
		5, N		32	0.0004001860	
		6, E		32	0.0004030821	
		4, Z	100	1	0.0142221575	2002-244:10.52.50
		5, N		1	0.0128059518	
		6, E		1	0.0128986306	
KMM	853	4, Z	100	1	0.0131056206	2003-048:18.08.49
		5, N		1	0.0131414299	
		6, E		1	0.0131505564	
NDN	856	4, Z	100	32	0.0004468545	2002-241:13.32.00
		5, N		32	0.0004445258	
		6, E		32	0.0004439007	
		4, Z	100	1	0.0142993456	2002-243:08.20.01
		5, N		1	0.0142248280	
		6, E		1	0.0142048199	
SKF	686	4, Z	100	1	0.0140285588	2002-241:10.00.54
		5, N		1	0.0127897355	
		6, E		1	0.0129261443	
		4, Z	100	32	0.0004383925	2002-242:13.31.29
		5, N		32	0.0003996793	
		6, E		32	0.0004039420	
		4, Z	100	1	0.0140285588	2002-242:14.20.32
		5, N		1	0.0127897355	
		6, E		1	0.0129261443	
SKV	852	4, Z	100	1	0.0129316621	2002-245:13.08.12
		5, N		1	0.0129759666	
		6, E		1	0.0128767031	
VGB	855	4, Z	100	32	0.0004051519	2002-242:10.29.42
		5, N		32	0.0004048055	
		6, E		32	0.0004075936	
		4, Z	100	1	0.0129648616	2002-243:10.45.58
		5, N		1	0.0129537756	
		6, E		1	0.0130429979	

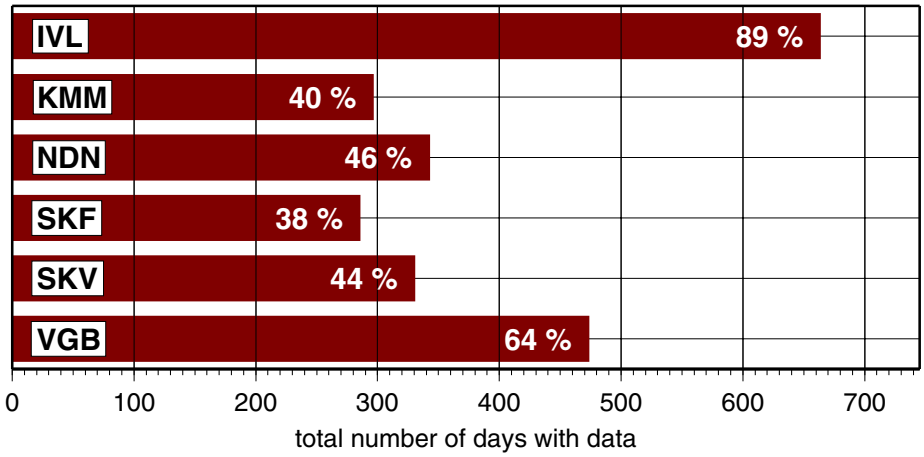

Fig. 6.4.3. Percentage of days of operation for each of the six temporary stations operating in northern Norway and Finland between 27 August 2002 and 9 September 2004. Continuous recording during the entire deployment period of 745 days corresponds to 100%.

Table 6.4.4. Data availability

Station	Year	Days of operation (Julian numbers)
IVL	2002 2003 2004	239-293, 314-365 001-017, 044, 049-173, 176-177, 180-220, 223-233, 236-317, 317-365 001-039, 040-115, 140-253
KMM	2003 2004	048-157, 176-224, 274-282, 316-365 001-016, 020, 039-047, 056, 140-191
NDN	2002 2003 2004	241-243 097-161, 164-240, 340-352, 355-357, 360-365 001-002, 005-007, 010-020, 023-038, 039-081, 139-152, 155-186, 189-191, 194-196, 199-208, 211-217, 220-247, 250-252
SKF	2002 2003	241-245, 248-320, 323-365 001-038, 053-098, 101-106, 123-197
SKV	2002 2003 2004	245-361 061-066, 069-176, 241-266, 297, 315-365 001-023
VGB	2002 2003 2004	242-314 097-098, 100-164, 177-244, 248-316, 340-365 001-004, 007-030, 035-036, 037-107, 133-202

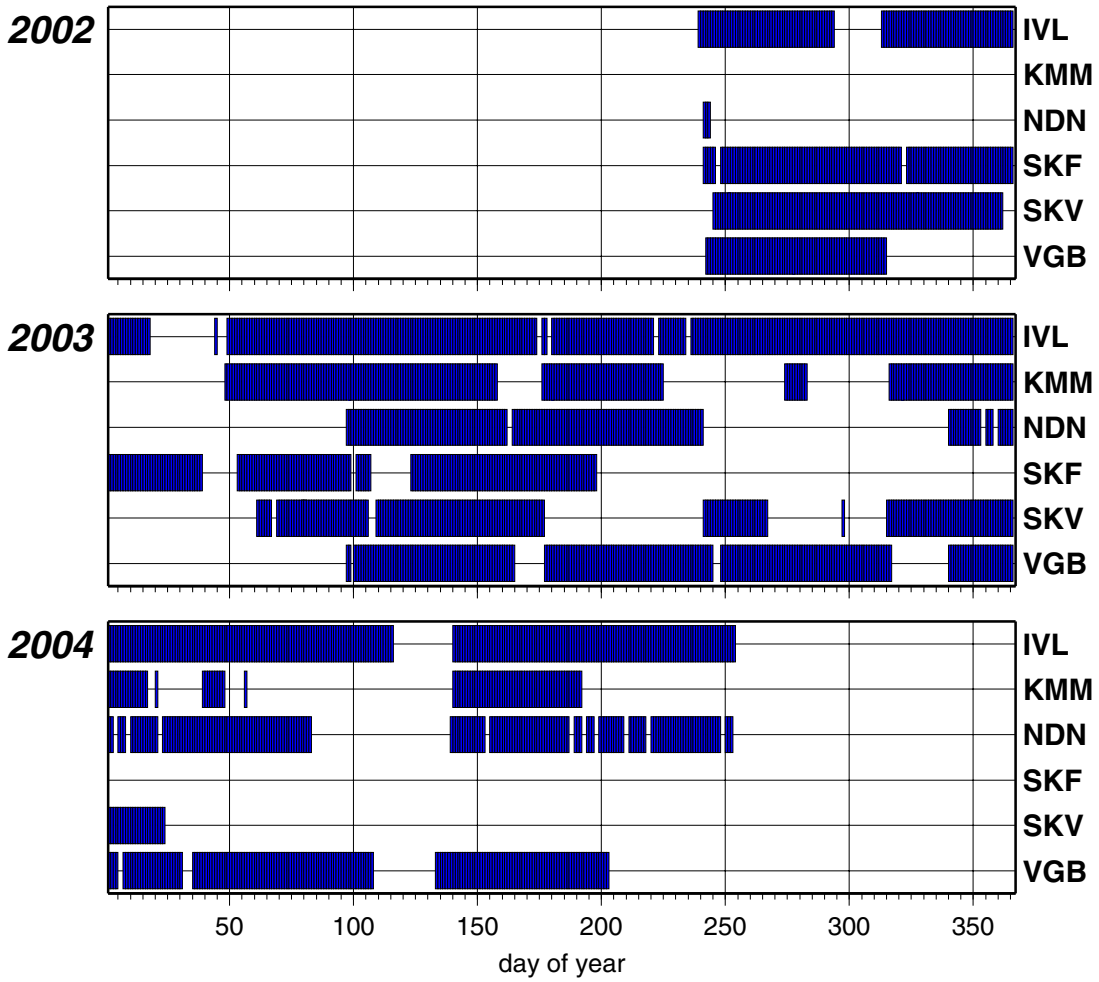

Fig. 6.4.4. Overview of days with data available from the six temporary stations operating in northern Norway and Finland between 27 August 2002 and 9 September 2004. The station locations are given in Fig. 6.4.1 and Table 6.4.1.

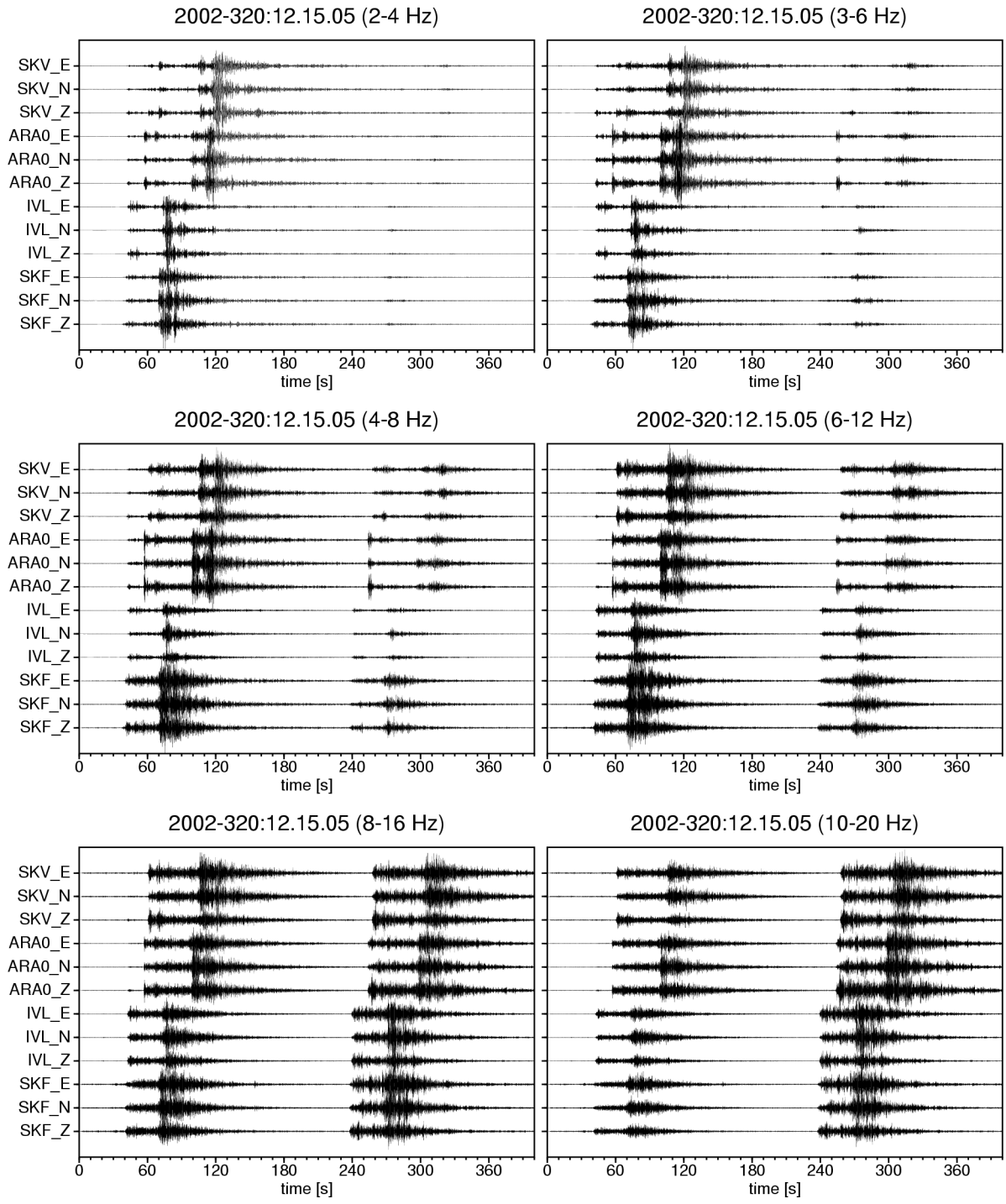

Fig. 6.4.5. The figure shows data from three of the temporary stations (SKF, IVL and SKV) as well as the three-component station ARA0 of the ARCES array for two explosions in the Khibiny massif (see the text for details on the explosions). The data are filtered in six different frequency bands, as shown in the headers. All seismograms have been trace normalized, and the plot start time is the origin time of the first explosion, also given in the headers.

6.5 The Sumatra M_W=9.0 earthquake as a high-end test of NORSAR's processing capability

6.5.1 Background

The Sumatra earthquake hit on December 26, 2004, and caused the most damaging tsunami historically recorded, and at the time of writing nearly 300,000 casualties have been confirmed. The M_W=9.0 megathrust earthquake was the globally largest in 40 years, and ruptured nearly 1200 km of the subduction zone separating the India and Burma plates. It was recorded on the NORSAR arrays in Norway at approximately 84 degrees distance, and examples of recordings at NORSAR stations are shown in Fig. 4.4.7 in Section 4. The first P-arrival reached the NOA array approximately 12 minutes after the rupture started.

The earthquake occurred along the NW part of the Sumatra-Java subduction zone, and the general plate convergence in this region is oriented towards NNE with an average velocity of 5.5 to 6.0 cm/year. Recent studies in the region have revealed that the rupturing segment of the plate boundary has been locked for quite some time since three large earthquakes (M>8.0) that occurred in the same general area in 1833, 1861 and 1881 (Simoes et al., 2004; Ortiz and Bilham, 2003). Fig. 6.5.1 shows the recent seismicity in the region, including also the largest historical events.

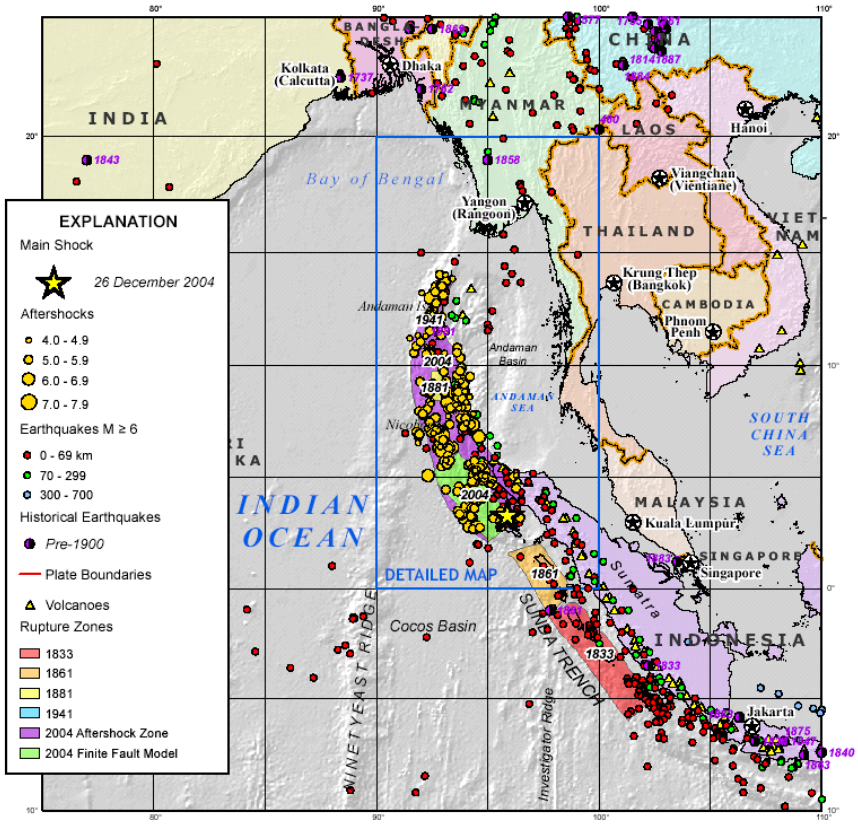

Fig. 6.5.1. Historical earthquakes and aftershocks following the 2004 megathrust earthquake. The historical large earthquakes are indicated with red circles. From USGS poster.

6.5.2 NORSAR's seismic processing system

NORSAR carries out routine detection processing and interactive analysis of seismic events, both globally (using mainly the teleseismic NOA array) and regionally (using the network of regional arrays in Fennoscandia and NW Russia). The processing algorithms in use at the NORSAR Data Center comprise the following steps:

- Automatic single array processing, using a suite of bandpass filters in parallel and a beam deployment that covers the main seismic phases for the region of interest.
- An STA/LTA detector applied independently to each beam, followed by broadband f-k analysis for each detected phase (best beam) in order to estimate azimuth and apparent velocity.
- Automatic single-array location of seismic events, by using a "beampacking" algorithm for teleseismic events and by associating P and S type phases for events at regional distances.
- For events at regional distances, the Generalized Beamforming (GBF) approach is used (Ringdal and Kværna, 1989) to associate phases from all stations in the regional network and thereby provide automatic network-based locations. Selected events are later analyzed interactively, and the results are published on the Internet.
- For teleseismic events detected by the NOA array, all detected events are reviewed by the analyst, and the reviewed solutions are published in the monthly NORSAR teleseismic event bulletin. This reviewed bulletin is also available on the Internet.

NORSAR has also developed an earthquake alert system, which has been described in a previous Semiannual Report (Schweitzer, 2003). In fact, two independent alert procedures are in effect at NORSAR: One is based on the automatic NOA teleseismic event list, and the second one uses the detection lists from all of the seismic arrays operated by NORSAR in order to provide automatic network-based event locations for large earthquakes. Whenever a large earthquake is detected by the system, alerts are generated automatically and sent to specific subscribers within minutes of the event. The performance of the alert system for the large Sumatra earthquake is described in more detail below. (The NOA processing include longer wait time to allow for teleseismic phase association.)

6.5.3 Processing of the 26 December earthquake

The travel time of seismic P-waves from Sumatra to Fennoscandia is about 12-13 minutes, and the time sequence of NORSAR's processing of the Sumatra earthquake is summarized in Table 6.5.1.

The first alert (based on joint processing of the Fennoscandian arrays) was issued at 01.18 GMT, i.e. about 19 minutes after the earthquake rupture started, and about 7 minutes after the signals were detected by the NORSAR array systems. The second alert (based on NOA single-array processing) was issued 2 minutes later, at 01.20 GMT.

Table 6.5.1 Time-line for NORSAR's processing of the Sumatra earthquake

Time (GMT) 26.12.04	Description
00.58.50	"Origin time" of the M=9.0 Sumatra earthquake. The fault rupture continued during 5-6 minutes.
01.10.45	Seismic P-wave arrival at the closest Fennoscandian array (FINES)
01.11.24	Seismic P-wave arrival at the large NOA array
01.18	Automatic alert message generated by the NORSAR NEWS system (based on network processing): 2004/12/26 00:59:04.97 4.59N 93.33E m_b=5.5 Message sent to EMSC as well as subscribing institutions/persons
01.20	Automatic alert message generated by the NOA single-array processing: 2004/12/26 00:58:59.4 2.7N 92.6E 33 m_b=6.3 Message sent to EMSC as well as subscribing institutions/persons

6.5.4 Epicenter locations

The source parameters for the main shock as provided by the NOA array's automatic location procedure and the US Geological Survey is provided in Table 1. The NOA solution locates the epicenter 378 km to the NW of the USGS epicenter, which is regarded as acceptable for a fully automated solution generated only minutes after the first arrivals hit the stations east of Hamar, Norway.

The automatic NOA solutions of the aftershocks were compared with the multi-station QED solutions published by USGS, and a median epicenter difference of 271 km was found between the two groups. Fig. 6.5.2 compares the aftershocks as located by the European-Mediterranean Seismological Centre (EMSC) with the NOA automatic solutions, and essentially shows the same situation. While the greater spread in the automatic NORSAR locations is evident, the location estimates concentrate well around the main rupture zone, lending credibility to the basic processing algorithms.

Table 6.5.2. Source parameters from NOA array's automatic single array location compared with the reviewed solution of USGS

Source parameter	NOA (automatic)	USGS (Manually corrected)
Magnitude	6.3 m_b	9.0 M_w
Origin time	Dec. 26; 00:58:59.4	Dec. 26; 00:58:53
Depth	33 km	30 km
Latitude	2.70N	3.307N
Longitude	92.60E	95.947E

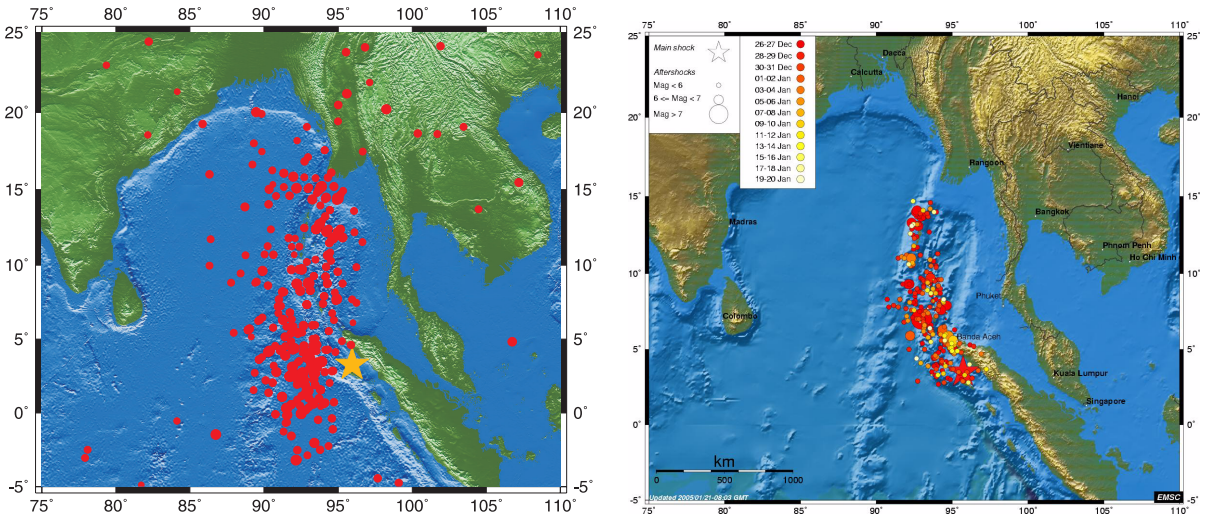

Fig. 6.5.2. Left: Automatic one-array NOA locations. Right: The aftershock distribution in the EMSC database (reviewed). Both maps show aftershock data recorded until January 20.

6.5.5 Aftershocks

The sensitivity of the NORSAR systems is indicated by the large number of aftershocks recorded. Until January 20, 2005, 736 aftershocks were detected and located by the NOA array as shown in Fig. 6.5.2. The NOA reviewed bulletin contained 274 aftershocks during the first day alone, and Fig. 6.5.3 shows the number of aftershocks during the first 21 days after the main earthquake.

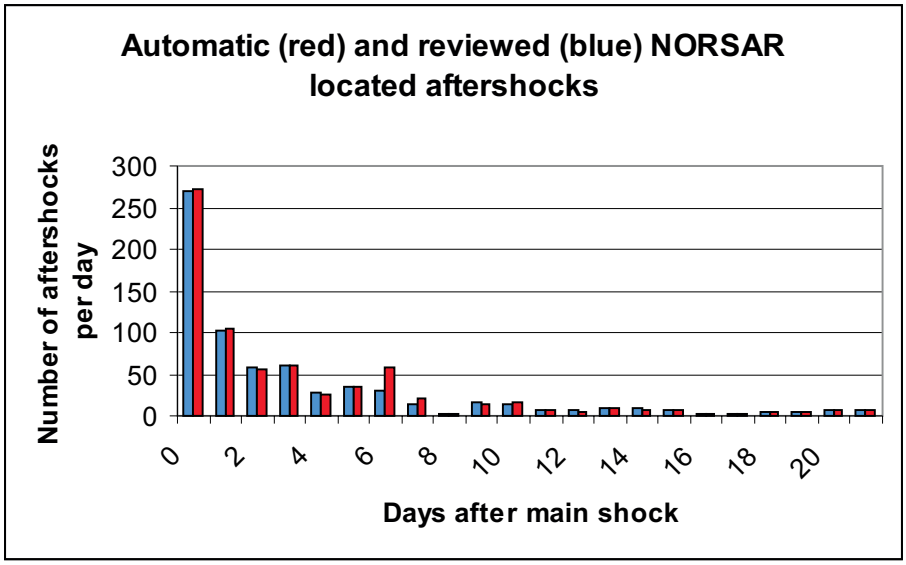

Fig. 6.5.3. Number of aftershocks recorded and located by NORSAR the first 21 days after the main event (from the automatic (red) and the reviewed (blue) bulletin)

6.5.6 Magnitudes

The epicenter to station azimuths for the Fennoscandian stations were 330 - 348 degrees, which is in the direction of the main rupture. At this time, we refrain from speculations on how this affected the magnitude calculations, and we refer to Schweitzer and Kværna (1999) for further discussions of this issue.

As described above, the two automatic systems for alerts reported m_b magnitudes of 5.5 and 6.3. The m_b 6.3 is obtained from the automatic large aperture array NOA processing. The amplitude is measured on a filtered beam (0.5-2.0Hz), and the time-window rule for picking the peak amplitude for the m_b measurement is to stay within 5 seconds after the P onset. An alert message reporting m_b magnitudes from 5.5 to 6.3 from a subduction zone is quite normal, and would not be considered as a possible catastrophic earthquake. In the search for other magnitude procedures, we therefore also measured manually the body wave maximum amplitude within 2 minutes after the P onset, and Table 6.5.3 show the results for m_b as well as for M_S measurements. As expected the m_b values are much larger than those measured during the first 5 seconds.

We normally see that large earthquakes have long P coda, and we see from Table 6.5.3 that extending the search time window for magnitude calculation results in significantly higher magnitudes. These results may indicate the need for a 2 step magnitude calculation: for the first alert messages, the first value (5 sec) is necessarily used, however, the first alert may be followed by a secondary processing (e.g. after 2 minutes) where additional measurements over longer time windows after the P arrival is used to verify or adjust the magnitude.

Table. 6.5.3. The m_b measurements were done in filter band 0.5-2Hz, whereas Ms was measured on unfiltered data

Station	m_b < 5 sec	m_b < 2 min	M_S
ARE0_bz	6.39	7.36	Clipped
SPA0_BHZ	6.58	7.72	9.05
NC405_bz	6.17	6.84	8.80
NC602_bz	6.10	7.21	9.03
FIA1_bz	6.28	7.28	Clipped
HFC2_bz	6.68	7.53	Clipped
JMIC_BHZ	6.66	7.24	Clipped

Finally, Fig. 6.5.4 compares 288 magnitude pairs in the aftershock sequence and demonstrate that the USGS reported magnitudes are systematically larger than the one-array NOA magnitudes. The difference is particularly pronounced at low magnitudes, and this illustrates the well-known "network magnitude bias" problem. In fact, the NOA single-array magnitudes are more consistent over the entire magnitude range than the network-based USGS magnitudes. Fig. 6.5.5 summarizes the magnitude differences in a cumulative probability distribution.

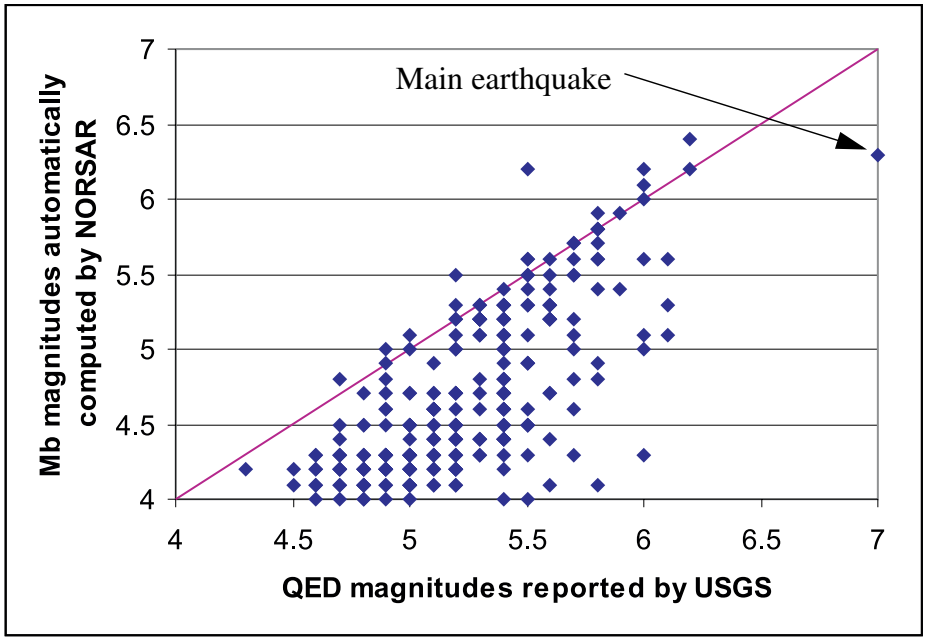

Fig. 6.5.4. Magnitudes for selected aftershocks (origin times within 60 seconds) for automatic NOA locations and QED reports from USGS.

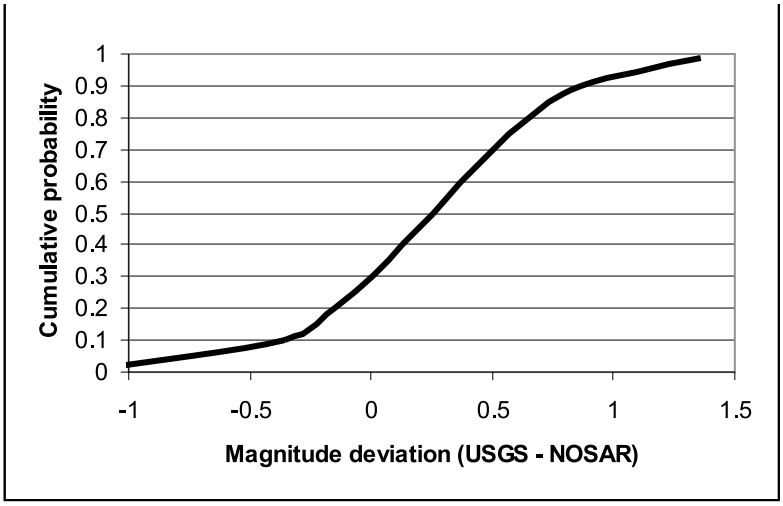

Fig. 6.5.5. Fig. 6.5.5. Magnitudes for selected aftershocks for automatic NOA locations and QED reports from USGS. Pairs of the earthquakes were matched if their origin time difference (NOA-QED) was within 60 seconds.

6.5.7 Conclusions

The Sumatra earthquake was the largest earthquake ever recorded by NORSAR, and consequently represented a test of the current instrumentation and processing algorithms. The alert system functioned well for the earthquake with reasonably precise location information relayed about 7 and 9 minutes after the first arrivals were recorded in Finland and Norway. The automatic magnitude estimates were considerably lower than later interactive measurements. While this is no surprise, it certainly represents a challenge for improving on magnitude determination algorithms for large earthquakes. Until January 20, 2005, 736 aftershocks were detected and located on the NOA array, and the automatic locations by and large delineate the main rupture.

Following this experience, some challenges for new developments have been identified: a) The processing could be optimized to provide the alert with a delay of some seconds rather than 7 and 9 minutes after data are recorded. Clearly, access to data from local or regional stations would enable even earlier alerts. b) The magnitude estimation (based on P-waves) should be improved for large events. Among the factors to take into account here are both the spectral properties of the signal and the duration of the P-wave train.

In summary we may state that:

- the NORSAR alert bulletins were functioning as intended, and with the appropriate precision for such distances.
- The processing of both main and aftershocks indicates adequate processing.
- The automatically computed m_b magnitudes are in principle not adequate for this size earthquakes.

- The automatic system may be improved on two particular targets: a) Improve the speed of the processing and b) develop/implement new magnitude estimation algorithms. For the latter it is possible to design a two-step alert system: the first step will be as today, however a delayed reprocessing (e.g. after 2 minutes) can be used to recalculate the magnitude from a longer time window.

References:

USGS poster on the 2004 Sumatra earthquake. http://neic.usgs.gov/neis/poster/2004/20041226_image.html.

Simoes, M., J. Avouac, R. Cattin, and P. Henry (2004): The Sumatra subduction zone: A case for a locked fault zone extending into the mantle, J. Geophys. Res., 109. doi:10:1029/2003JB00295.

Schweitzer J. (2003): NORSAR's Event Warning System (NEWS). NORSAR Scientific Report No. 1-2003, pp. 27-30.

Ortiz, M., and R. Bilham (2003): Source area and rupture parameters of the 31 Dec. 1881 Mw =7.9 Car Nicobar earthquake estimated from Tsunamis recorded in the Bay of Bengal. J. Geophys. Res. 2002JB001941RR 2003.

Ringdal F. and Kvaerna T. (1989): A multi channel processing approach to real time network detection, phase association, and threshold monitoring. Bull. Seism. Soc. Am., 79, pp. 1927-1940.

Conrad Lindholm
Frode Ringdal
Jan Fyen